의학박사 학위논문

Elucidation of the Biochemical Regulatory Mechanism of the Cys/N-Degron Pathway for Stress Sensing, Proteolysis, and Signaling

시스테인/N-말단 법칙을 통한 스트레스 센싱과 그에 따른 단백질 분해, 신호전달의 생화학적 조절 기작 규명

2022년 2월

서울대학교 대학원

의과학과 의과학 전공

허 아 정

시스테인/N-말단 법칙을 통한 스트레스 센싱과 그에 따른 단백질 분해, 신호전달의 생화학적 조절 기작 규명

지도 교수 권 용 태

이 논문을 의학박사 학위논문으로 제출함
2021년 10월

서울대학교 대학원
의과학과 의과학 전공
허 아 정

허아정의 이학박사 학위논문을 인준함

2022년 1월

위 원 장 이 민 재 (인)

부위원장 권 용 태 (인)

위 원 전 양 숙 (인)

위 원 한 도 현 (인)

위 원 송 현 규 (인)

Elucidation of the Biochemical Regulatory Mechanism of the Cys/N-degron Pathway for Stress Sensing, Proteolysis, and Signaling

Yong Tae Kwon

Submitting a Ph.D. Dissertation of
Medical Science

October 2021

Seoul National University
Biomedical Science Major

Ah Jung Heo

Confirming the Ph.D. Dissertation written by
Ah Jung Heo
January 2022

Chair	이 민 재	(Seal)
Vice Chair	권 용 태	(Seal)
Examiner	전 양 숙	(Seal)
Examiner	한 도 현	(Seal)
Examiner	송 현 규	(Seal)

Abstract

Elucidation of the Biochemical Regulatory Mechanism of the Cys/N-Degron Pathway for Stress Sensing, Proteolysis and Signaling

Ah Jung Heo

Major in Biomedical Sciences

Department of Biomedical Sciences

Seoul National University Graduate School

Cellular homeostasis requires the adaptation to a dynamically changing environment, which necessitates an equally flexible system that senses and responds to said changes. In the cellular scheme of sensing and adapting to change, the final determinants as executors are proteins. To adapt to various cellular stresses, modifications that deviate proteins apart from the basic function are required. In conjunction with this, cells routinely regulate the levels of proteins via transcriptional upregulation, alteration of protein stability, and post-translational modification that directly correlates to a change in function.

In this thesis paper, I will focus on the role of the Cys/N-degron pathway in the cellular response to oxidative stress, focusing on its modulation of both protein stability and post-translational modifications. The N-degron pathway, which is evolutionarily conserved throughout all the kingdoms, states that the exposed N-terminal residue of a

protein dictates the stability of a given protein. Amongst the diverse and many branches and sub-pathways of the N-degron pathway, the Cysteine branch of the Arg/N-degron pathway is unique in that it is the only residue capable of being modified by, and thus sensing oxygen atoms. This unique feature naturally imbues the Cys/N-degron pathway a key position to sense and respond to cellular oxidative stress within the N-degron pathway.

The first part of this thesis will elaborate on the intra-cellular system designed to maintain a delicate balance of cellular oxidative and reductive power in terms of proteolysis. Mechanistic insights to sense acute-to-prolonged hypoxia with subsequent oxidative stress, and to respond to those stresses via modulation of protein structure, function and metabolic fate dependent on its N-terminally exposed Cys residue will then be presented. Among the possible sources of the N-terminal arginine (Nt-Arg) residue, the two different pre-Arg secondary N-degrons, namely Cys-sulfinic acid ($CysO_2$) and Cys-sulfonic acid ($CysO_3$), bifurcate the metabolic fate of the substrate in question into either the ubiquitin-proteasome system (UPS) or the autophagy-lysosome system (ALS) respectively. This bifurcation is responsible for the crosstalk between the novel N-recognin KCMF1-UBR4 circuit and canonical UBR1/UBR2 circuit, resulting in the repriming of the ubiquitin code. This finding will expand the field of the N-degron pathway by elucidating the identity of second-position N-degron as a functional degradation determinant beyond that of subordination or sequel to the primary Arg/N-degron.

Subsequently, the physiological relevance of this oxidative stress-sensing, regarding the linkage between Cys/N-degron circuit and mitochondrial homeostasis will be investigated specifically under oxidative stress. E3 ligase and ubiquitin-dependent autophagic N-recognin KCMF1 will also be compared with the conventional autophagic shuttling adaptor N-recognin p62.

The following part of the thesis will broaden the scope to cell-to-cell communication comes in a sequel of stress sensing mechanism and how this inter-cellular signaling is mediated via Arg/N-degron pathway. I will focus on elucidating the mechanism of Arg/N-degron pathway mediated exocytosis. Specifically, RILP, which undergoes oxidative stress-induced cleavage and subsequent arginylation, settles a formation of MVB-ARL8b-kinesin complex formation for multivesicular body transport toward the plasma membrane. Moreover, ATE1 mediated arginylation also regulates the formation of intraluminal vesicles inside MVB. Through these dual regulatory steps of exosome biogenesis and transport, cells can reach intercellular homeostasis against oxidative stress beyond a single cellular level.

In the final section of my thesis, I will conclude with an overall summary and discussion of my findings. These series of findings will provide a complete and integrated view of the evolutionarily conserved cysteine branch of the Arg/N-degron pathway for both mammalian intra- and inter-cellular homeostasis against oxidative stress via bimodal proteolysis followed by oxidation and exosome secretion, respectively.

*The first part of the Results section was published in [Heo *et al.* 2021. The N-terminal Cysteine is a Dual Sensor of Oxygen and Oxidative Stress. *Proc.Natl. Acad. Sci. U.S.A.*, *in press*] (please refer to CV).

**The second part of the Results section is being prepared for submission.

Keywords: Cys/N-degron pathway, Arg/N-degron pathway, oxidative stress sensor, hypoxia sensor, KCMF1, exocytosis

Student ID: 2014-25077

Table of Contents

List of figures

Introduction

Results

The N-terminal Cysteine is a Dual Sensor of Oxygen and Oxidative Stress

Acronyms and abbreviations

AKT: Protein kinase B
ALP: Autophagy-Lysosome Pathway
ANXA1: Annexin A1 protein
AMPK: AMP-activated protein kinase
ARL8B: ADP ribosylation factor like GTPase 8B
ATE1: Arginyltransferase 1
ATG: Autophagy-related gene/protein
BAF: Bafilomycin A1
BiP: Binding Immunoglobulin Protein
CHOP: C/EBP Homologus Protein
CRT: Calreticulin
$CoCl_2$: Cobalt chloride
$CysO_2$: Cysteine sulfinic acid
$CysO_3$: Cysteine sulfonic acid
Degron: Degradation signal
ERK: Extracellular signal-regulated kinase
ESCRT: Endosomal sorting complex required for transport
GCN2: General control nonderepressible 2; Ser/Thr protein kinase
GPX3: Glutathione peroxidase 3
HCQ: Hydroxychloroquine
HIF1a: Hypoxia-inducible factor 1-alpha
IB: Immunoblotting
ICC: Immunocytochemistry
ILV: Intraluminal vesicles
iNOS: inducible nitric oxide synthase
IP: Immunoprecipitation
IRE1: Inositol-requiring enzyme 1
KDEL: Lys-Asp-Glu-Leu
KEAP1: Kelch-like ECH-associated protein
LIR domain: LC3-Interacting Region domain
MAPK: Mitogen-activated protein kinase
MEF: Mouse embryonic fibroblast
MetAP2: Methionine aminopeptidase 2
MG132: Carbobenzoxy-Leu-Leu-leucinal
Mitophagy: selective autophagic degradation of the mitochondria
MVB: Multivesicular body
NF-κB: Nuclear factor kappa-light chain-enhancer of activated B cells
NRF2: Nuclear factor erythroid-2-related factor 2
Nt-Arg: N-terminal arginine
Nt-Cys: N-terminal cysteine
Nt-Cys2: N-terminal cysteine located at second position
p62/SQSTM1: Ubiquitin-binding protein p62/Sequestosome-1
PARP: Poly (ADP-ribose) polymerase
PB1 domain: Phox and Bem1 domain
PDI: Protein Disulfide Isomerase
PERK: Pancreatinc ER kinase
PHDs: prolyl hydroxylase domain proteins
PI3K: Phosphatidylinositol 3-kinase
PPI: Protein-protein interaction

pQc: Protein quality control
PTM: Post translational modification
pVHL: Von Hippel-Lindau tumor suppressor E3 ligase
RHD: Rel homology domain
RILP: Rab interacting lysosomal protein
ROS: Reactive Oxygen Species
SDS-PAGE: Sodium Dodecyl-Sulfate Polyacrylamide gel
SLR: Sequestosome1-Like Receptor
SOD1: Superoxide dismutase 1
tBHP: tert-Butyl hydroperoxide
TGF-beta: Transforming growth factor beta
Ub: Ubiquitin
UBD/UBA: Ubiquitin-Binding Domain/Ubiquitin-Associated
UPR: Unfolded Protein Response
UPS: Ubiquitin-Proteasome System
VPS22/SNF8: Vacuolar protein-sorting-associated protein 22
VPS34: Phosphatidylinositol 3-kinase VPS34
VPS36: Vacuolar protein-sorting-associated protein 36
WB: Western blotting
WIPI2: WD-repeat domain phosphoinositide-interacting protein 2

Global Introduction

Overview & background

An organism is defined as the unit of life comprised of an organized structure, reaction to stimuli, growth, reproduction, adaptation, and maintenance of homeostasis. Among these, homeostasis - maintenance of a stable internal environment - is critical for the proper function and maintenance of life, the final gateway, and executors of which are proteins. Proteins, the most basic component of any cellular compartment, are the principal workhorses for all cellular functions. The function of a protein depends primarily on its structure. Cellular homeostasis and the proper structure/function of proteins are elegantly interconnected with one another in that one cannot exist without the other. Various extracellular and intracellular factors affect protein folding and protein-protein interactions. Any internal/external environmental changes can induce cellular stress by modifying the structure of macromolecules, primarily proteins. Thus, acute maintenance and rapid restoration of cellular homeostasis necessitate an equally swift and dynamic sensory system, by which cells can sense and respond appropriately to changing environmental factors such as hypoxia, oxidative stress, extreme temperatures, and nutrient starvation.

Homeostasis at the organismal level is achieved via both intracellular and intercellular signaling followed by signal transduction. Intracellular signaling involves a series of signal propagation mediated by modulation of protein structure and thus function carried out thoroughly various types of post-translational modifications (PTMs). PTMs are the core dynamics underlying the alteration of protein functionality, reversibly or irreversibly. Quite literally, PTMs are the conjugation of small proteins or chemical functional groups to an internal amino acid residue of a protein. Typical chemical PTMs include phosphorylation, glycosylation, hydroxylation, methylation, and acetylation among others. PTMs regulate cellular signaling by altering partly the interactome and partly the stability of a given protein via modulation of its structural conformation, which changes the critical recognition domain or substrate itself. As an archetypal example and

one of the earliest PTMs discovered and critically involved in signaling cascades, phosphorylation introduces a phosphate group to the serine, threonine, and tyrosine residue of a protein and results in a net charge of -2, which induces a major change in its structural conformation (1, 2). This altered structure, along with the added phosphoryl group, enables recognition by binding partners via specific domains such as SH2 (Src homology domain 2), phosphotyrosine-binding domain (PTB), or forkhead-associated domain (3, 4).

Furthermore, conjugation of the small proteins can also modulate target protein for further functional and stability regulation of the protein for the response for sensing and adaptation. Ubiquitin and other ubiquitin like proteins (UBLs) are studied in a different context to broaden the horizon of protein modifications. SUMO (small ubiquitin-like modifier) (5, 6), NEDD8 (neural precursor cell expressed developmentally downregulated protein 8) (7-9), and ISG15 (interferon stimulated gene 15) (10-12) are regulated via manner similar to ubiquitylation mechanism to regulate various cellular processes including transcription, damage repair response, activate E3 ligases, autophagy, protein translation, and exosomal secretion. Amongst all, a 76-amino-acid-residue protein ubiquitin, an epitome of “degron”, a signal for degradation (13), becomes a subject of the most extensive study. Requiring sequential action of three enzymes, C-terminal glycine residue of ubiquitin is activated by E1 ATPase for the formation of ubiquitin adenylate and transferred to active site Cys residue of the E2 ubiquitin-carrier protein (14-17).Then E3 ubiquitin ligase links the C-terminus of the ubiquitin to ε-amino group of the lysine residue of the specific substrate protein with isopeptide bond (2). Substrate selectivity of the ubiquitylation established on over 600 genes for E3 ligases each accompanied with specified substrate recognition motif. However diverse the composition of its domain for substrate protein recognition, E3 ligase must possess two domains: one of the RING (Really Interesting New Gene), HECT (Homologous to E6AP C-terminus), and RBR

(RING-in-between-RING) domain responsible for ubiquitin ligation and the other one responsible for the recognition of the substrate signal (18). Upon substrate recognition by E3 ubiquitin ligase, a substrate is ubiquitylated by single or multiple ubiquitin residues. Monoubiquitylation of the substrate protein was widely known for a nonproteolytic reversible modification that regulates the functionality of proteins specifically in endocytic trafficking, histone activity, DNA repair, virus budding, etc (19). Monoubiquitylation can occur in single as well as multiple lysine residues of the substrate protein. Serving a basis for multiple ubiquitin ligation, initial ubiquitin residue can build more ubiquitin as a form of chain at 7 lysine internal residues (K6, K11, K27, K29, K33, K48, and K63) and initial methionine residue to form homotypic and heterotypic poly-ubiquitin chains responsible for different conformational arrangement for further ubiquitin recognition components. The ubiquitin code dedicated by those homotypic and heterotypic linkages is mostly decoded for the ubiquitin chain as a determinant for protein degradation signal. Among the 8 identified homotypic chain linkage types, K11, K29, and K48-linked chains have been widely reported as proteasomal degrons, while K63-linked chains have been associated with autophagic delivery of substrates (20-22). However, ubiquitin can also assemble into the single Lys residue for the formation of heterotypic Ub linkage as a mixed or branched conformation. A limited number of studies have identified the function of heterotypic Ub chain linkages, such as K11 and K63 mixed chains for endocytosis, K63 and M1 hybrid linkage for immune signaling, K29/K48 and K11/K48 branched chains for protein degradation, and K63-K48 branched linkage for NF-κB signaling (23-28). However, other types of heterotypic Ub chain linkages and their functions have yet to be fully elucidated. These discrete types of ubiquitin chain become a basis to modulate cellular signaling and response to stress via protein degradation. The ubiquitin code is a single encompassing theme for the two major branches of the protein degradation pathway, the ubiquitin-proteasome system (UPS) and autophagy-lysosomal

system (ALS). Forementioned K11, K29, K48-linked homotypic ubiquitin chains as well as K29/K48 and K11/K48 branched ubiquitin chains are responsible for the proteasomal degradation of substrate proteins (25, 26, 29, 30). Also, for larger substrates incapable of passing the 20S core compartment of the proteasome, substrate proteins are targeted to autophagic degradation. Along with substrate recognition specificity mediated by the E3 ligase, these complexities of the ubiquitin code are responsible for the selectivity of the protein degradation.

One of the two major axes of protein degradation, autophagy is categorized into macro- and selective autophagy. Macroautophagy is a catabolic process by which cytoplasmic constituents such as misfolded proteins and organelles are sequestered by autophagosomes and digested by lysosomal hydrolases (31, 32). The targeting of autophagy cargoes often involves specific receptors such as p62/Sequestosome-1 and Neighbor of BRCA gene 1 (NBR1) (33-35) whose UBA and LIR domains enable recognition of both ubiquitin (Ub) chains on protein cargoes and LC3 on autophagosomes, respectively (36, 37). Selective autophagy by LIR-containing receptors facilitates the removal of various subcellular cargoes, including protein species ranging from monomers to aggregates, organelles, and infectious pathogens.

One of the major challenges for the cells for a swift and dynamic sensor/responder system is the availability of oxygen. Cellular O_2 reserve at any given moment in time is critical for cellular homeostasis due to energy production in the mitochondria via oxidative phosphorylation. Known mammalian O_2 sensing mechanisms involve HIF-1α (hypoxia-inducible factor 1α) for oxygen homeostasis and subsequent transcriptome change (38). As an O_2 sensor, the transcription factor HIF-1α is normally hydroxylated by PHD (prolyl-hydroxylase) and degraded through ubiquitylation by the von Hippel-Lindau (VHL) E3 ligase. Under hypoxia, HIF-1α is not oxidized and thus metabolically stabilized, leading to the transcriptional induction of hypoxia-responsive

proteins (39-41). However, as this chronic sensor of hypoxia typically requires at least 2-4 hours (42) to adjust stress response pathways, it remains an outstanding question how cells sense and react to acute hypoxia.

Dysregulation of O_2 homeostasis can cause the excessive accumulation of ROS, leading to oxidative stress (43). In response to the increases in ROS levels, cells attempt to maintain homeostasis by activating stress-specific signaling cascades (Figure 1), such as the Keap1-Nrf2, NF-κB, AKT, and MAPK pathways (44). While the functions and mechanisms of anti-oxidative stress pathways are now fairly well understood, little is known about how cells initially sense the accumulation of ROS. Moreover, despite the fact that O_2 and ROS are chemically and physiologically related to each other, it has remained unclear how sensing systems for O_2 and ROS are in crosstalk with each other, especially when ROS begin to accumulate as a consequence of chronic O_2 deficiency (i.e., hypoxia).

The Arg/N-degron pathway (previously called the "The Arg/N-end rule pathway") can target a protein that bears a destabilizing N-terminal (Nt-) residue for degradation by the proteasome or via autophagy (Figure 2) (37, 45-49). The set of N-degrons encompasses Nt-arginine (Nt-Arg). While this N-degron can be present constitutively, it can also be generated conditionally, through arginylation of Nt-aspartate (Asp) or Nt-glutamate (Glu) by arginyl-tRNA protein transferase 1 (ATE1 R-transferase). The resulting Nt-Arg is bound by the UBR box of the N-recognins UBR1 and UBR2 that promote ubiquitylation and proteasomal degradation of native substrates (50). In addition to Nt-Asp and Nt-Glu, Nt-Cys can be Nt-arginylated following its chemical or enzymatic oxidation(51-54). The Nt-Cys-carrying substrates of arginylation include a set of GTPase-activating proteins (RGS4, RGS5, and RGS16) and interleukin-32 (IL-32) that carry the Nt-Met-Cys motif as a pro-N-degron (51, 52, 55, 56). The RGS proteins are normally degraded through the Ub-proteasome system (UPS), during which their Cys2 residue is

N-terminally exposed as a pro-N-degron, following Nt-Met excision. This Nt-Cys residue is subsequently oxidized into $CysO_2$ (Cys-sulfinic acid) by mammalian ADOs (cysteamine (2-aminoethanethiol) dioxygenase) or plant PCOs (plant cysteine oxidases) (Figure 3) and arginylated by ATE1, leading to substrate ubiquitylation and proteasomal degradation (53, 56). However, under hypoxia, the oxidation of the Nt-Cys residue is inhibited, resulting in the metabolic stabilization and adjustment of downstream signaling pathways (52, 53). Through O_2-dependent degradation, the Nt-Cys can function as an O_2 acceptor in a cellular sensing system for acute hypoxia (53, 56-58). However, the role of the Nt-Cys residue in chronic hypoxia and oxidative stress remains unknown.

The autophagic Arg/N-degron pathway facilitates autophagic degradation of not only N-degron substrates but also other cellular proteins via activation of the autophagic adaptor p62/SQSTM1/Sequestosome-1. Specifically, the accumulation of autophagic cargoes such as ubiquitinated proteins and aggregates induces the Nt-arginylation of ER-resident chaperones. As a prime example, Nt-arginylated BiP (R-BiP) is associated with misfolded proteins, and its N-terminal Arg binds the ZZ domain of p62(47, 59). This Nt-Arg mediated interaction induces a conformational change of p62, exposing its PB1 and LC3-interacting domains, which functionally activates both itself and cellular autophagy, ranging from autophagosome biogenesis and autophagy flux. Thus, the macroautophagy modulator p62 is an N-recognin of the Arg/N-degron pathway specifically validated for Asp-, and Glu- bearing secondary N-degron substrate proteins in response to proteotoxicity. However, the exact ramifications and mechanistic relevance of p62 with respect to the Cys/N-degron pathway under oxidative stress have not yet been fully explored.

As mentioned earlier, cells necessarily communicate for initiation of the instant protection against incoming damage. For cell-to-cell communication cells utilize exocytosis machinery for the secretion of intracellularly synthesized signaling molecules

(Figure 4). Although mechanism and initiating signals for the regulated secretion and constitutive secretion is thoroughly studied, mechanism and signal for releasing exosome has not been elucidated well.

For the first part of the thesis, I will show that the Nt-Cys2 of the Cys/N-degron pathway mediates the intracellular sensing of and response to acute and chronic hypoxia as well as oxidative stress. The second part of the thesis will elaborate on how the Arg/N-degron pathway regulates oxidative stress-induced exosome secretion via dual regulatory mechanisms of MVB transport complex formation and ILV biogenesis.

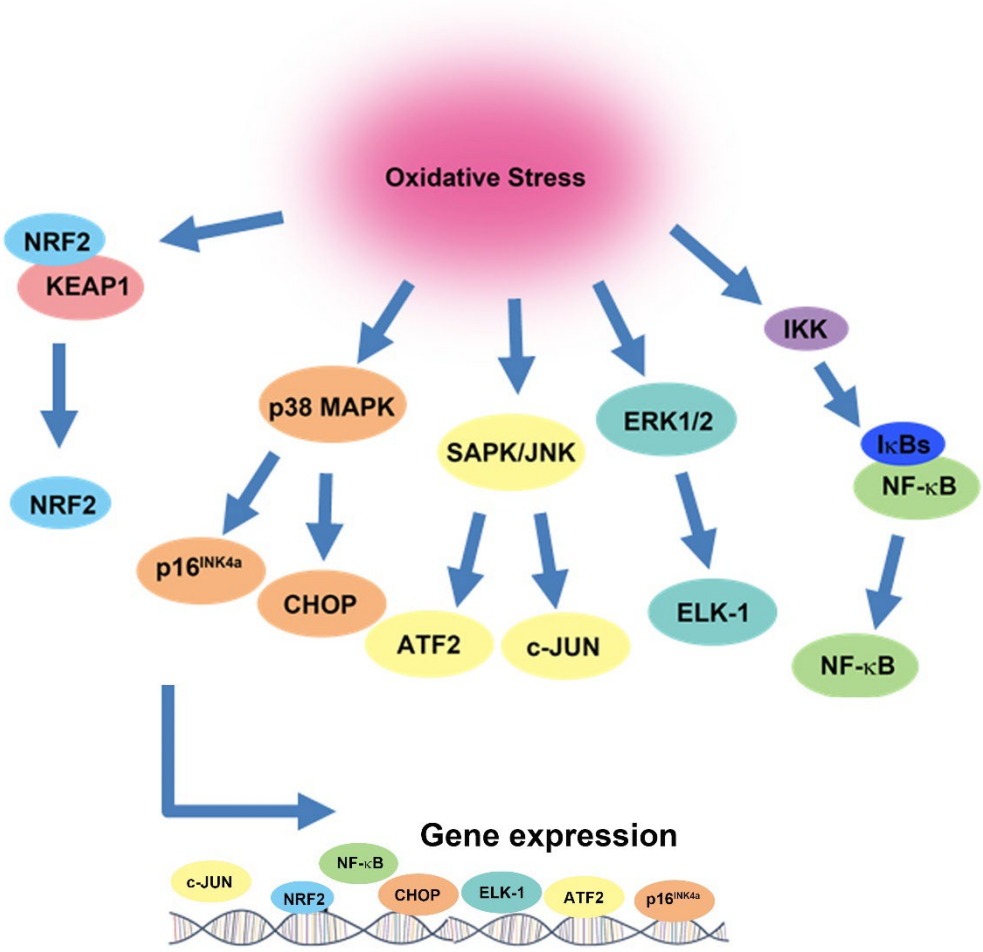

Figure 1. Oxidative stress-induced signaling pathway

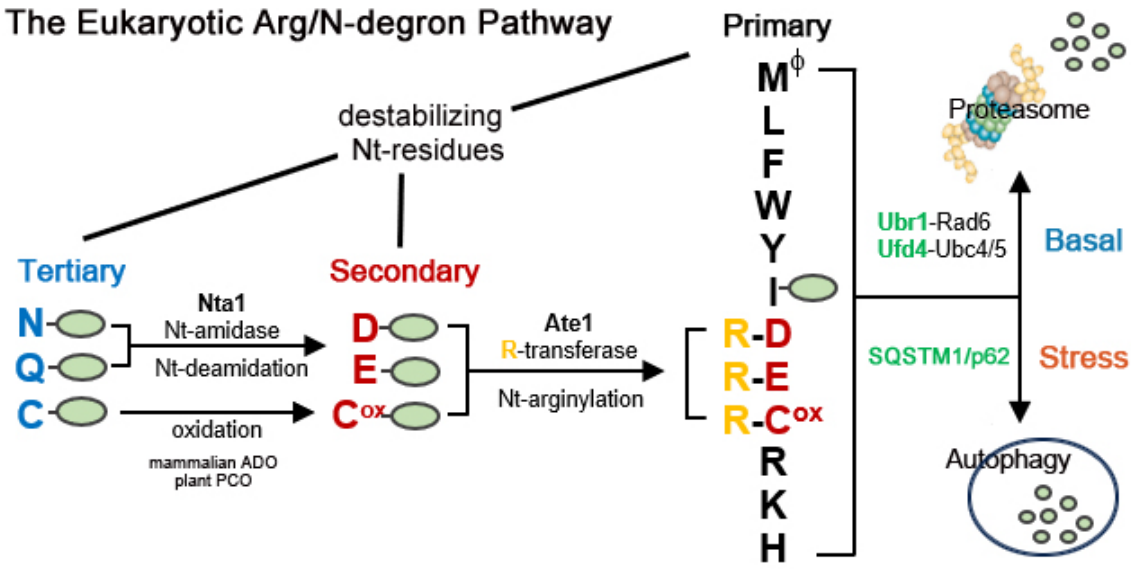

Figure 2. The eukaryotic Arg/N-degron pathway

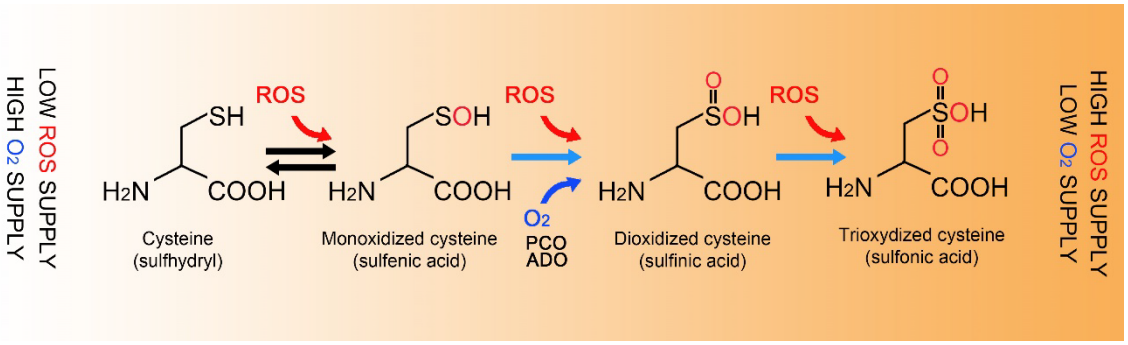

Figure 3. Redox potential of the Nt-cysteine side chain – sulfhydryl group may accept up to three oxygen atoms

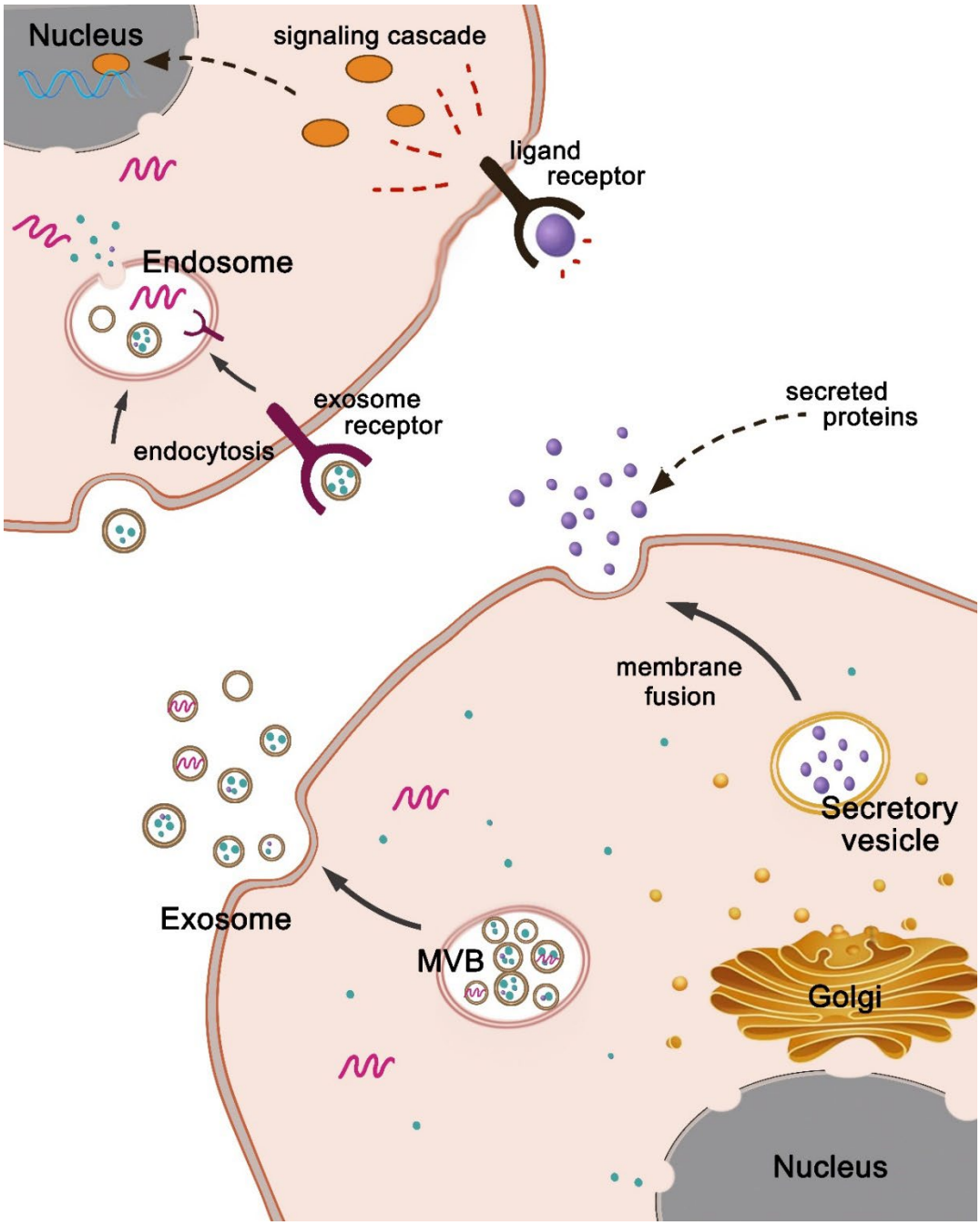

Figure 4. Exocytosis-mediated intercellular and intracellular signaling

Chapter 1

The N-terminal Cysteine is a Dual Sensor of Oxygen and Oxidative Stress

Introduction

Cellular resiliency involves the sensing of and adaptation to a dynamically changing environment often challenged with various stresses. It has been an outstanding question how cells sense environmental factors and intracellular stresses, including posttranslational modifications to macromolecules, O_2 deprivation, oxidative stress, extreme temperatures, and nutrient starvation. Notable examples include ATM (ataxia-telangiectasia mutated), ATR (ATM- and Rad3-Related), and DNA-PKcs (DNA-dependent protein kinase) that together sense DNA damage (60, 61). GCN2 (general control nonderepressible 2 kinase) and AMPK (5' AMP-activated protein kinase) respectively sense amino acid and glucose starvation (62, 63). In contrast, O_2 levels can be sensed via PHD (prolyl-hydroxylase)-mediated oxidation of HIF-1α (hypoxia-inducible factor 1α), which induces transcriptional adaptations to hypoxia for O_2 homeostasis (39-41). To date, however, the mammalian first-line sensing system for oxidative stress, such as that induced by reactive oxygen species (ROS), have not yet been fully elucidated.

The N-degron pathway dictates the *in vivo* half-life of a protein based on its destabilizing N-terminal amino acid, called an N-degron (45-47). In this pathway, the N-degron Arg can be generated by conjugation of L-Arg to Nt-Asp or Nt-Glu by arginyl-tRNA protein transferase 1 (ATE1), which is recognized by UBR box-carrying E3 ligases such as UBR1 and UBR2 that promote ubiquitination and proteasomal degradation (50). When autophagic cargoes such as misfolded proteins and their aggregates accumulate under stresses, the Nt-Arg is generated on various non-Nt-Cys substrates to bind p62 via its ZZ domain, resulting in self-oligomerization and increased LC3-interaction of p62 for co-degradation of itself and its cargoes by lysosomal hydrolases (47, 50, 59).

Although the pVHL-HIF-1α circuit has been identified as an O_2 sensor, this chronic sensor takes 2-4 hours to induce the expression of its target genes (64), raising an outstanding question on how cells sense fluctuating O_2 levels in a real-time basis. Our earlier work has shown that the Cys/N-degron pathway functions as an acute O_2 sensor (52, 55). In this sensing system, the Nt-Cys2 residue of RGS4 and RGS5, exposed from the second position, is co-translationally oxidized into Cys sulfinic acid ($CysO_2(H)$) in normoxia, which was later found to be mediated by ADO (52, 56). The C^{O2} N-degron is subsequently conjugated with the amino acid L-arginine (L-Arg) by *ATE1*-encoded R-transferases (Kwon et al., 1999; 2002). The resulting R-C^{O2} N-degron is recognized by UBR boxes of the N-recognins UBR1 and UBR2 that promote ubiquitination and proteasomal degradation. Under hypoxia, however, the oxidation of Nt-Cys2 is inhibited, and the resulting degron-less Cys substrates are metabolically stabilized to modulate hypoxia responses, thereby functioning as an O_2 sensor (57). The role of the Nt-Cys in O_2 sensing was further supported by the findings in plants where a set of transcription factors mediate hypoxia responses through oxidation of their Nt-Cys2 by plant cysteine oxidases, generating the R-C^{O2} N-degron via arginylation (65-67). In plants, cysteine oxidases (PCOs) was found to conjugate O_2 to Nt-Cys to generate the C^{O2} N-degron (53, 58). These substrates are metabolically stabilized under abiotic stress-linked hypoxia, modulating hypoxic stress responses (65-68). It is now increasingly clear that the Cys/N-degron pathway functions as an acute oxygen sensor as compared with chronic oxygen sensing by the pVHL-HIF-1α pathway.

One outstanding question, however, is how Cys substrates under hypoxia are degraded even though they cannot be oxidized and, thus, lack, the C^{O2} N-degron. Compared with Nt-Arg, the role of Nt-Cys remains controversial as Nt-Cys is stabilizing in *S. cerevisiae* (69, 70) but can act as a pro-N-degron for the Arg-N-degron pathway via the UPS in plant and mammalian systems (55). In plants, responses to

hypoxia are mediated by the Nt-Cys2 residue on a set of hypoxia-sensitive Nt-Cys-carrying transcription factors (65-67). Plant cysteine oxidases (PCOs) conjugate O_2 to Nt-Cys to form a Cys^{O2} (53, 58). Abiotic stress-linked hypoxia impairs the degradation of such substrates, thereby modulating the hypoxic stress response. (65-68). In mammalian systems, the Nt-Cys substrates such as regulator of G-protein signaling 4 (RGS4), RGS5, and RGS16, are regularly oxidized to generate Nt-Cys^{O2} by ADO for ubiquitination and proteasomal degradation, the process of which is blocked by hypoxic stress (52, 56). The Nt-Cys2-containing substrates are oxidized by ADO and arginylated by ATE1, leading to proteasomal degradation (52, 56). Prolonged exposure to this hypoxic stress inevitably generates non-oxidized and thus non-degraded Nt-Cys substrates and presents a dilemma for intracellular proteolysis. However, mechanisms and pathways for the intracellular proteolysis of Nt-Cys substrates under hypoxia have not yet been identified.

Sensing of molecular oxygen and generation of reactive oxygen species (ROS) are intrinsically intertwined with each other. Interestingly, either the presence (due to oxidative phosphorylation) or absence of O_2 can produce ROS (43). Disruption of this delicate balance in oxygen homeostasis, which is normally maintained by dynamic levels of cytosolic antioxidant buffers, results in excessive ROS accumulation, causing oxidative stress, inflammation and ultimately cell death. ROS-induced oxidative stress mediates the pathogenesis of various diseases, including neurodegeneration, via processive and systematic structural modifications on various cellular components ranging from macromolecules to organelles (71-75). Thus, sensing and adaptation to oxidative stress as well as pharmacological modulation of such responses have been a subject of extensive research. To date, however, little is known about how cells initially sense and react to ROS by triggering oxidative stress responses and how this sensing system is linked to O_2 sensors.

In this study, we show that the Nt-Cys2 residue is a dual sensor for both O_2 and oxidative stress. In normoxia, the Nt-Cys2 is enzymatically oxidized into R-C^{O2} via arginylation, acting as an O_2-dependent N-degron inducing K48-linked ubiquitination and proteasomal degradation. Under prolonged hypoxia or oxidative stress, the Nt-Cys2 is chemically oxidized into C^{O3} by ROS and arginylated into R-C^{O3}. The R-C^{O3} redirects the substrates to autophagy via K27/K63-linked ubiquitination, whose chains are recognized by p62 for lysosomal targeting of the substrate. The Nt-R-C^{O3} proteins that escape from arginylation are cytotoxic and imported into the mitochondrion for degradation via MAGIC (mitochondria as a guardian in cytosol). Through this bifunctional sensor involving two structurally distinct oxygen-containing degrons, neuronal cells sense and coordinate both O_2 and oxidative stress into various biological processes including proinflammatory signals. We also developed small molecular ligands that modulate the degradation of Cys/N-degron substrates and, thus, protect dopaminergic neurons from degeneration and death, which is critical to the pathogenesis of Parkinson's disease.

Results

The Nt-Cys residue plays a key role in sensing acute and chronic hypoxia as well as oxidative stress though its oxidation

To understand the role of the Nt-Cys residue in sensing O_2 and ROS and how the two sensing systems are intertwined with each other, I first characterized the metabolic fate and their N-terminal modifications of Nt-Cys proteins under acute vs. chronic hypoxia. Degradation assays showed that RGS4, RGS5, RGS16 and IL32 were normally degraded via the UPS (Figure 5A-D). This degradation required Nt-arginylation of their Cys2 residues, as evidenced by their stabilization under chemical inhibition of ATE1 by tannic acid (Figure 6) or Cys2 mutation to Val (Figure 7). Consistent with our previous finding that the Nt-Cys is oxidized to facilitate proteasomal degradation of N-degron substrates (56), the Nt-Cys proteins were drastically stabilized under hypoxia (Figure 8). These results reiterate the role of Nt-Cys in proteolysis via the N-degron pathway and sensing acute hypoxia in mammalian cells.

I also determined whether the Nt-Cys acts as a sensor of ROS under oxidative stress. Importantly, normally short-lived Cys/N-degron substrates turned to long-lived when cells under normoxia were exposed to ROS-inducing chemicals such as tert-butyl hydroperoxide (tBHP) and cobalt chloride ($CoCl_2$) (Figure 9A, 9B). This ROS-induced stabilization occurred as early as 0.5 h and continued up to 6 h post-treatment with ROS inducers (Figure 10), independent of transcriptional alteration (Figure 11A, 11B). These Nt-Cys proteins, metabolically stabilized by tBHP or $CoCl_2$, (Figure 12A, 12B, 12C) returned back to be short-lived when ROS was scavenged using N-acetyl cysteine (NAC) (Figure 13A, 13B). In contrast, C2V-RGS4 mutant was unconditionally long-lived under all conditions tested (Figure 12A, 12B). These results suggest that normally short-lived Nt-Cys proteins are metabolically stabilized under oxidative stress through chemical

oxidation of their Nt-Cys by ROS.

To determine the role of the Nt-Cys residue as a sensor of chronic hypoxia, I also tested the hypothesis that chronic hypoxia generates ROS, which in turn chemically oxidizes Nt-Cys bearing proteins. Indeed, DCHF-DA assays showed that prolonged hypoxia led to the excessive production of ROS, which was counteracted by NAC (Figure 14). Consistently, RGS16 were long-lived under chronic hypoxia and became short-lived following NAC treatment (Figure 15). These results collectively suggest that the Nt-Cys residue represents a cellular sensing system for acute and chronic hypoxia as well as oxidative stress in HIF-1α-independent manner.

Proteolytic flux in the Cys/N-degron pathway is shifted from the proteasome to the lysosome under chronic hypoxia and oxidative stress

To investigate the role of the Nt-Cys residue as an oxidative stress-specific N-degron, I characterized the metabolic fates of Nt-Cys-carrying proteins. Cycloheximide-chase assays showed that Cys/N-degron substrates were stabilized in an Nt-Cys-dependent manner when cells were treated with $CoCl_2$ (Figure 16A, 16B). When proteolytic flux was analyzed using the proteasomal inhibitor MG132 or the lysosomal inhibitor bafilomycin A1, they were normally degraded via the UPS but redirected to autophagy in response to oxidative stress induced by $CoCl_2$ or tBHP (Figure 17A, 17B, 18A, 18B, 18C, 18D). Such a proteolytic re-routing occurred as early as 0.5 hr post-exposure to ROS (Figure 19). In co-localization analyses, Nt-Cys proteins under oxidative stress were targeted to $p62^{+}LC3^{+}$ autophagic membranes through the activity of their Nt-Cys (Figure 20A, 20B, 21, 22, 23). Their degradation via macroautophagy was abolished by chemical inhibition or genetic ablation of ATE1 (Figure 24A, 24B, 24C). Thus, the Nt-Cys residue exposed to oxidative stress redirects proteolytic flux from the UPS to macroautophagy through its oxidation and arginylation.

Next, I determined the role of the Nt-Cys residue in autophagic proteolysis under chronic hypoxia. Proteolytic flux assays showed that Cys/N-degron substrates were normally subject to acute degradation via the UPS with cooperation of ADO1 (Figure 25) but drastically stabilized when hypoxia was prolonged to 6 hrs (Figure 26A, 26B). The apparent stabilization was attributed to re-routing from UPS-mediated acute degradation to lysosome-mediated chronic degradation (Figure 27). The autophagic degradation was abrogated by genetic depletion (Figure 28A) or chemical inhibition (Figure 28B) of ATE1. Thus, proteolytic flux of Cys/N-degron substrates is re-directed from the UPS to autophagy if hypoxia is prolonged.

The Nt-Cys under oxidative stress is oxidized and arginylated to generate the N-degron Arg-CysO_3

Previous studies showed that when cells sense acute changes in O_2 levels, the Nt-Cys residue is enzymatically oxidized to the CysO_2 N-degron by plant PCO1 or mammalian ADO1 (53, 56, 58). I therefore tested whether ADO1 mediates oxidation of the Nt-Cys under chronic hypoxia. Importantly, ADO1 knockdown cells under chronic hypoxia retained significant autophagic flux of Cys/N-degron substrates (Figure 29), suggesting that Cys/N-degron substrates may be at least in part chemically oxidized by ROS under chronic hypoxia or oxidative stress. I therefore characterized the modifications of Nt-Cys under oxidative stress and chronic hypoxia by employing mass spectrometry of RGS4. LC/MS analysis showed that, while an expected modifications of the Nt-Cys product of RGS4 protein following oxidation under normoxia is CysO_2 (53, 56), Nt-Cys residue of RGS4 in cells exposed to tBHP was mostly modified into CysO_3 (Cys sulfonic acid) (Figure 30). Critically, the levels of Nt-CysO3-carrying RGS4 peptides destined to oxidative stress-associated autophagy were 73-fold higher than those destined to the UPS under normoxia (Figure 31A, 31B). Thus, under chronic hypoxia or

oxidative stress, the Nt-Cys residue is chemically oxidized and arginylated into the autophagic N-degron Arg-$CysO_3$.

Autophagic targeting of Cys/N-degron substrates is mediated via K63 and K27-linked ubiquitylation

Previous studies showed that RGS4 and RGS5 under normoxia are assembled with K48-linked Ub chains by the N-recognin UBR1 and UBR2 (76). To elucidate the mechanisms by which the Cys/N-degron pathway modulates bidirectional proteolysis via the Arg-$CysO_2$ or Arg-$CysO_3$ degron, I characterized the Ub codes of Nt-Cys proteins under oxidative stress and chronic hypoxia. Denaturation immunoprecipitation (IP) assays under normoxia confirmed that polyubiquitylation of RGS4 led to acute degradation by the proteasome (Figure 32; lanes 3 vs. 4). Notably, RGS4 was also polyubiquitylated in the presence of excessive ROS, which lead to degradation by the lysosome but not the proteasome when proteolytic flux was analyzed using MG132 and bafilomycin A1 (lanes 6 vs. 7). To determine whether the Cys2 residue is essential for RGS4 ubiquitylation, X-nsP4 (X= Cys or Arg) was expressed in *ATE1*$^{-/-}$ mouse embryonic fibroblasts (MEFs) using Ub fusion technique (UFT) (Figure 33). Whereas Arg-RGS4 was ubiquitylated in both +/+ and *ATE1*$^{-/-}$ cells, Cys-RGS4 was conjugated with poly-Ub chains only in +/+ cells but not *ATE1*$^{-/-}$ cells (Figure 34). These results suggest that Nt-arginylation is essential for ubiquitylation of Nt-Cys-carrying proteins for degradation via both the UPS and autophagy.

Our results suggest that the Nt-Cys residue is enzymatically oxidized to Arg-$CysO_2$ under normoxia and chemically oxidized to Arg-$CysO_3$ under chronic hypoxia and oxidative stress. I therefore characterized the differences in Ub chain linkages conjugated to substrates bearing the Arg-$CysO_2$ or Arg-$CysO_3$ degron with respect to their proteolysis via the UPS and autophagy, respectively. As expected, K48-ubiquitylated RGS4 was

selectively enriched upon inhibition of the proteasome (Figure 35, lanes 3 vs. 2, K48-Ub) but not the lysosome under oxidative stress (lanes 4 vs. 2). In contrast to K48-Ub chains, K63-Ub chains exhibited significant proteolytic flux upon lysosomal inhibition in cells treated with tBHP (lanes 4 vs. 2, K63-Ub). Such a proteolytic flux of K63-chains via autophagy was diminished in ATE1-deficient cells (Figure 36, lanes 3 vs. 4, K63-Ub). Under these oxidative stress conditions, autophagic flux was observed with K63-Ub chains (Figure 37, lanes 4 vs. 3) but not K48-Ub chains (lanes 4 vs. 3). These results suggest that Cys/N-degron substrates are tagged with K63-linked Ub chains.

To identify additional Ub modifications on RGS4 that facilitate autophagic flux, I used single-lysine (Lys)-only Ub mutants in which all Lys residues except one are substituted with Arg. When visualized using immunostaining analyses, RC^{ox}-RGS4 formed cytosolic puncta that co-localized solely with K63-only or K27-only mutant Ub bodies (Figure 38, 39). In denaturation IP assays under oxidative stress, autophagic flux was observed with K63-only- (Figure 40A, 40B) and K27-only (Figure 41) Ub mutants conjugated to Nt-Cys substrates but not with K48-only mutants (Figure 42). These results suggest that RGS4 conjugated with K63/K27-linked Ub chains are selectively degraded by autophagy. I therefore asked whether K63/K27-ubiquitylation occurs on other Nt-arginylation substrates that enter autophagic flux independent of Nt-Cys. $RD\text{-}CDC6^{FLAG}$, a model Nt-Arg substrate known to be destined to autophagic degradation under proteotoxic condition (77), was not K63-ubiquitylated in either oxidative or proteotoxic stress (Figure 43A, 43B). These results show that the tri-oxidized Nt-Cys residue functions as an autophagic N-degron that targets substrates to the lysosome via arginylation-dependent Ub re-priming with K63/K27 chains under oxidative stress.

KCMF1 is an oxidative stress-specific N-recognin that K63-ubiquitylates Nt-Cys substrates.

To identify the E3s that mediate K63- and/or K27-linked Ub chains on Nt-Cys bearing proteins, I measured the binding of UBR1 to RGS4. Co-IP analyses showed that the binding affinity significantly weakened under oxidative stress as compared with normal conditions (Figure 44). Moreover, the genetic ablation of both UBR1 and UBR2 did not blocked but rather accelerated autophagic targeting of Nt-Cys substrates (Figure 45A, 45B, 46, 47, 48). As these results suggest that UBR1 and UBR2 preferentially recognize Arg-$CysO_2$ over Arg-$CysO_3$, I screened for oxidative stress-specific E3s that recognize Arg-$CysO_3$ and promote K27- or K63-ubiquitylation. Co-IP analyses coupled with mass spectrometry identified KCMF1 as an E3 responsible for K63-ubiquitylation of Nt-Cys substrates. Mapping analyses showed that KCMF1 bound Arg-$CysO_3$ through the ZZ domain (Figure 49). The ZZ domain of KCMF1 shared sequence similarity with the UBR box of UBR1 and the ZZ domain of the autophagic N-recognin p62, including those required for binding Nt-Arg (Figure 50). I therefore determined how the binding affinity of KCMF1 and UBR1 to the RC^{ox} degron is modulated under oxidative stress using *in vitro* peptide pulldown and co-IP assays. In basal conditions, similar amounts of KCMF1 and UBR1 were co-precipitated with RGS4 (Figure 51). However, under oxidative stress, the RC^{ox} exhibited higher affinity to KCMF1 and weaker affinity to UBR1 as compared with basal conditions (Figure 52A, 52B). Pulldown assays confirmed that the ZZ domain of KCMF1 is essential for the recognition of the Nt-Arg-$CysO_3$ degron (Figure 53). These results suggest that KCMF1 is an oxidative stress-specific N-recognin that K63-ubiquitylates Nt-Cys substrates.

Next, I characterized the role of KCMF1 in targeting Nt-Cys proteins to autophagy. Denaturation IP assays confirmed that the genetic interference of *KCMF1* (Figure 54) abolished the conjugation of K63-linked Ub chains on Nt-Cys substrates and their ROS-induced autophagic turnover (Figure 55). Co-localization assays revealed that interference of *KCMF1* abolished both the formation and subsequent co-localization of

recombinant RGS4^{+}p62^{+} punctate structures (Figure 56). In contrast, no such impairment in K63-ubiquitylation was observed in *UBR1*$^{-/-}$*UBR2*$^{-/-}$ cells (Figure 57A, 57B). These results suggest that KCMF1 is essential for targeting Cys/N-degron substrates to autophagy.

UBR4 assembles K27-linked Ub chains on K63-ubiquitylated Nt-Cys substrates

To identify the E3 responsible for the assembly of K27-linked Ub chains on K63-ubiquitylated Nt-Cys bearing proteins, I screened UBR box proteins. Autophagic flux assays showed that the loss of both UBR1 and UBR2 accelerated the autophagic degradation of Nt-Cys proteins under oxidative stress (Figure 58). UBR5-knockdown cells also retained the capacity to target K63-ubiquitylated RGS4 to autophagy (Figure 59). By contrast, UBR4 deficiency did not affect K63-ubiquitylation of RGS4 (Figure 60, lanes 4 vs. 3) but abolished its K27-ubiquitylation (Figure 61). Consistently, *UBR4*$^{-/-}$ MEFs under oxidative stress failed to target RGS4 to p62^{+} autophagic membranes, which otherwise would form RGS4^{+}p62^{+} cytosolic puncta (Figure 45A, 45B, 62, 63). As a consequence, lysosomal degradation of Nt-Cys substrates was disrupted in *UBR4*$^{-/-}$ MEFs (Figure 64A, 64B) as well as UBR4 knockdown cells (Figure 65). Thus, UBR4 is essential for the assembly of K27-linked Ub chains on K63-ubiquitylated Nt-Cys proteins.

Next, I determined whether UBR4 acts as an N-recognin that directly binds the Arg-CysO_3 N-degron of Nt-Cys. In pulldown analyses, UBR4 did not bind Nt-CysO_3 carrying RGS4 peptides (Figure 66). Instead, UBR4 bound KCMF1 to form a complex (Figure 67) suggesting that KCMF1 serves as a scaffold on which UBR4 K27-ubiquitylates Nt-Cys substrates without a direct interaction.

p62 recognizes K63/K27-linked Ub chains to target Cys/N-degron substrates to macroautophagy

I investigated how ubiquitylated Cys/N-degron substrates are delivered to autophagy. Loss-of-function analyses of candidate proteins revealed that the autophagy receptor p62 is critical for autophagic targeting (Figure 68) and degradation (Figure 69) of RGS4. Mapping analyses using p62 fragments showed that UBA (Figure 70) domain-lacking p62 mutant (ΔUBA) could not bind Nt-Cys-RGS4 (Figure 71). Given our earlier finding that p62 is an autophagic N-recognin that binds the Nt-Arg (47, 48), these results suggest that both the Arg-$CysO_3$ and K63/K27-linked Ub chains may synergistically facilitate interaction between p62 and RGS4. This is in direct contrast to non-Cys Arg/N-degron substrates such as RD-$CDC6^{FLAG}$ (Figure 72) that bind p62 solely via their ZZ domains (77). I therefore determined whether p62 is essential for targeting Nt-Cys proteins to autophagic membranes. In immunostaining analyses, RGS4 failed to form autophagic puncta in p62 knockdown SH-SY5Y cells as well as *p62*$^{-/-}$ MEFs expressing $p62^{\Delta UBA}$-MYC (Figure 68, 73). These results suggest that p62 delivers K63/K27-ubiquitylated RGS4 to autophagic membranes via UBA domain.

I have previous developed a chemical mimicry (YOK-1104; Figure 74) of the Arg N-degron that binds to ZZ domain of the p62 and conformationally and functionally activates p62 as an autophagic receptor (48). To test whether the Arg-$CysO_3$ activates p62 in targeting Nt-Cys proteins to autophagy, cells were treated with YOK-1104. Indeed, YOK-1104 facilitated the co-targeting of RGS4 and p62 to autophagy under oxidative stress, leading to the formation of $RGS4^{+}p62^{+}$ puncta and their lysosomal degradation (Figure 75). In contrast, YOK-1104 did not alter KCMF1 mediated K63-ubiquitylation status of RGS4 (Figure 76). These results suggest that the Arg-$CysO_3$ binds p62 and facilitates co-degradation of p62 in complex with oxidized and ubiquitylated RGS4 via autophagy.

The Cys/N-degron pathway is required for cellular homeostasis in response to oxidative stress and chronic hypoxia

To determine the role of the Cys/N-degron pathway in cellular responses to oxidative stress, I monitored signaling pathways in cells challenged with tBHP. Chemical inhibition of Nt-arginylation using tannic acid significantly impaired the transcriptional activation of oxidative stress-responsive proteins, including SOD1, TGF-β, iNOS and COX2 (Figure 77A, 77B). Consistently, tannic acid rendered cells hypersensitive to $CoCl_2$-induced oxidative stress, leading to apoptosis as evidenced by the cleavage of caspase-3 and PARP (Figure 78). Next, I investigated whether the KCMF1-UBR4 circuit is also required for cellular responses to oxidative stress. Indeed, siRNA-mediated knockdown of either *KCMF1* or *UBR4* retarded the nuclear translocation of a set of transcription factors sensitive to oxidative stress including NRF2, p-p65 and HIF-1α (Figure 79). Such an impairment was associated with hypersensitivity to ROS-induced ER stress (Figure 80). Given the results with oxidative stress, I also performed analogous assays in cells under chronic hypoxia. A similar impairment in the transcription of iNOS, GPX3, SOD1, and TGF-β was observed when ATE1 was depleted using siRNA (Figure 81A) or inactivated using tannic acid (Figure 81B). These results suggest that the Cys/N-degron pathway is required for cellular responses to oxidative stress.

The homeostasis of the Nt-$CysO_3$ proteome is maintained by mitochondrial quality control

To further characterize the protective role of the Cys/N-degron pathway in the pathogenesis driven by oxidative stress, SH-SY5Y cells were treated with 6-hydroxydopamine (6-OHDA), a known oxidative stressor that induces mitochondrial damage leading to death of dopaminergic neurons and followed by development of Parkinsonism (78). When monitored using immunocytochemistry analyses, ATE1 knockdown cells exhibited drastically increased mitochondrial fragmentation in response to 6-OHDA treatment, resulting in apoptotic cell death (Figure 82A, 82B). A similar degree of mitochondrial fragmentation and apoptosis was observed in cells deficient in

KCMF1 or UBR4 (Figure 82A, 82C). These results highlight the importance of the Cys/N-degron pathway in cellular homeostasis in response to oxidative stress. Moreover, while RGS4 overexpression promoted apoptosis under the same condition (Figure 83), These results imply that the overload (due to increased synthesis or inhibited degradation) of non-arginylated and thus non-degradable Cys/N-degron substrates beyond autophagic capacity of the ATE1-KCMF1-UBR4 circuit induces hypersensitivity to oxidative stress-induced mitochondrial fragmentation and apoptosis.

I next characterized the mechanisms by which overload of Cys/N-degron substrates hypersensitizes cells to oxidative stress. It is known that excessive mitochondrial import of cytotoxic protein cargoes beyond mitochondrial capacity can induce their fragmentation and subsequent programmed cell death (79). I therefore hypothesized that non-arginylated and non-degraded Cys/N-degron substrates might translocate to within the mitochondria and cripple mitochondrial proteostasis. Subcellular fractionation, immunocytochemistry and immunoblotting assays with oxidative stressors including 6-OHDA showed that non-arginylated/ubiquitinated and non-degradable Nt-Cys proteins are indeed imported from the cytosol to the mitochondria and sequestered within (Figure 84, 85A, 85B, 85C, 86), at least partly due to TOM70-mediated transport/import (Figure 87A, 87B). On the other hand, C-terminal fragments of cytosolic CDC6 carrying the Nt-Asp degron accumulated only in the cytosol (Figure 88). These results indicate that the homeostasis of the Nt-CysO3 proteome is maintained by mitochondrial quality control, possibly via MAGIC (mitochondria as a guardian in cytosol) (80).

To obtain the pharmaceutical means to protect cells from oxidative stress, cells challenged with 6-OHDA were treated with YOK-1104, the p62 activating ligand (47, 48). The chemical activation of p62 ZZ domain stimulated p62-associated autophagic degradation of Cys/N-degron substrates (Figure 89) and rescued cells from mitochondrial

fragmentation and apoptosis (Figure 90A, 90B). The cytoprotective efficacy was abolished when either macroautophagy or UBR4 was inactivated (Figure 91), indicating that the recognition of ubiquitinated Cys/N-degron substrates by p62 is the final autophagic delivery determinant in the KCMF1-UBR4 circuit (Figure92). These results suggest that the activation of ATE1-KCMF1-UBR4-p62 circuit could be a therapeutic target in the pathogenesis driven by oxidative stress.

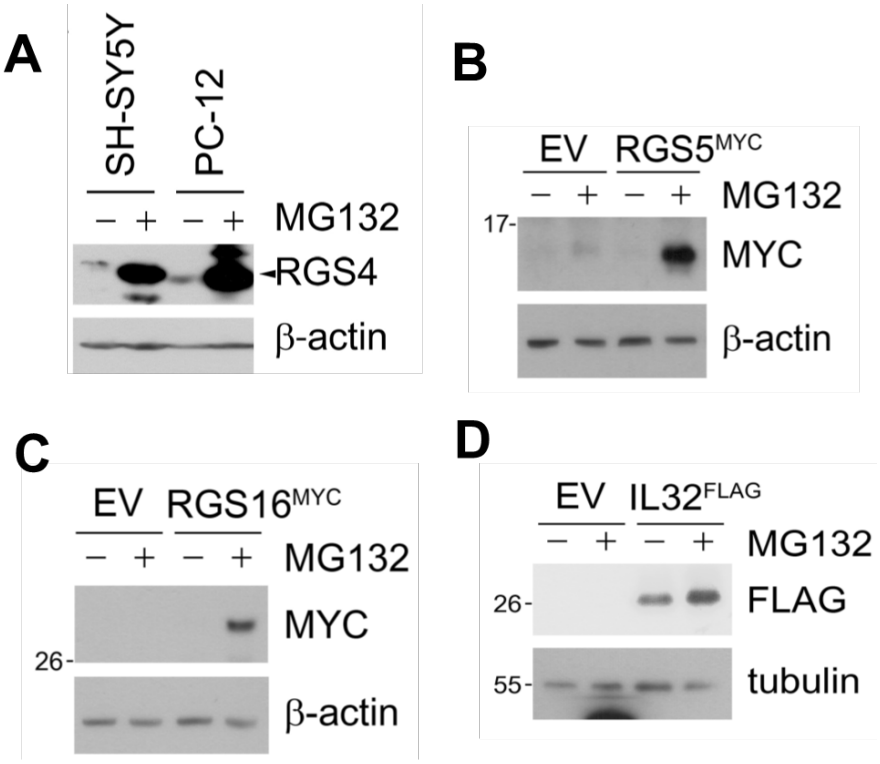

Figure 5. Nt-Cys bearing proteins are degraded via 26S proteasome. (A) WB of endogeneous RGS4 in SH-SY5Y and PC-12 cells treated with MG132 (10 μM, 6 h). (**B,C,D**) WB of $RGS5^{MYC}$, $RGS16^{MYC}$ and $IL32^{FLAG}$-overexpressing HEK293T cells treated with MG132 (10 μM, 6 h).

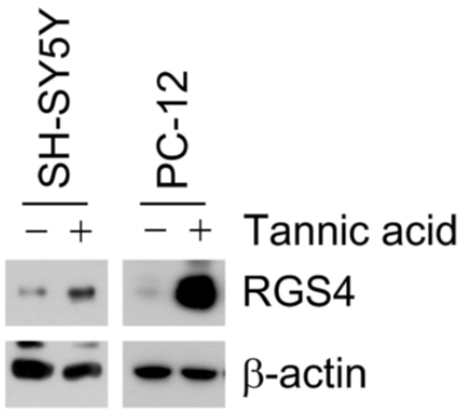

Figure 6. Nt-Cys possessing proteins are Arg/N-degron substrates. WB of endogeneous RGS4 in SH-SY5Y and PC-12 cells treated with tannic acid (35 μM, 24 h).

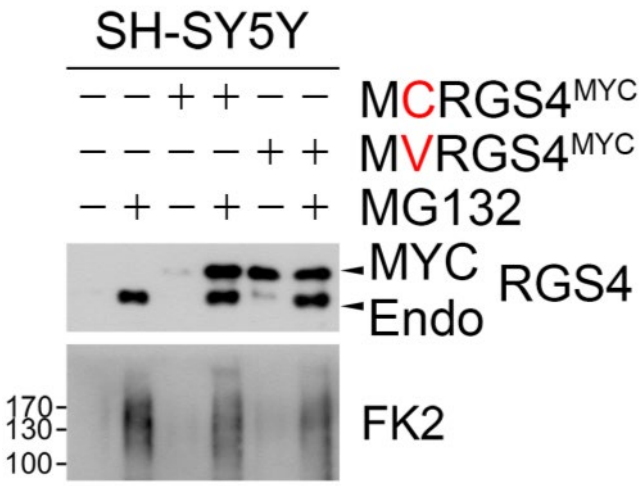

Figure 7. Cys/N-degron proteins undergo proteasomal degradation in Nt-Cys dependent manner. WB of RGS4 in SH-SY5Y expressing WT or C2V RGS4^{MYC} treated with MG132 (10 μM, 6 h).

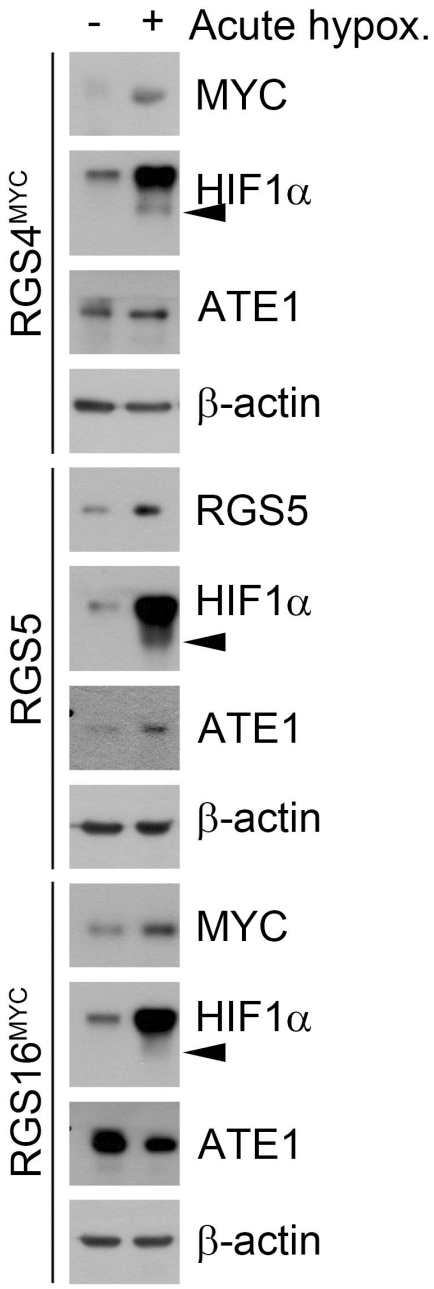

Figure 8. Cys/N-degron proteins are stabilized under acute hypoxia. WB of $RGS4^{MYC}$, $RGS5^{MYC}$, and $RGS16^{MYC}$ -overexpressing HEK293T cells exposed to acute hypoxia (1% O_2, 6 h).

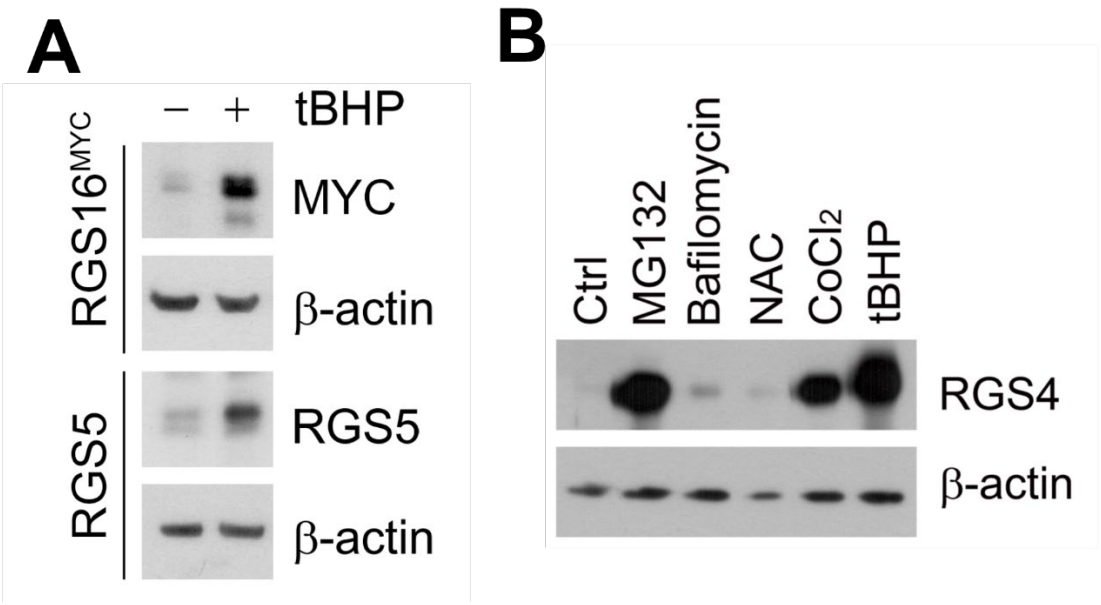

Figure 9. Cys/N-degron proteins are stabilized under oxidative stress. (A) WB of 293T cells expressing RGS5 or $RGS16^{MYC}$ and treated with 6h tBHP (250 μM, 6 h). **(B)** WB of RGS4 in SH-SY5Y cells treated with a combination of MG132 (10 μM), BAF (200 nM), NAC (0.5 mM), $CoCl_2$ (250 μM) and tBHP (250 μM) for 6h.

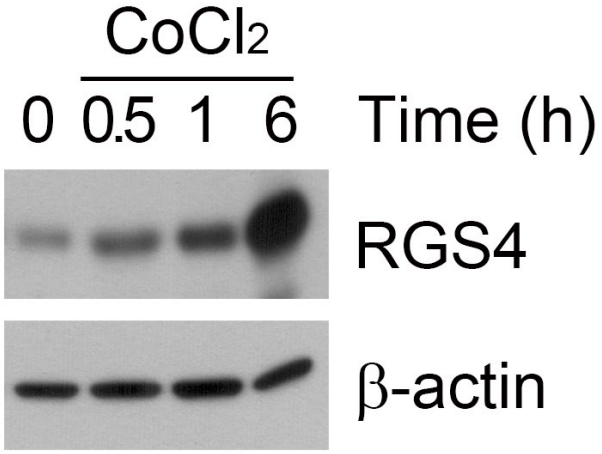

Figure 10. Cys/N-degron proteins undergo protein level stabilization as early as 0.5 h upon exposure to oxidative stress. WB of SH-SY5Y cells treated with $CoCl_2$ (250 μM) for indicated time.

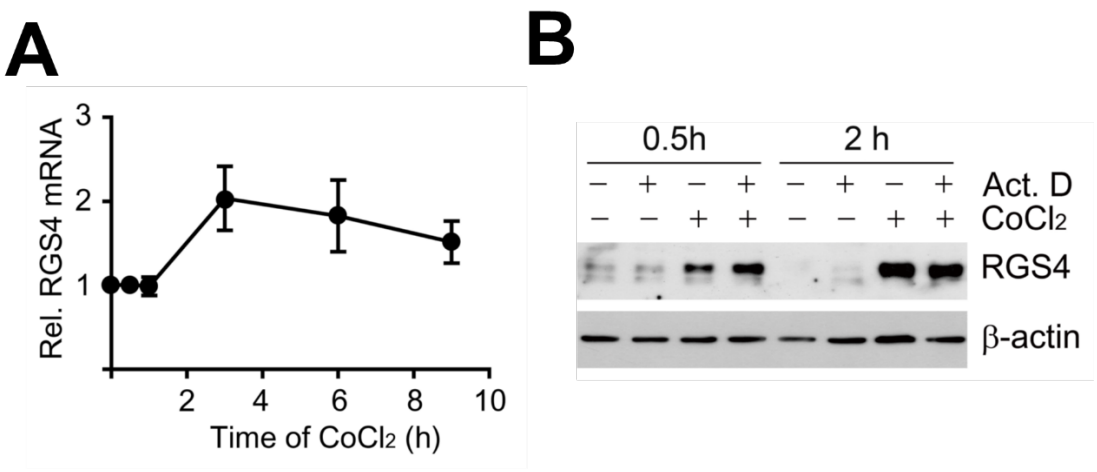

Figure 11. Cys/N-degron proteins undergo protein level stabilization under oxidative stress independent of transcriptional upregulation. (A) Relative RGS4 mRNA levels in SH-SY5Y cells treated with $CoCl_2$ (250 μM) at the indicated time points **(B)** WB of RGS4 in SH-SY5Y cells treated with actinomycin D (5 nM) and $CoCl_2$ (250 μM).

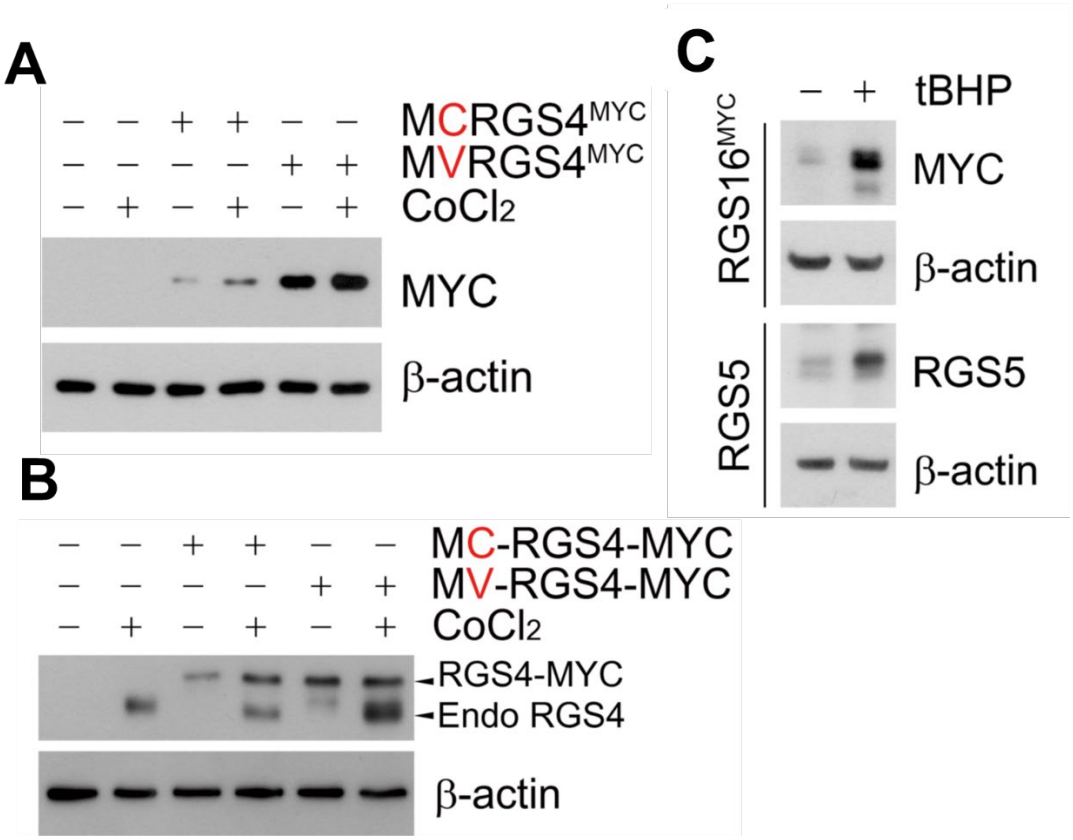

Figure 12. Oxidative stress induced cysteine dependent stabilization of Cys/N-degron protein. (A, B) WB of ectopically expressing WT and C2V-RGS4 in 293T cells treated with $CoCl_2$ (250 μM, 6 h) immunoblotted with **(A)** anti-MYC antibody or **(B)** anti-RGS4 antibody. (C) WB of 293T cells expressing $RGS16^{MYC}$ or RGS5 treated with tBHP (250 μM, 6 h).

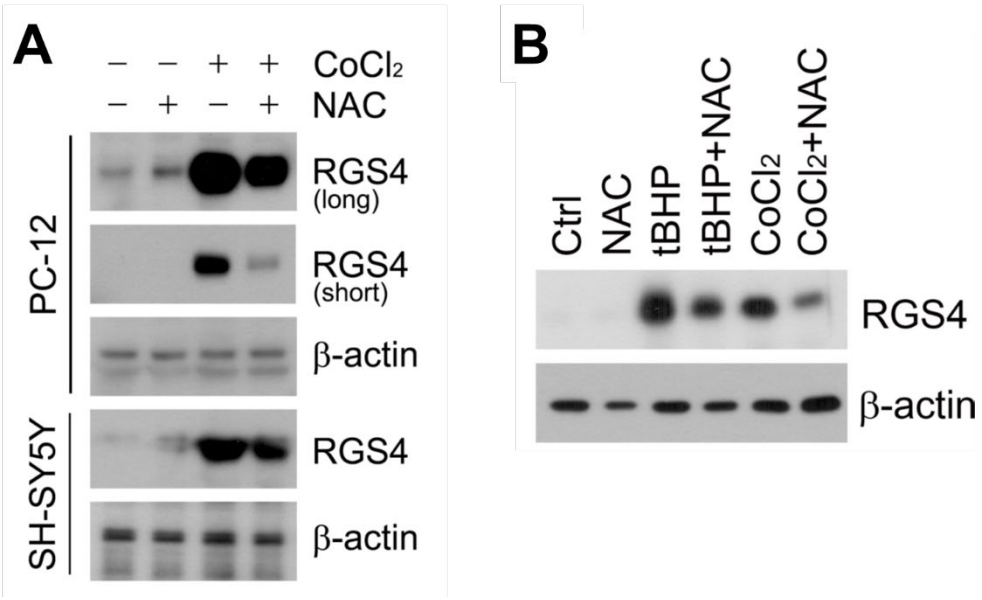

Figure 13. Oxidative stress induced Cys/N-degron substrate stabilization is rescued by ROS scavenger treatment. (A) SH-SY5Y cells were treated with $CoCl_2$ and NAC (0.5 mM) for 6h and immunoblotted. **(B)** WB of RGS4 in SH-SY5Y cells treated with a combination of NAC (0.5 mM), $CoCl_2$ (250 μM) and tBHP (250 μM) for 6h.

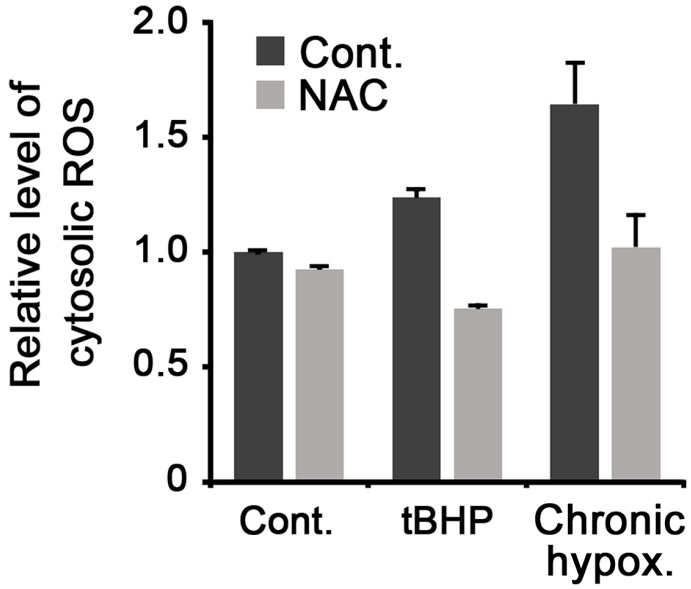

Figure 14. tBHP and chronic hypoxia generate cytosolic ROS. relative cytosolic ROS level measured upon exposure to tBHP (250 μM, 6 h) under chronic hypoxia (1% O_2, 48h) with combination treatment of NAC (0.5 mM) on 293T cells.

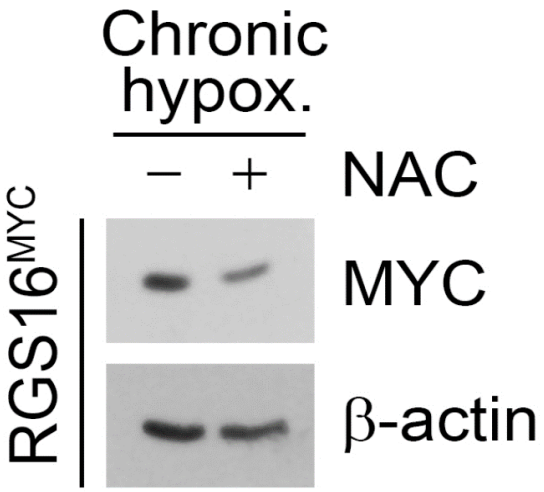

Figure 15. chronic hypoxia induced Nt-Cys protein stabilization is rescued by ROS scavenger treatment. WB of 293T cells expressing $RGS16^{MYC}$ and exposed to chronic hypoxia (1% O_2 ,48 h).

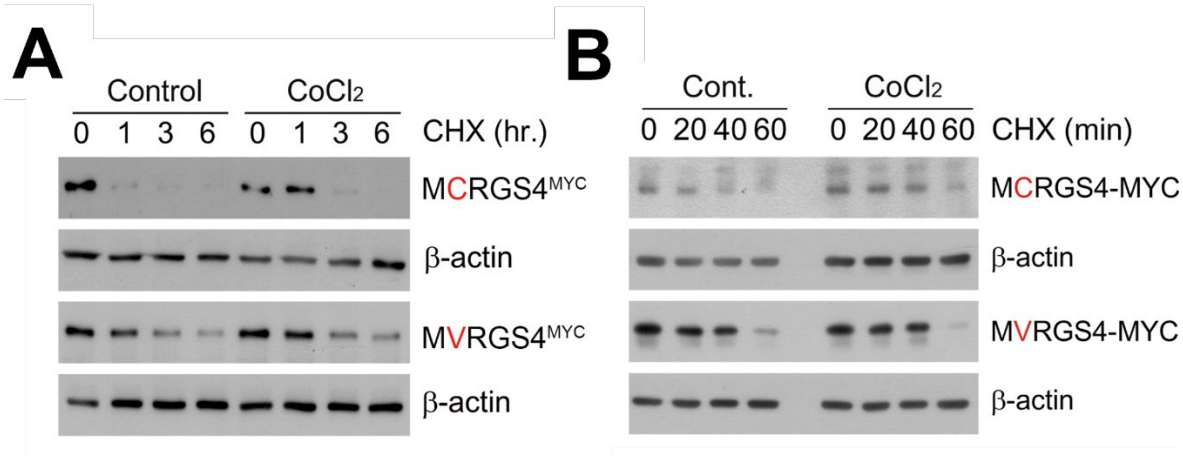

Figure 16. Oxidative stress increased half-life of the Cys/N-degron substrate protein. **(A, B)** CHX chase assay in HEK293T cells expressing WT or C2V RGS4-MYC and treated with $CoCl_2$ (250 μM) for indicated time points.

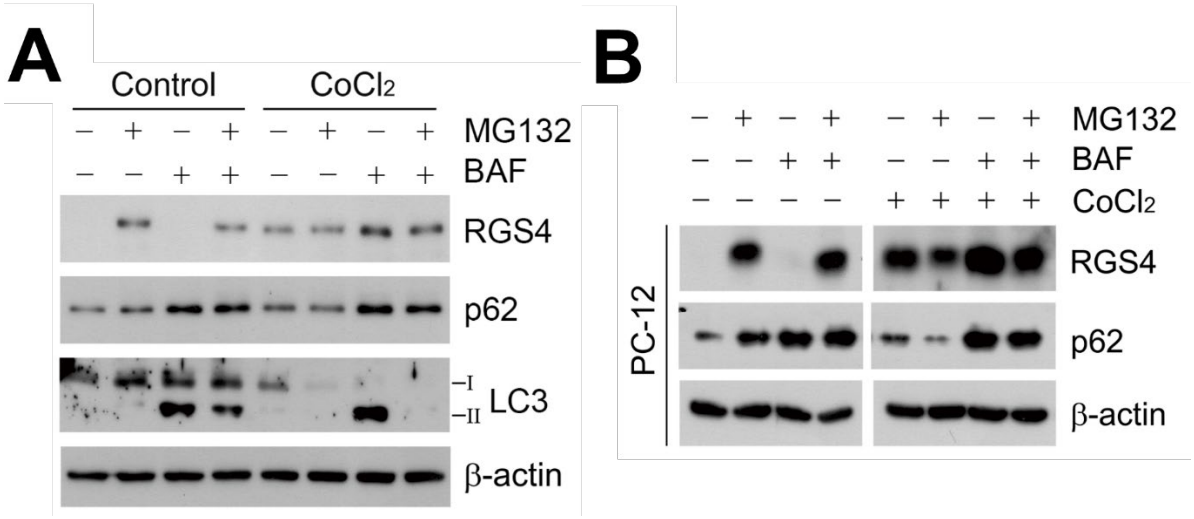

Figure 17. Oxidative stress re-routed RGS4 to autophagic degradation. WB of RGS4 treated with $CoCl_2$ WB of endogeneous RGS4 with combination of MG132 (10 μM, 6 hr), BAF (200nM, 6 hr), and $CoCl_2$ (250 μM) treatment for 6h in (**A**) SH-SY5Y cells and (**B**) PC-12 cells.

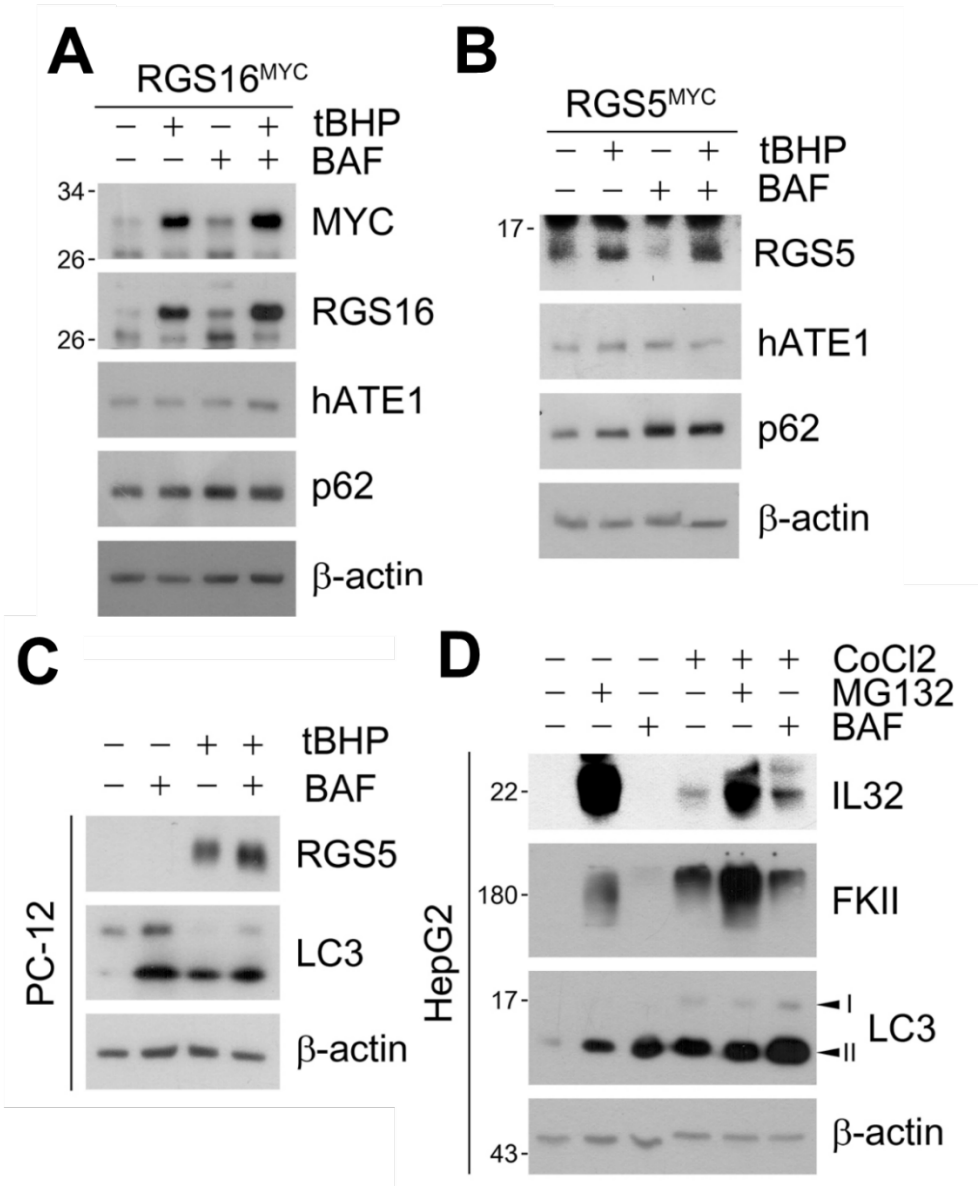

Figure 18. Oxidative stress re-routed Cys/N-degron substrate proteins to autophagic degradation. (**A,B**) WB of $RGS16^{MYC}$ (**A**) or $RGS5^{MYC}$ (**B**) overexpressed 293T cells treated with tBHP (250 μM, 6 h), BAF (200 nM, 6 hr) or both. **(C)** WB of PC-12 cells treated with combination of BAF (200nM, 6 hr) and tBHP (250 μM) treatment for 6h. (**D**) WB of HepG2 cells treated with combination of MG132 (10 μM, 6 hr), BAF (200nM, 6 hr), and $CoCl_2$ (250 μM) treatment for 6 hr.

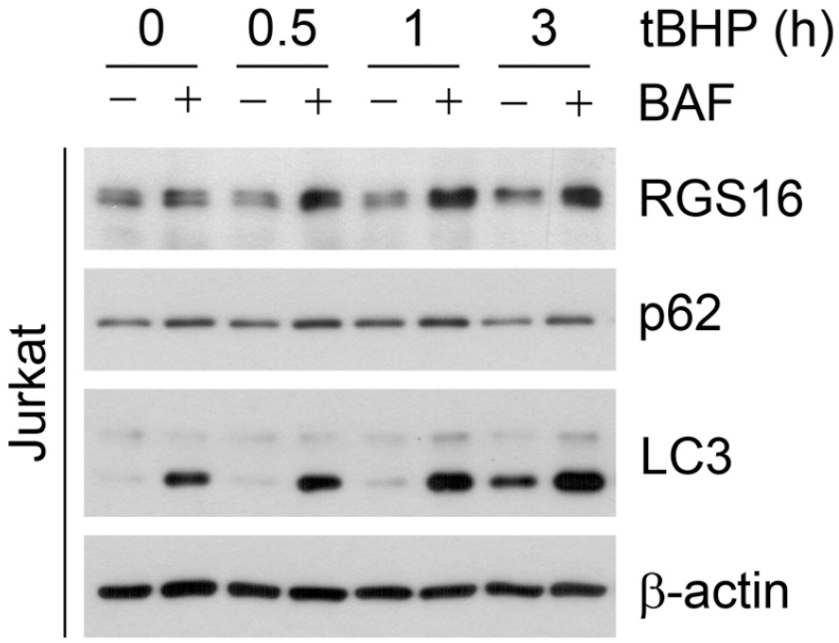

Figure 19. Oxidative stress swiftly re-routed Cys/N-degron substrate proteins to autophagic degradation. WB of endogeneous RGS16 in Jurkat cells treated with tBHP (250 μM) and BAF (200 nM, 6 h) for indicated time.

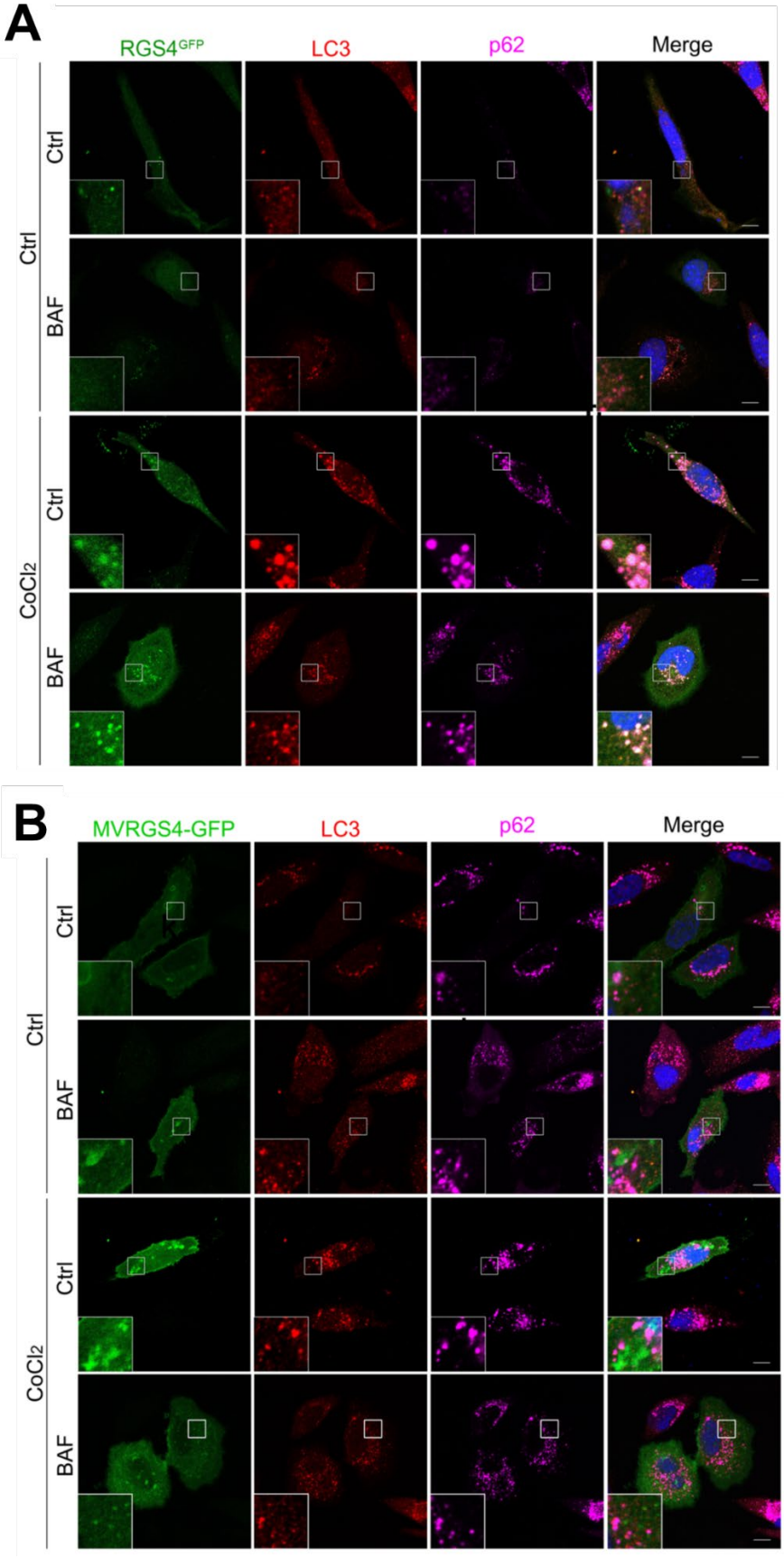

Figure 20. Under oxidative stress, RGS4 is targeted to autophagy with Nt-Cys dependent manner. Co-localization assay of the GFP, p62 and LC3 puncta in RGS4-GFP expressing HeLa cells treated with 6h BAF (200 nM, 6h), $CoCl_2$, or both. Scale bar, 10 μm.

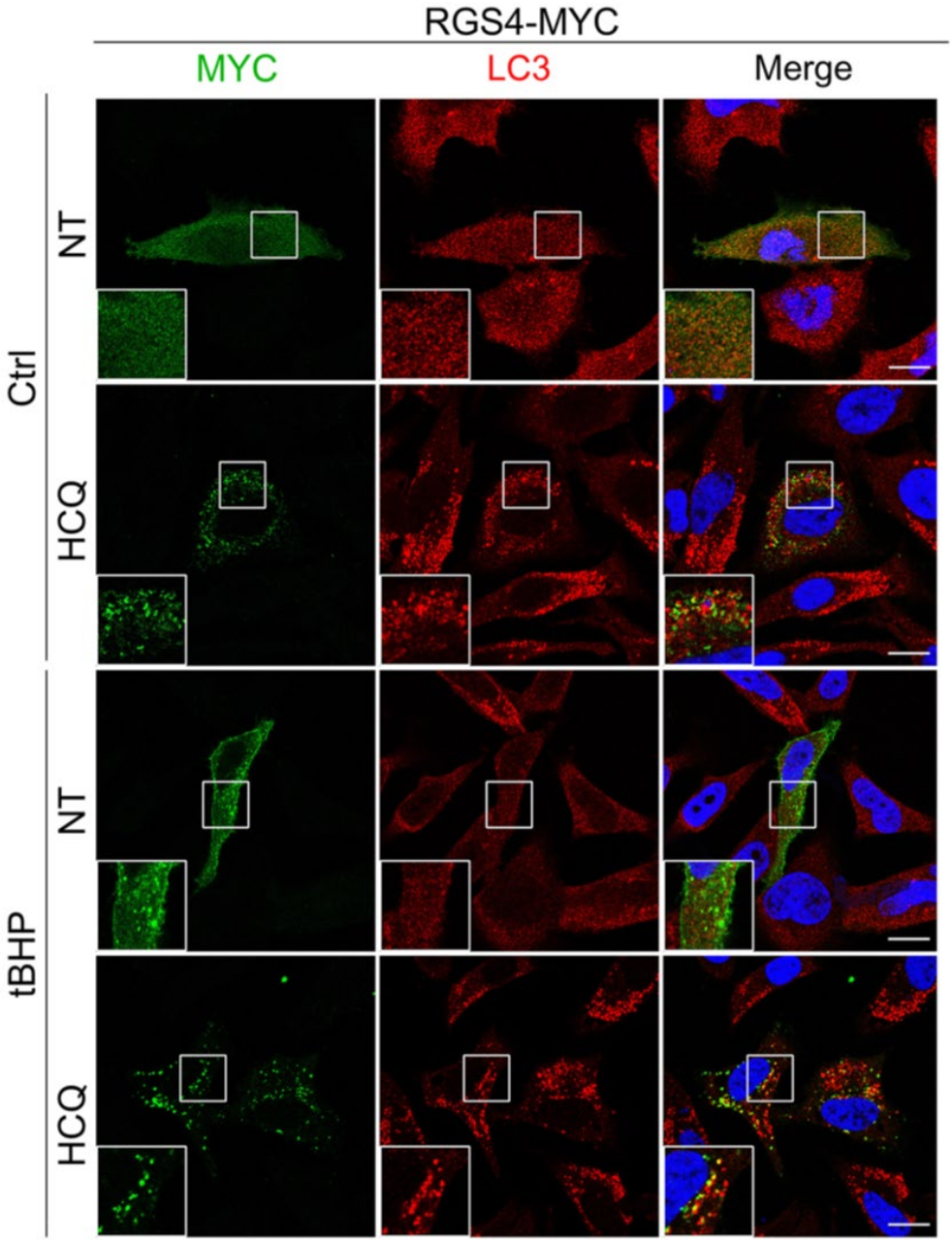

Figure 21. Under oxidative stress, RGS4 is targeted to autophagy. (**A**) Co-localization assay of the MYC and LC3 puncta in RGS4^{MYC} expressing HeLa cells treated with HCQ (25 nM, 6h) with tBHP (250 µM, 6 h). Scale bar, 10 µm

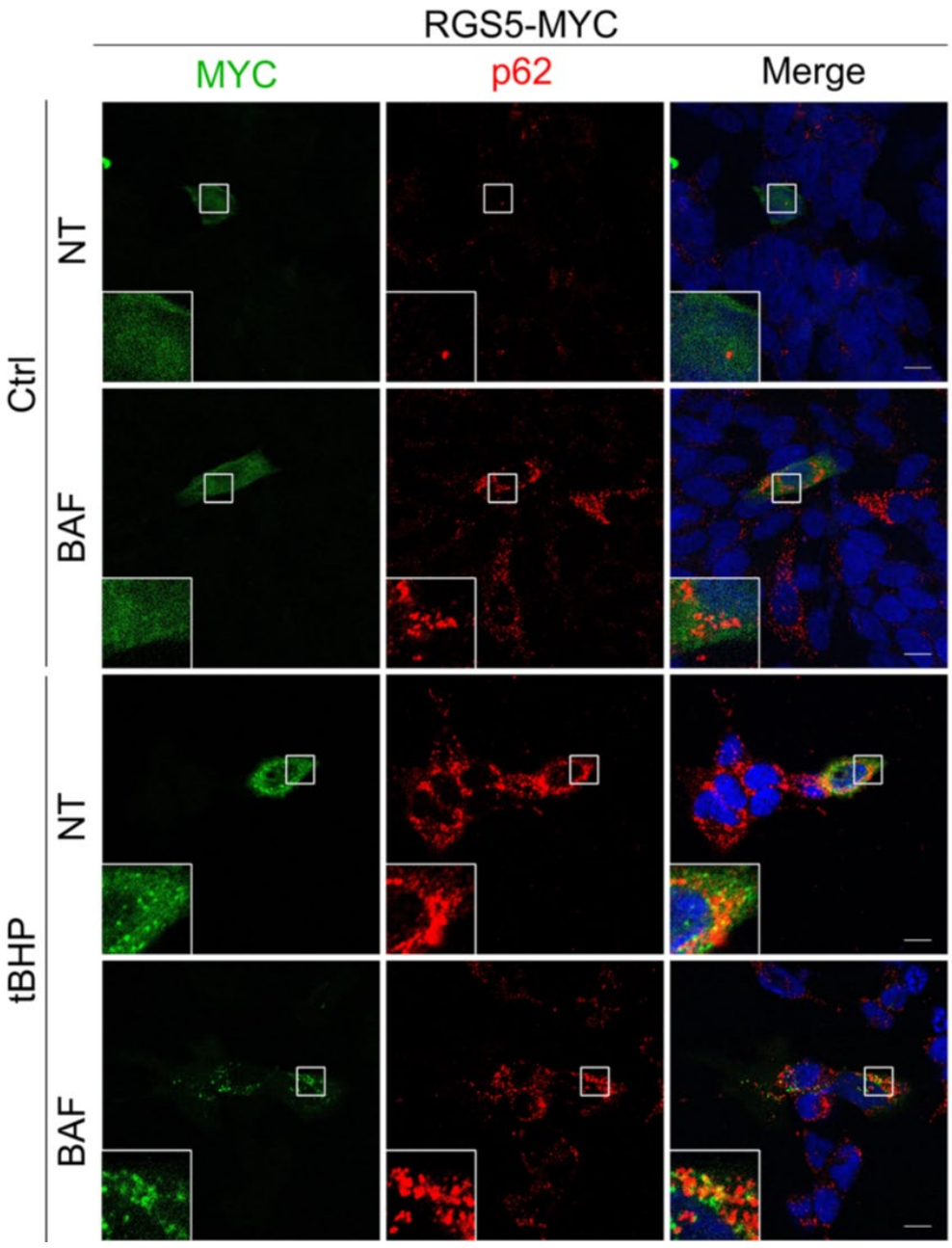

Figure 22. Under oxidative stress, RGS5 is targeted to autophagy. Co-localization assay of the MYC and p62 puncta in RGS5^{MYC} expressing HeLa cells treated with 6h BAF (200 nM, 6h), tBHP (250 μM, 6 h) or both. Scale bar, 10 μm.

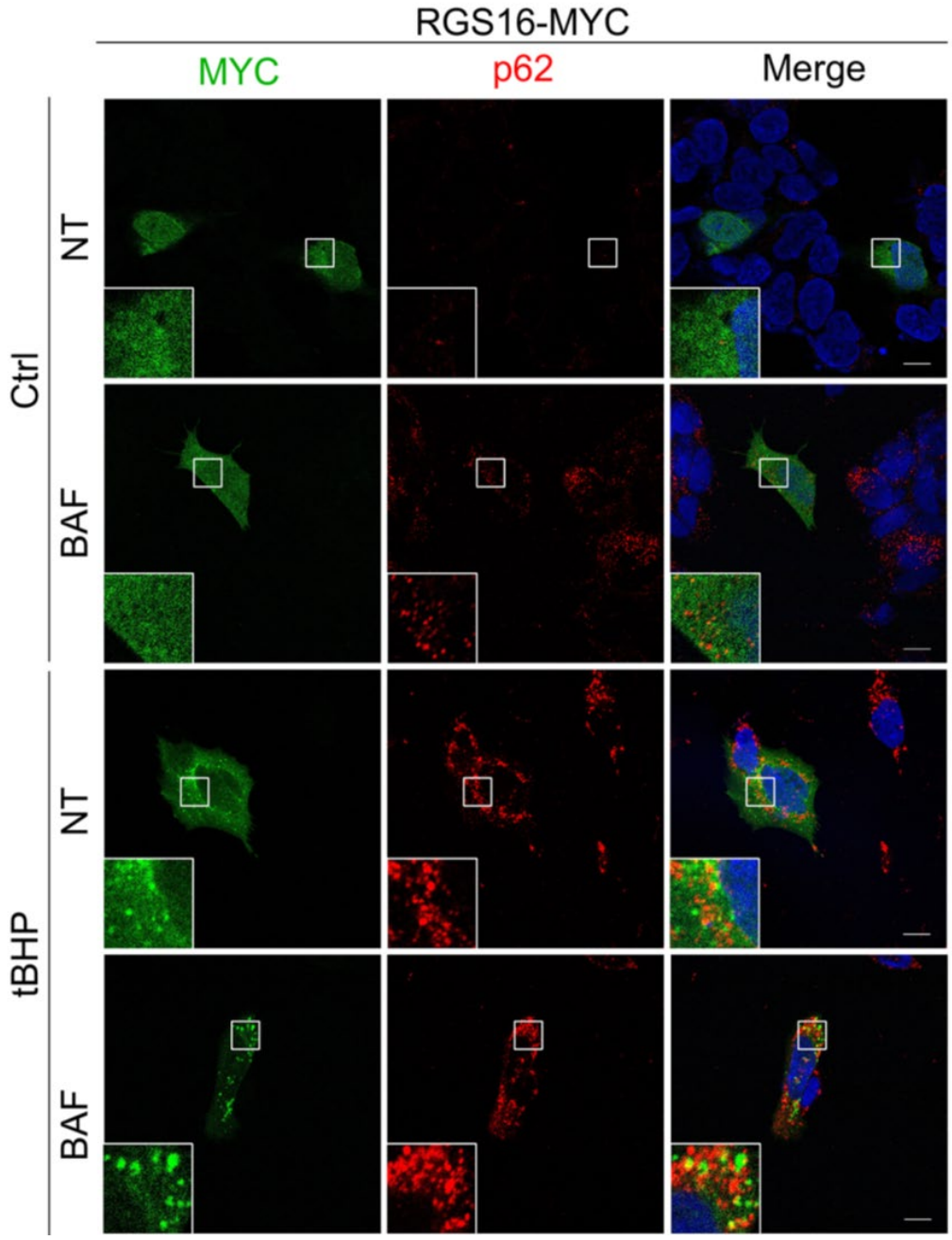

Figure 23. Under oxidative stress, RGS16 is targeted to autophagy. Co-localization assay of the MYC and p62 puncta in RGS16^{MYC} expressing HeLa cells treated with 6h BAF (200 nM, 6h), tBHP (250 μM, 6 h) or both. Scale bar, 10 μm.

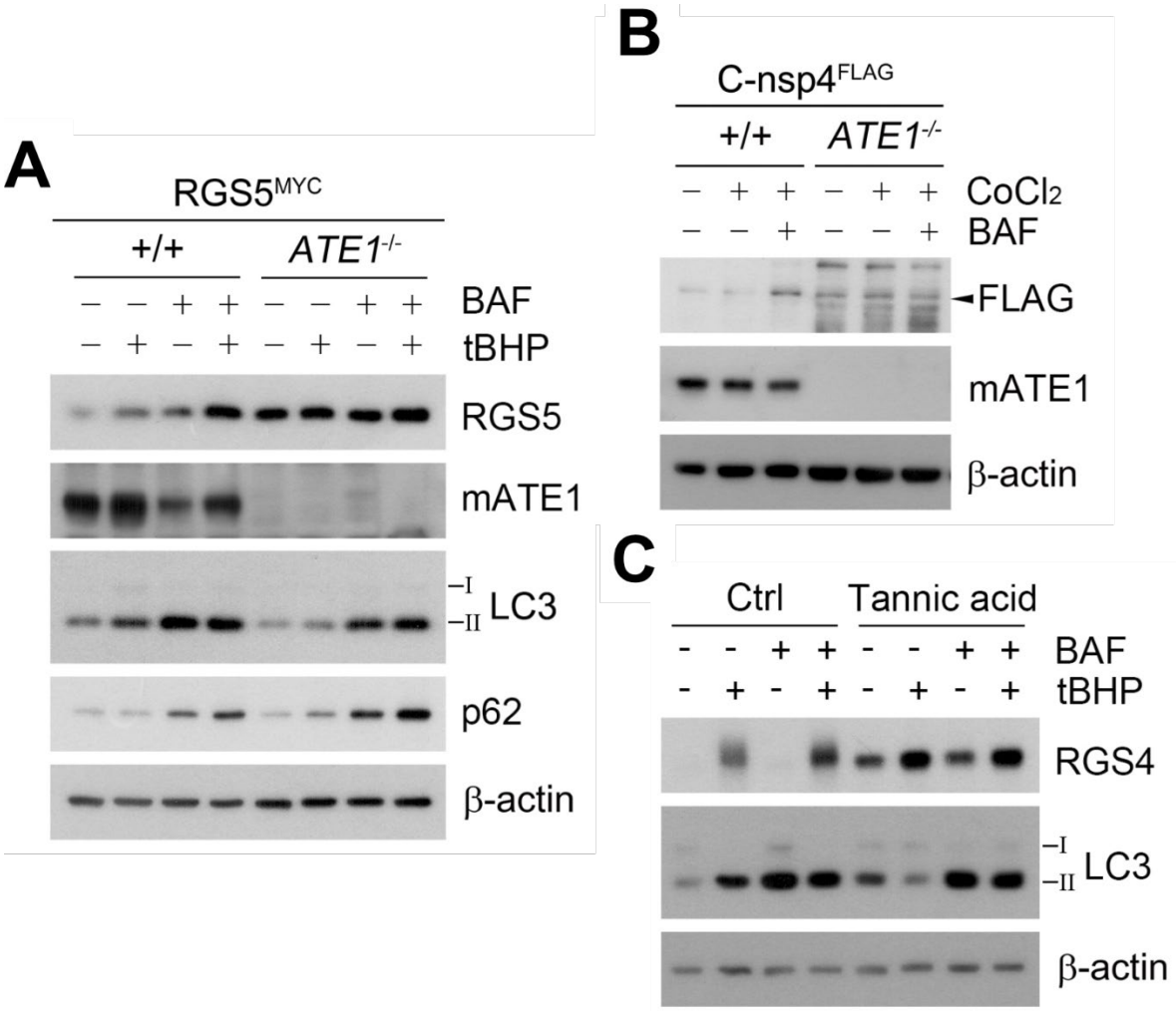

Figure 24. Oxidative stress induced autophagic degradation of the Cys/N-degron substrates are determined by ATE1 function. (**A,B**) WB of RGS5^{MYC} (**A**) or C-nsp4^{FLAG} (**B**) overexpressed +/+ and ATE1$^{-/-}$ MEF cells treated with tBHP (250 μM, 6 h), BAF (200 nM, 6 h) or both. **(C)** WB of SH-SY5Y cells treated with combination of tannic acid (35μM, 24 h), BAF (200nM, 6 h) and tBHP (250 μM, 6 h) treatment.

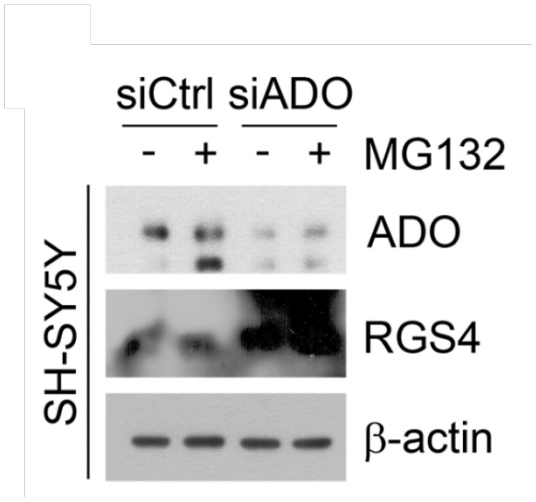

Figure 25. ADO1 is responsible for proteasomal degradation of Nt-Cys substrates. WB of SH-SY5Y cells under *ADO1* interference (20 nM, 48 h) treated with MG132 (10 μM, 6h).

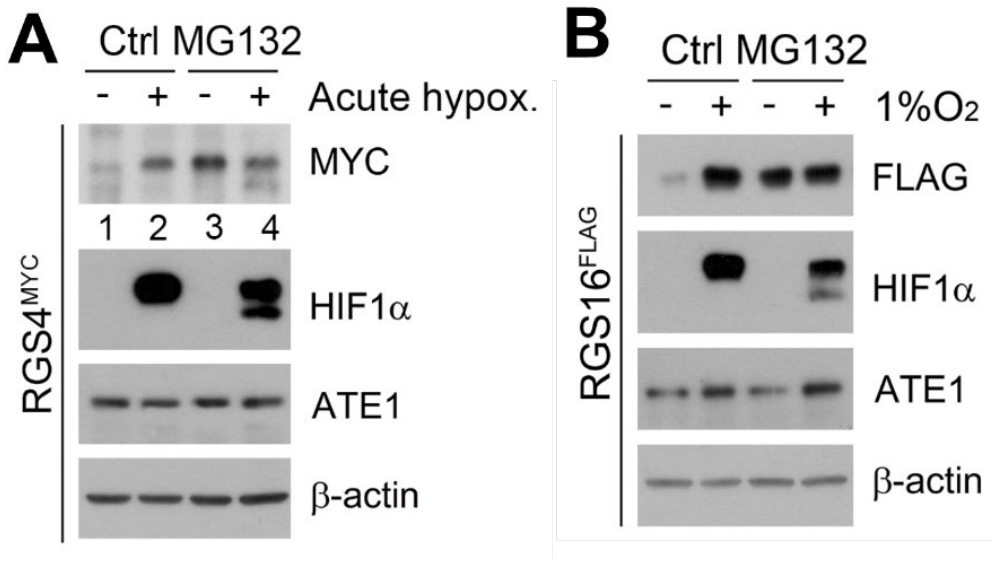

Figure 26. Acute hypoxia obstructs proteasomal degradation of Nt-Cys substrates. (**A,B**) WB of 293T cells expressing $RGS4^{MYC}$ (**A**) or $RGS16^{FLAG}$ (**B**) and exposed to acute hypoxia (1% O_2, 6 h) and MG132 (10 μM, 6 h).

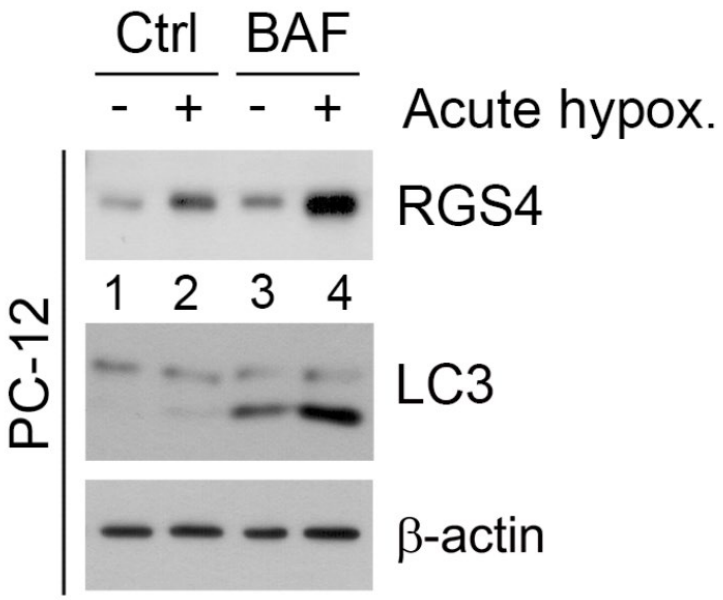

Figure 27. Chronic hypoxia induces autophagic degradation of Nt-Cys substrates. WB of SH-SY5Y cells exposed to chronic hypoxia (1% O_2, 24 h) treated with BAF (200 nM, 6h).

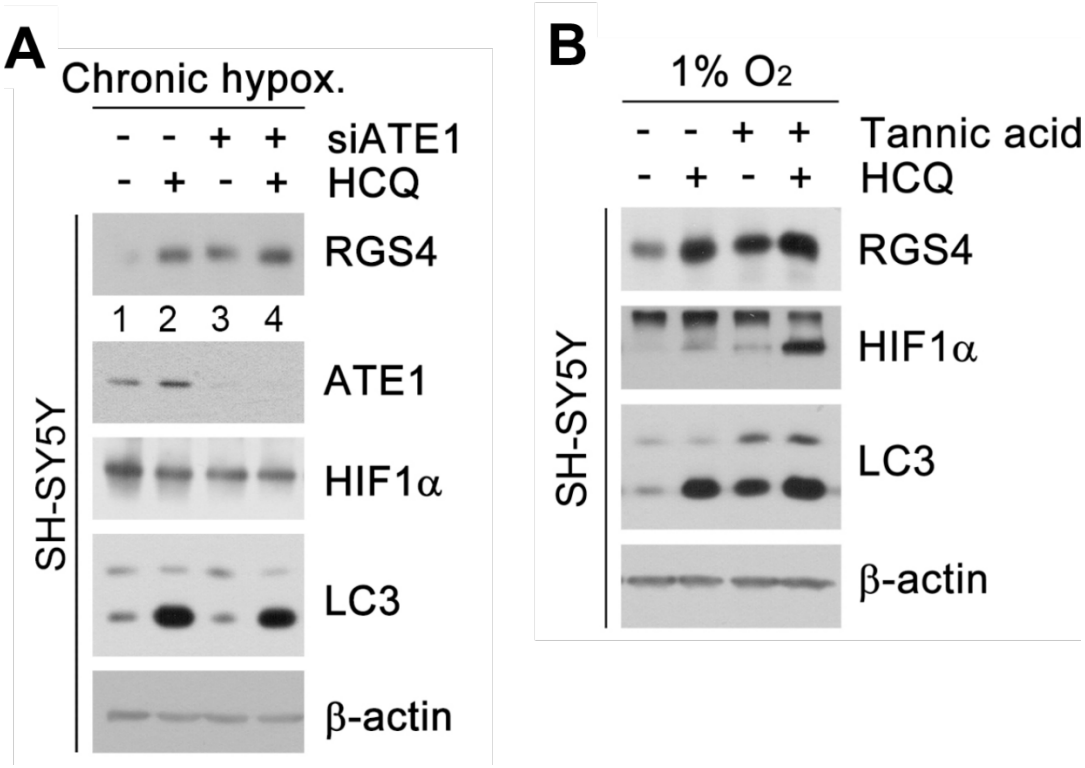

Figure 28. Chronic hypoxia induces autophagic degradation of Nt-Cys substrates via ATE1 mediated arginylation. (A) WB of SH-SY5Y cells with si*ATE1* (40 nM, 48 h) and exposure to chronic hypoxia(1% O_2, 24h) and HCQ (25 nM) for 24h. **(B)** WB of SH-SY5Y cells with tannic acid (35 μM, 24 h) and exposure to chronic hypoxia(1% O_2, 24h) and HCQ (25 nM) for 24h.

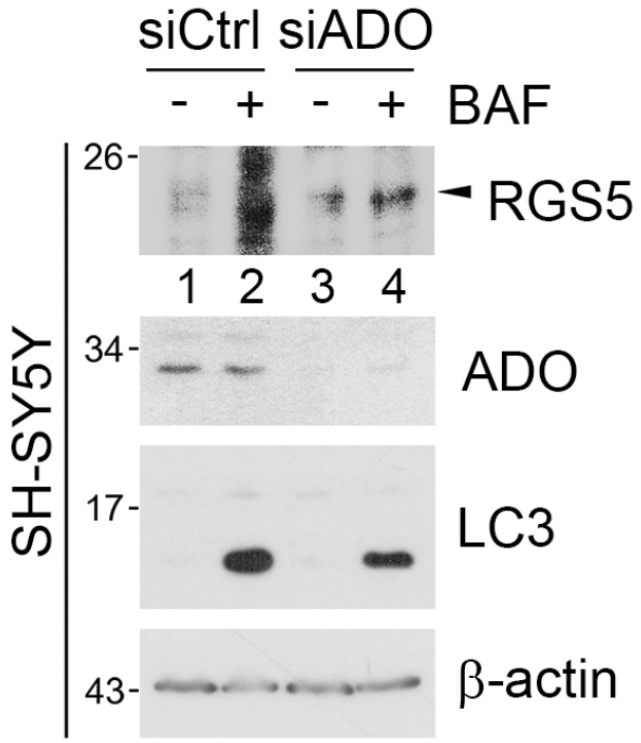

Figure 29. Chronic hypoxia induced autophagic degradation of Nt-Cys substrates is independent of ADO1 activity. WB of SH-SY5Y cells under *ADO1* interference (20 nM, 48 h) treated with BAF (20 nM, 6h).

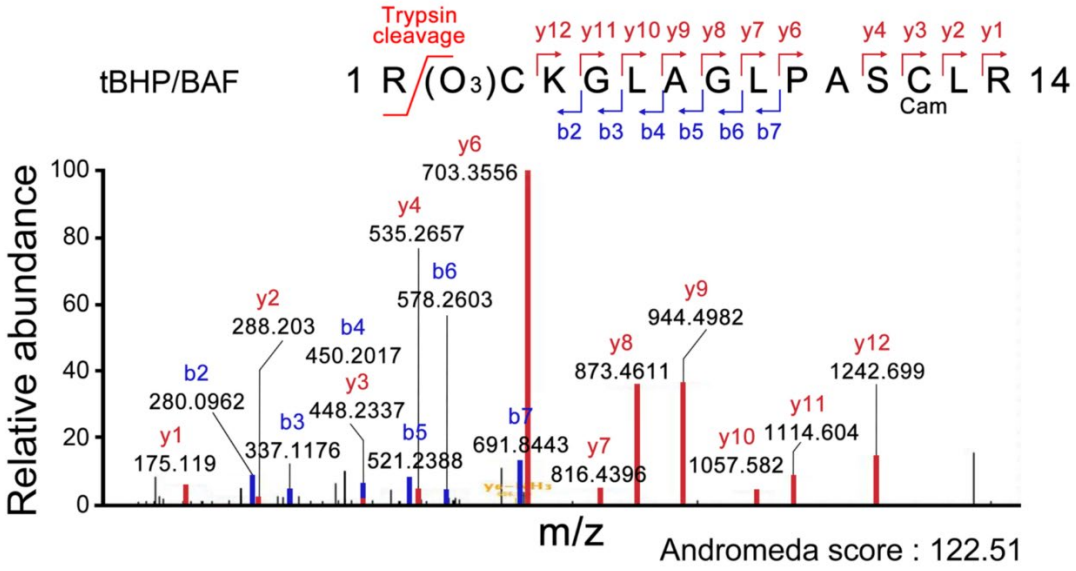

Figure 30. Nt-Cys is modified into $CysO_3$ under oxidative stress. LC/MS spectrum of $CysO_3$ containing peptide from immunoprecipitated RGS4 sample harvested from HEK293T cells expressing $RGS4^{MYC}$ with co-treatment of tBHP (250 μM, 6 h) and BAF (200 nM, 6 h). The sequence contains the Nt-Arg which is expected to be cleaved off during trypsin digestion.

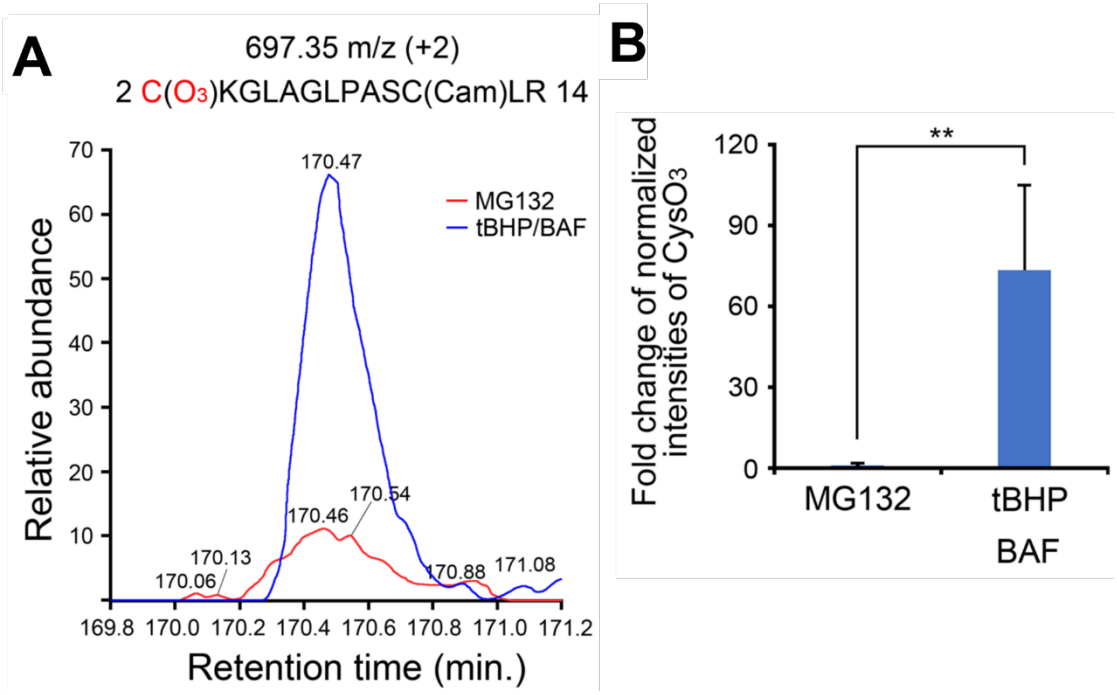

Figure 31. Nt-CysO$_3$ formation is drastically increased under oxidative stress. (A, B) LC/MS mass spectrometry assay of HEK293T cells expressing RGS4^{MYC} and treated with tBHP (250 μM, 6 h) and BAF (200 nM, 6 h) or MG132 (10 μM, 6 h), shown in XIC graph **(A)** and bar graph **(B)** reflecting relative fold change of the normalized intensity of CysO$_3$ containing peptide purified from MG132 (10 μM, 6h) and tBHP and BAF co-treated samples.

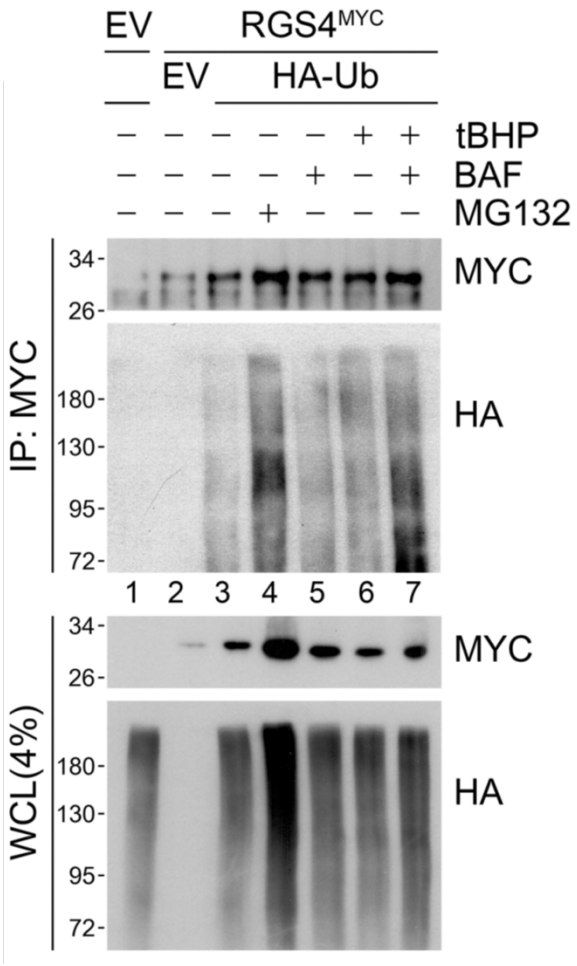

Figure 32. Oxidative stress induced autophagic degradation of Nt-Cys substrate is ubiquitylated. Denaturation IP of RGS4^{MYC} and HA-Ub expressing HEK293T cells treated with a combination of BAF (200 nM), tBHP (250 μM), MG132 (10 μM) for 6 h.

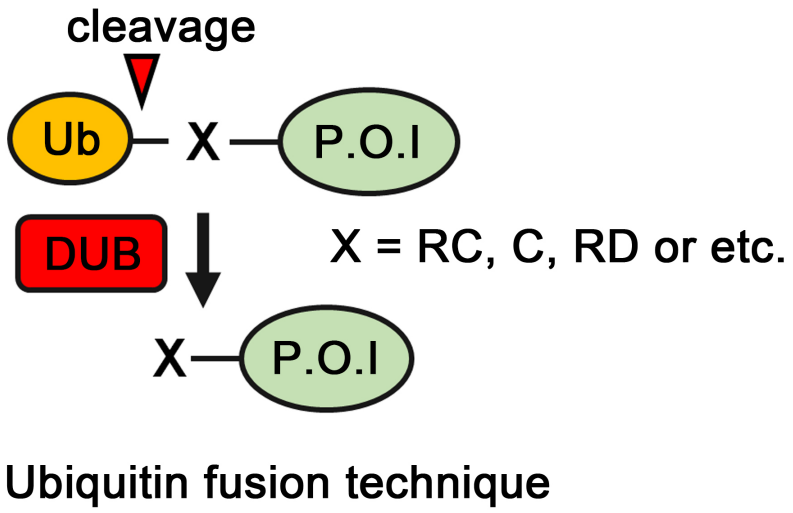

Figure 33. Graphical demonstration of the ubiquitin fusion technique (UFT).

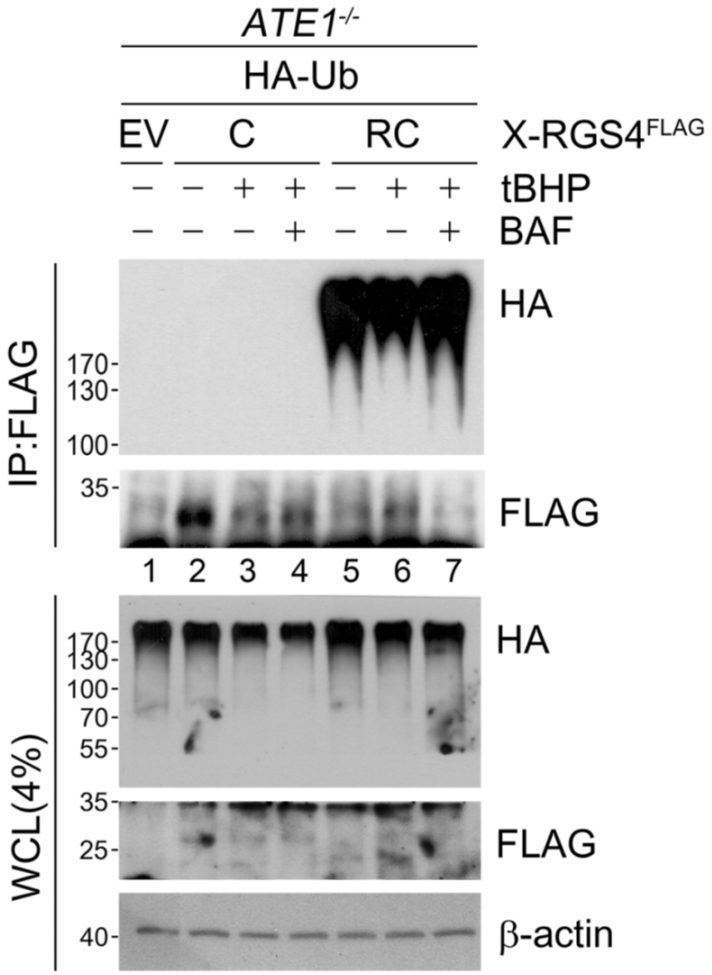

Figure 34. ATE1 mediated Nt-arginylation is required for oxidative stress induced ubiquitylation of Cys/N-degron substrate. Denaturation IP of C and RC-RGS4^{FLAG} with HA-Ub expressing *ATE1*$^{-/-}$ MEF cells treated with a combination of BAF (200 nM), tBHP (250 μM), MG132 (10 μM) for 6 h.

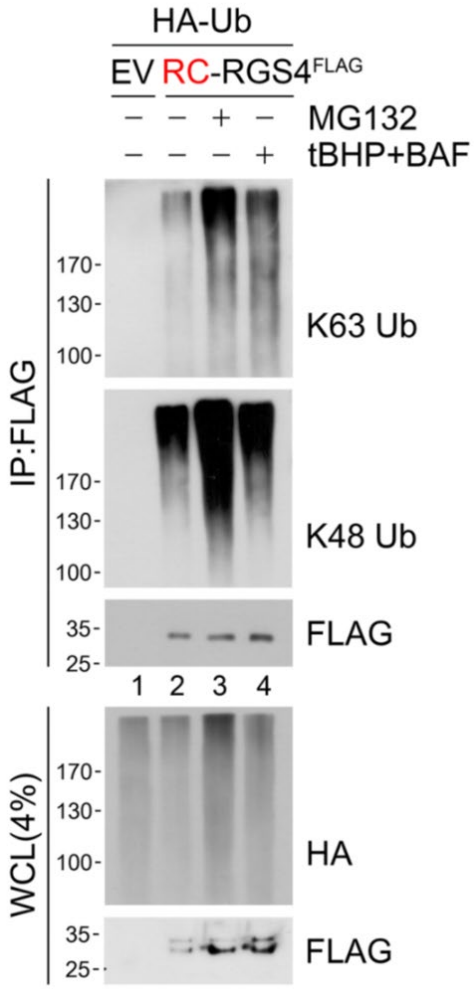

Figure 35. Nt-arginylated Cys/N-degron substrate undergo K63-linked ubiquitylation for autophagic degradation. Denaturation IP of RC-RGS4^{FLAG} with HA-Ub expressing 293T cells treated with co-treatment of BAF (200 nM) and tBHP (250 μM) or MG132 (10 μM) for 6 h.

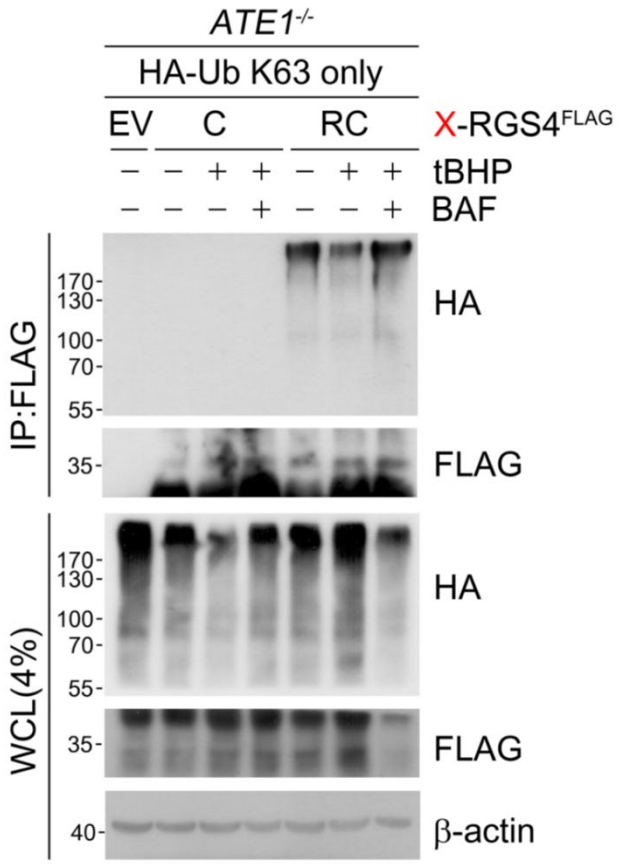

Figure 36. Nt-arginylation is required for oxidative stress induced K63-linked polyubiquitylation of Cys/N-degron substrate. Denaturation IP of C and RC-RGS4^{FLAG} with HA-Ub-K63 only expressing *ATE1*$^{-/-}$ MEF cells treated with a combination of BAF (200 nM), tBHP (250 μM), MG132 (10 μM) for 6 h.

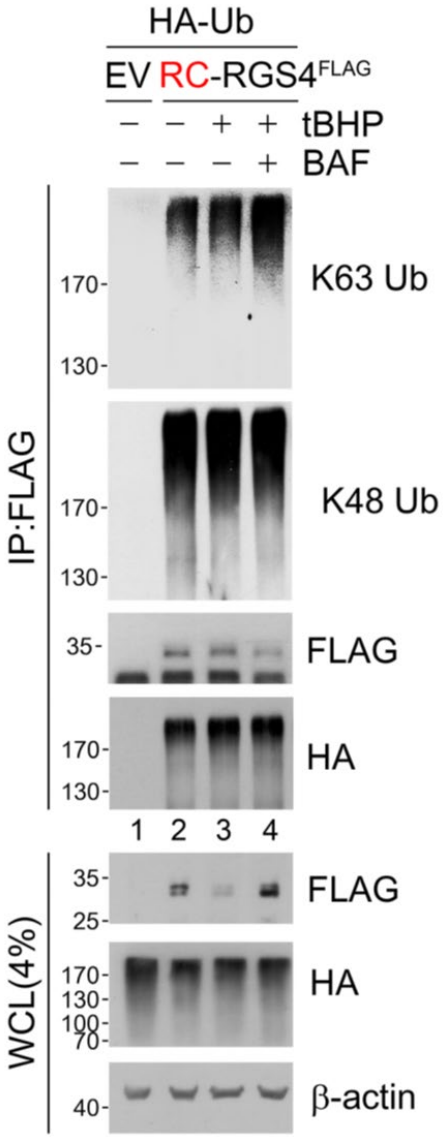

Figure 37. Autophagy targeted Nt-arginylated Cys/N-degron substrate possesses K63-linked polyubiquitylation. Denaturation IP of RC-RGS4^{FLAG} with HA-Ub expressing 293T cells treated with a BAF (200 nM) and tBHP (250 μM) or MG132 (10 μM) for 6 h.

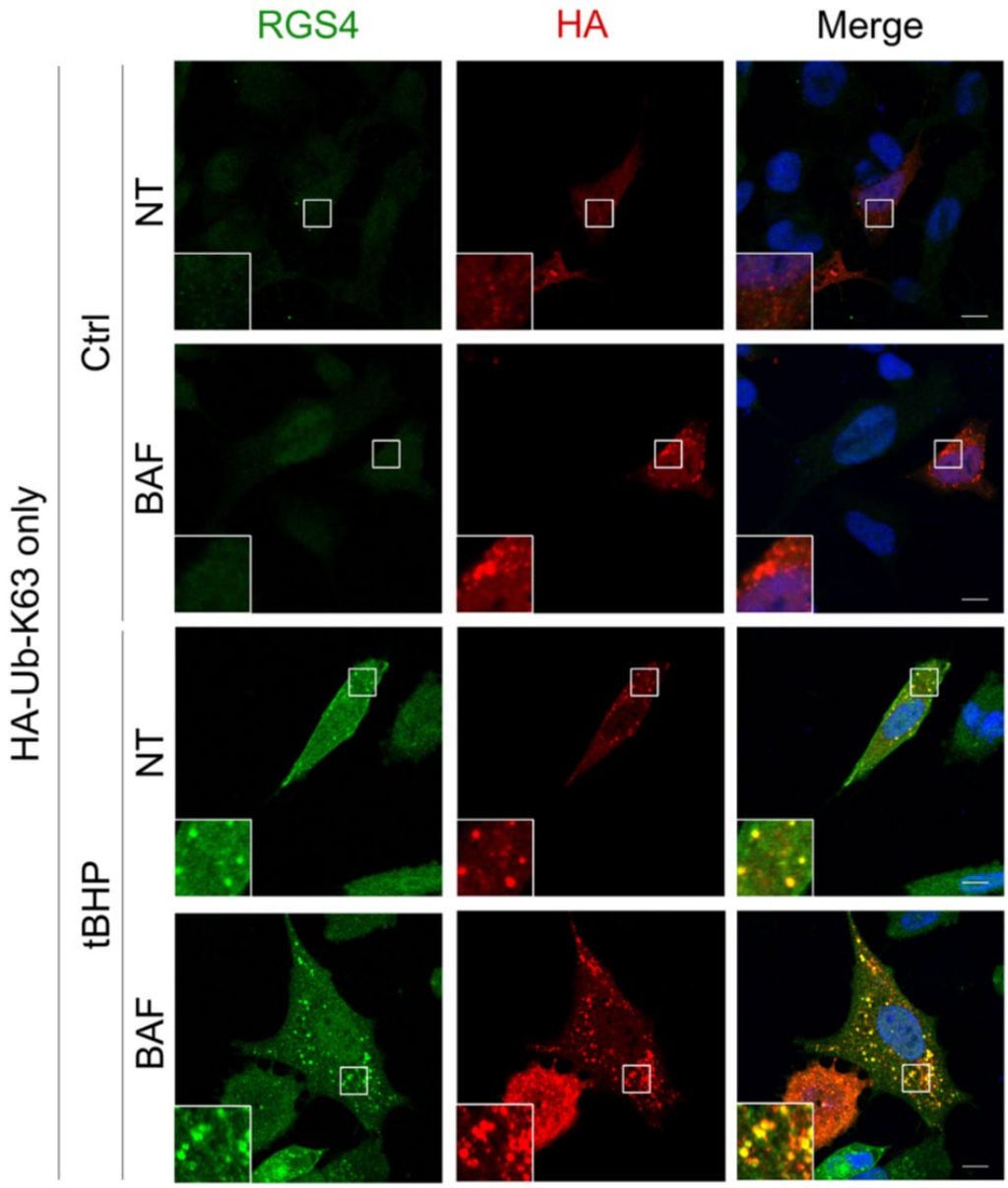

Figure 38. Cys/N-degron substrates are K63-linked ubiquitylated and form puncta structure upon oxidative stress. (A) ICC in SH-SY5Y cells expressing K63 only ub treated with a combination of BAF (200 nM), tBHP (250 μM) for 6 h.

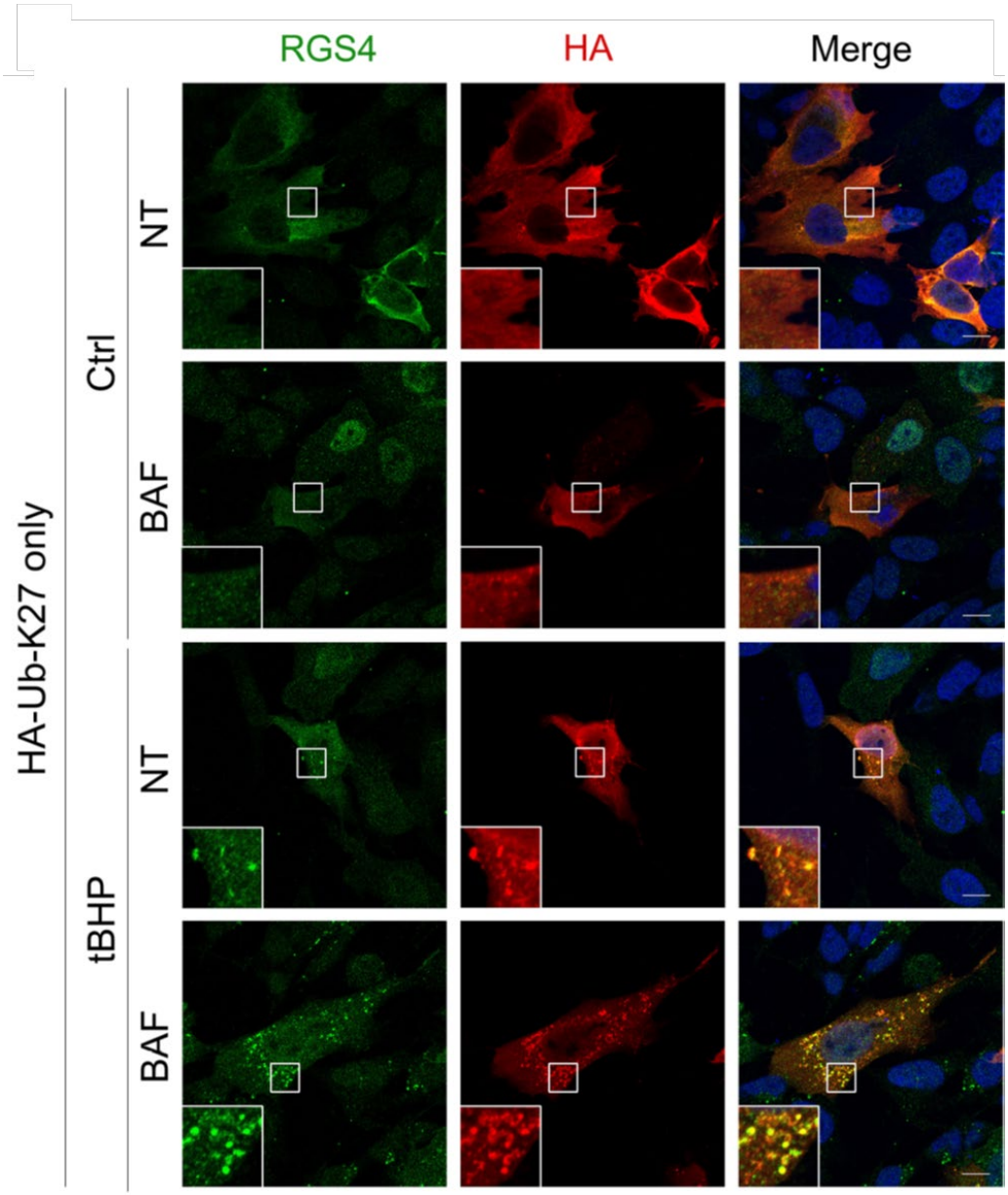

Figure 39. Cys/N-degron substrates are K27-linked ubiquitylated and form puncta structure upon oxidative stress. (A) ICC in SH-SY5Y cells expressing K27 only ub treated with a combination of BAF (200 nM), tBHP (250 μM) for 6 h.

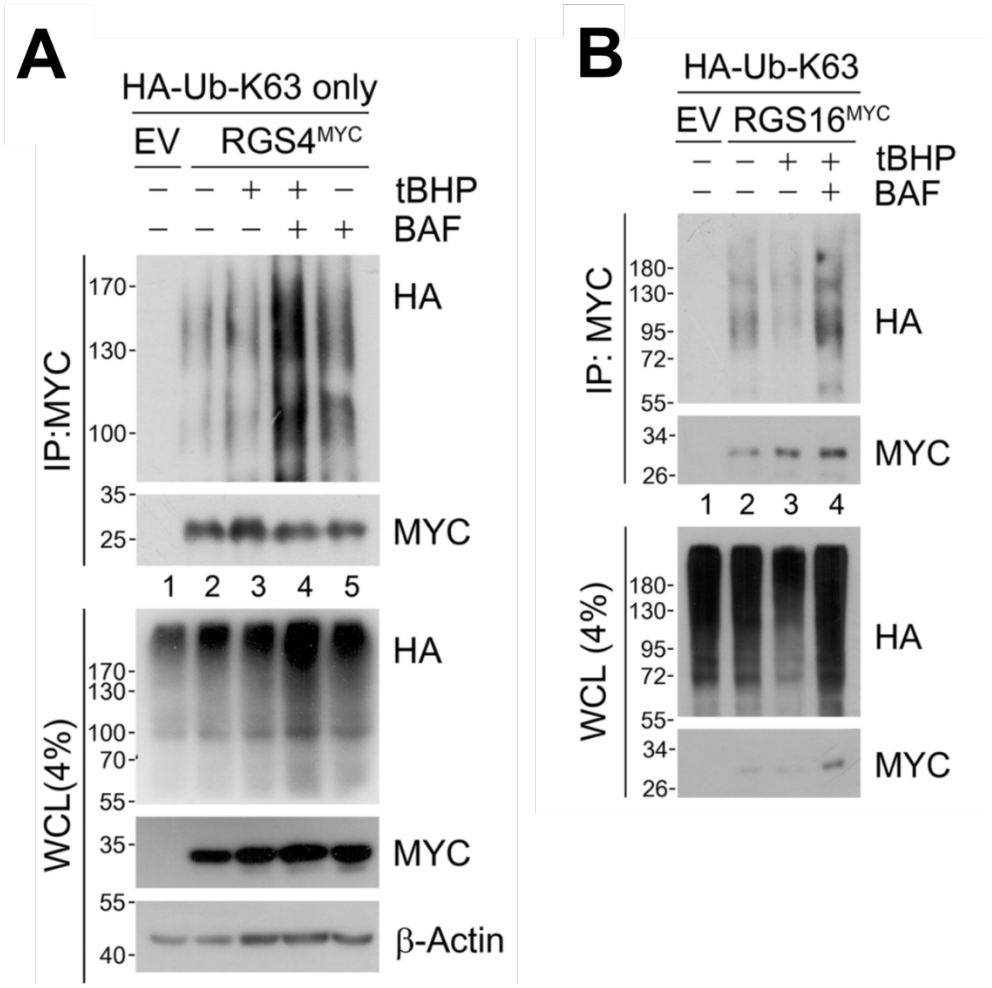

Figure 40. Oxidative stress induced autophagic degradation of Nt-Cys substrates requires K63-linked ubiquitylation. (**A**) Denaturation IP of RGS4^{MYC} and HA-Ub-K63 only expressing HEK293T cells treated with a combination of BAF (200 nM) and tBHP (250 μM) for 6 h. (**B**) Same as **A** but with RGS16^{MYC} expression.

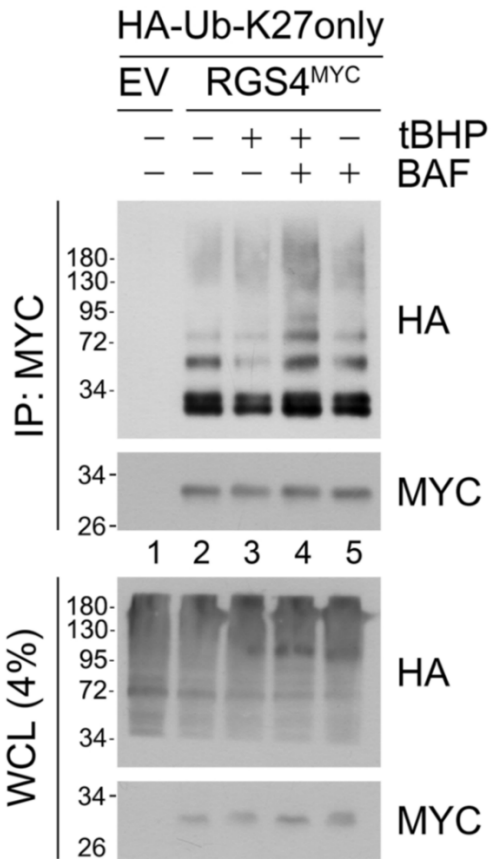

Figure 41. Oxidative stress induced autophagic degradation of Nt-Cys substrates requires K27-linked ubiquitylation. Denaturation IP of $RGS4^{MYC}$ and HA-Ub-K27 only expressing HEK293T cells treated with a combination of BAF (200 nM) and tBHP (250 μM) for 6 h.

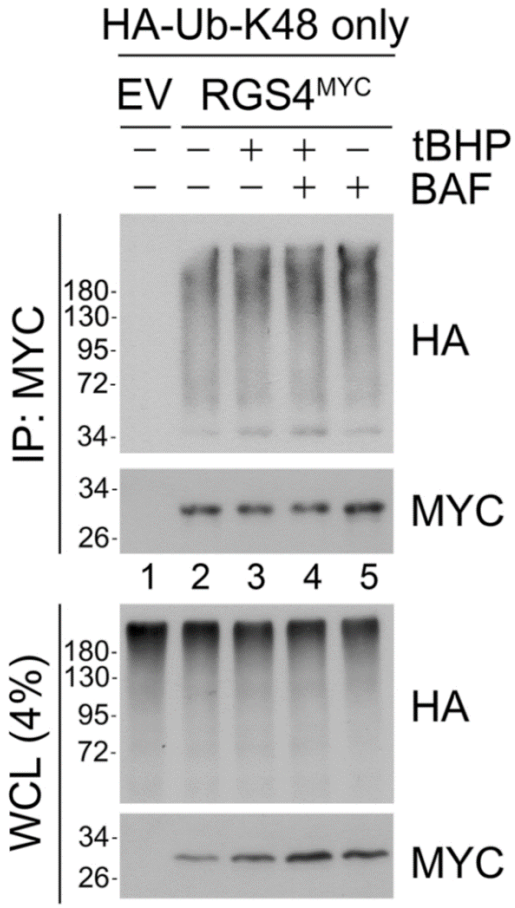

Figure 42. Oxidative stress induced autophagic degradation of Nt-Cys substrates is not affected by K48-linked ubiquitylation. Denaturation IP of $RGS4^{MYC}$ and HA-Ub-K48 only expressing HEK293T cells treated with a combination of BAF (200 nM) and tBHP (250 μM) for 6 h

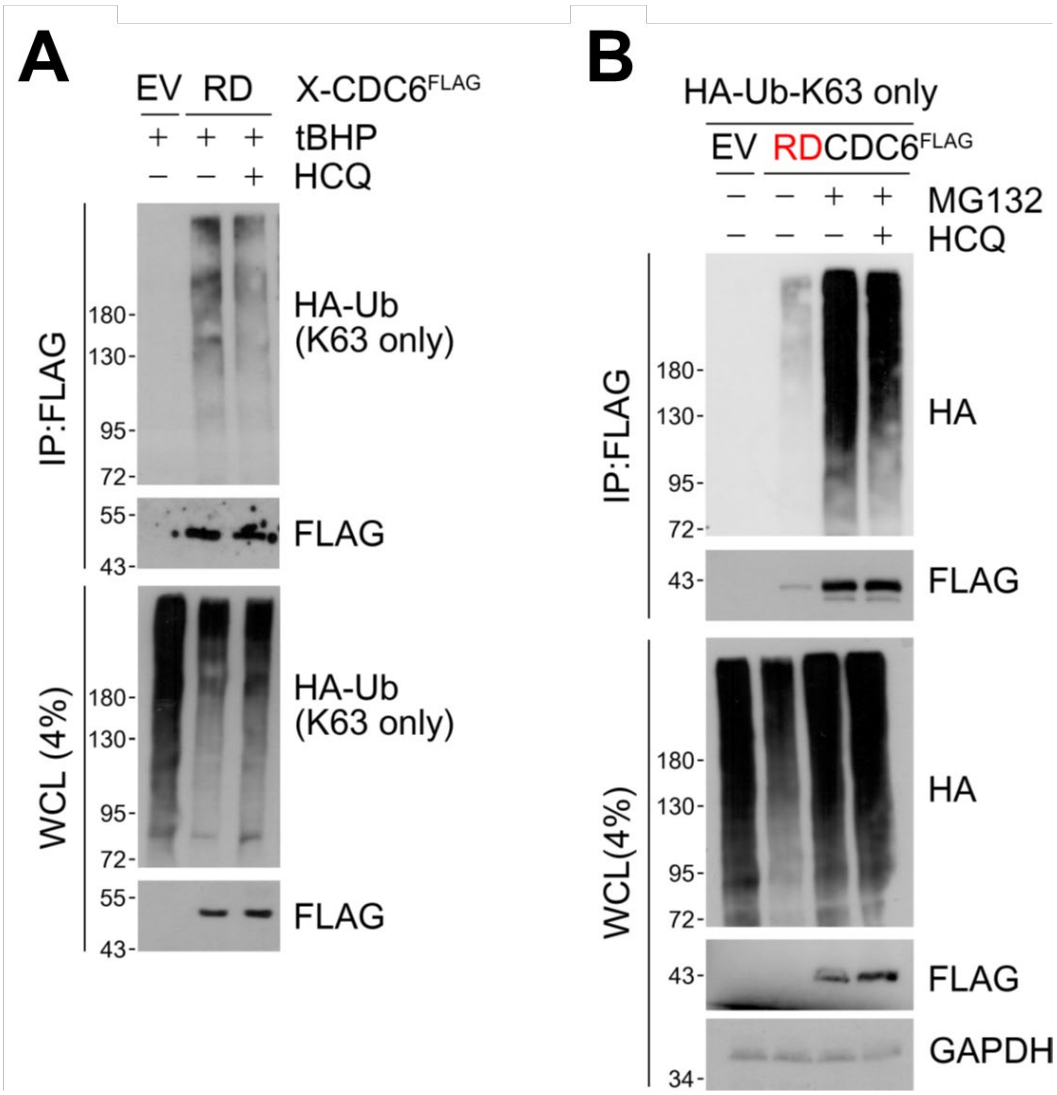

Figure 43. Autophagic degradation of Cys/N-degron specifically requires K63-linked ubiquitylation. (**A**) Denaturation IP of Denaturation IP assay in RD-CDC6FLAG and HA-Ub-K63-only mutant-expressing HEK293T cells treated with tBHP (250 μM, 6 h) and HCQ (25 nM, 24 h). **(B)** Same as with **C** but treated with MG132 (3 μM, 24 h) and HCQ (25 nM, 24 h).

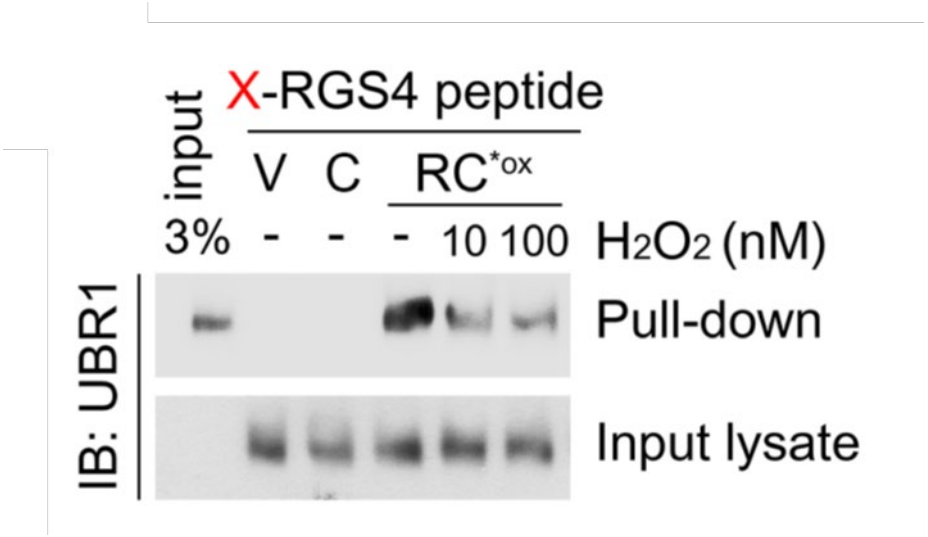

Figure 44. Nt-arginylated RGS4 loses its interaction with canonical N-recognin E3 ligase UBR1 upon exposure to oxidative stress. (A) *In vitro* X-RGS4 (X = V, C, or RC^{O3}) peptide pulldown assay with H_2O_2 added to lysate with indicated concentrations.

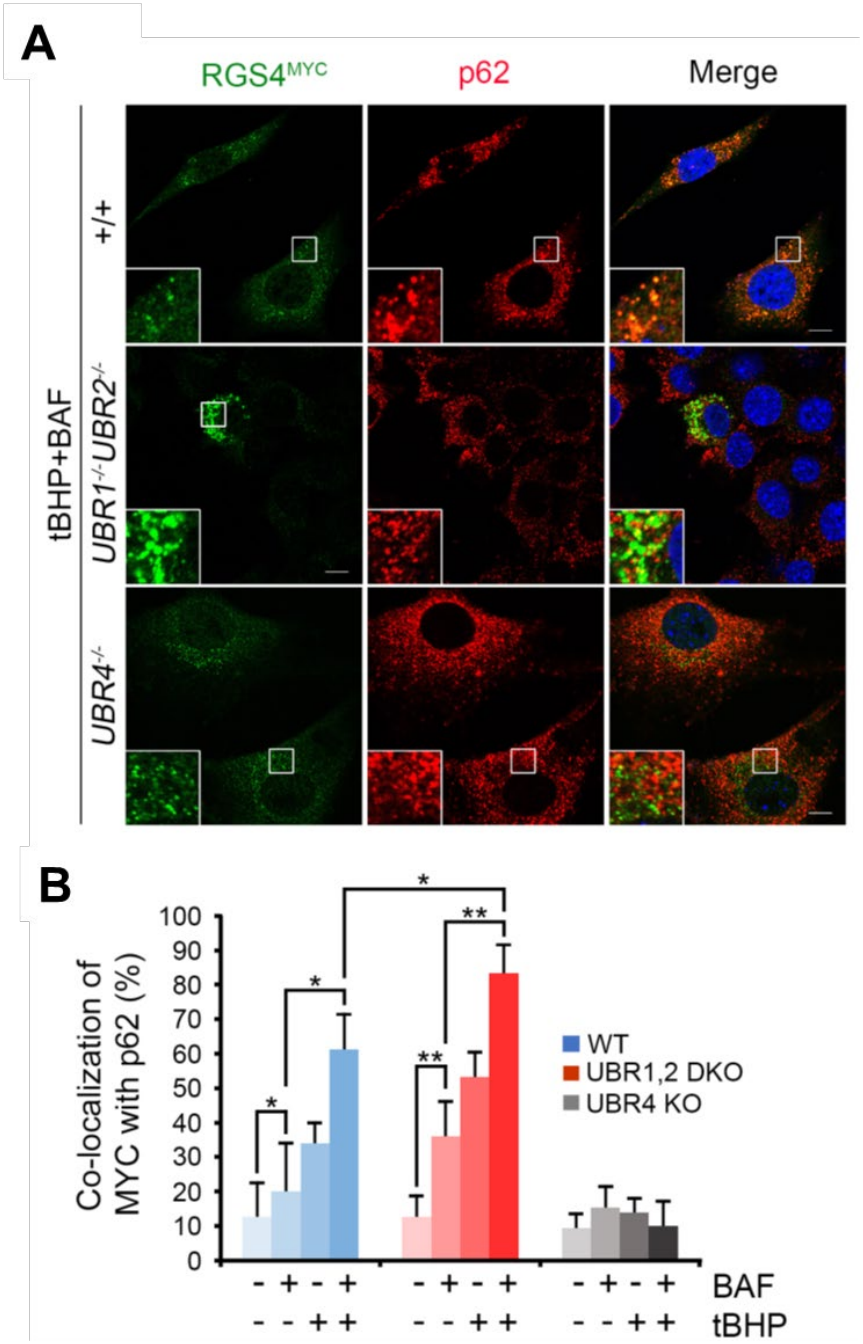

Figure 45. Oxidative stress induced autophagic targeting of Nt-Cys substrates requires non-canonical N-recognin E3 ligase other than UBR1 and UBR2. (A) ICC of WT, *UBR1/UBR2*$^{-/-}$, and *UBR4*$^{-/-}$ MEFs expressing RGS4^{MYC} and treated with treated with tBHP (250 μM, 6 h) and BAF (200 nM, 6 h). Scale bar, 10 μm. **(B)** Quantification of **A** (n=50 cells).

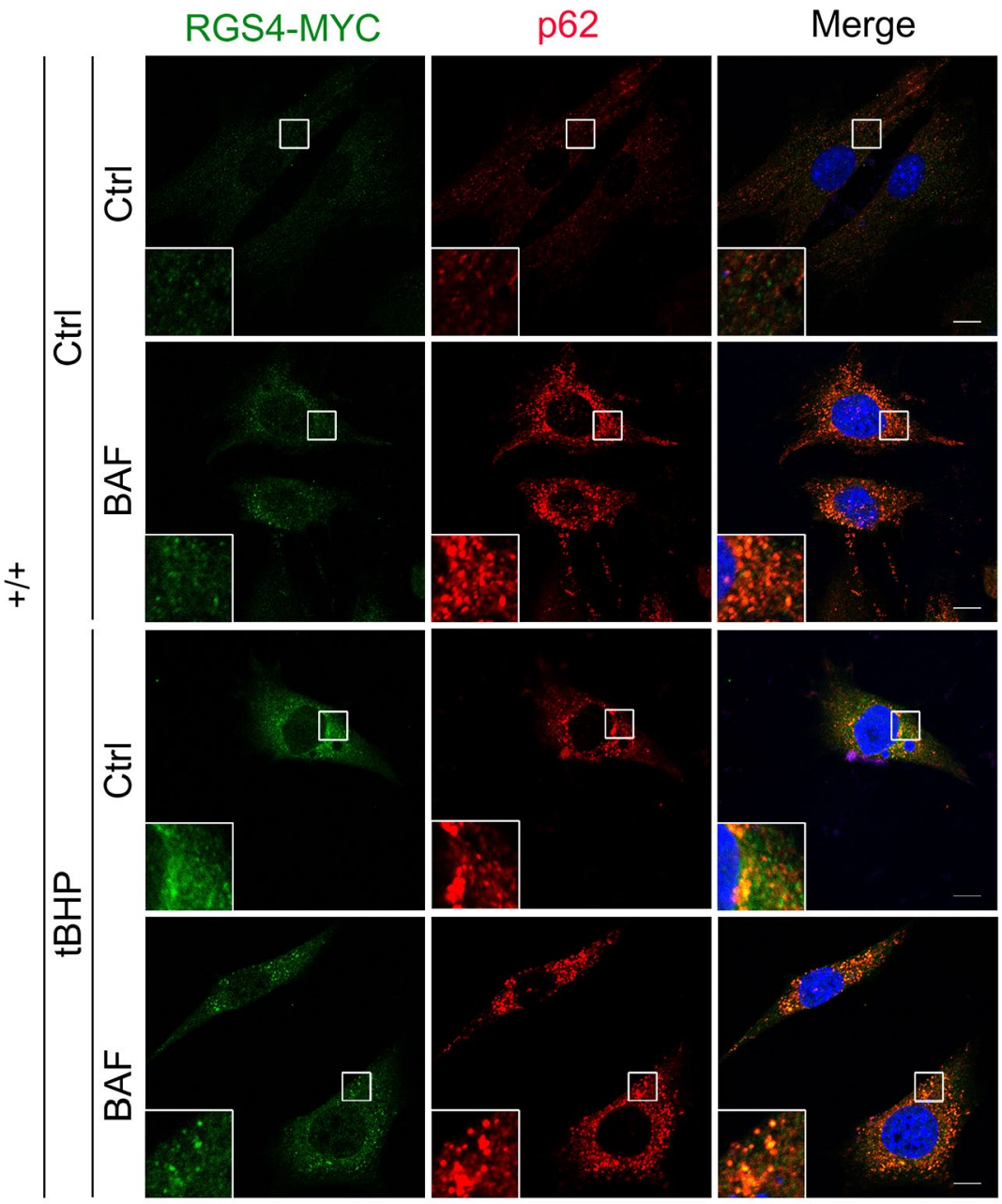

Figure 46. Oxidative stress induces autophagic targeting of RGS4. ICC of WT MEFs expressing $RGS4^{MYC}$ and treated with treated with tBHP (250 µM, 6 h) and BAF (200 nM, 6 h). Scale bar, 10 µm.

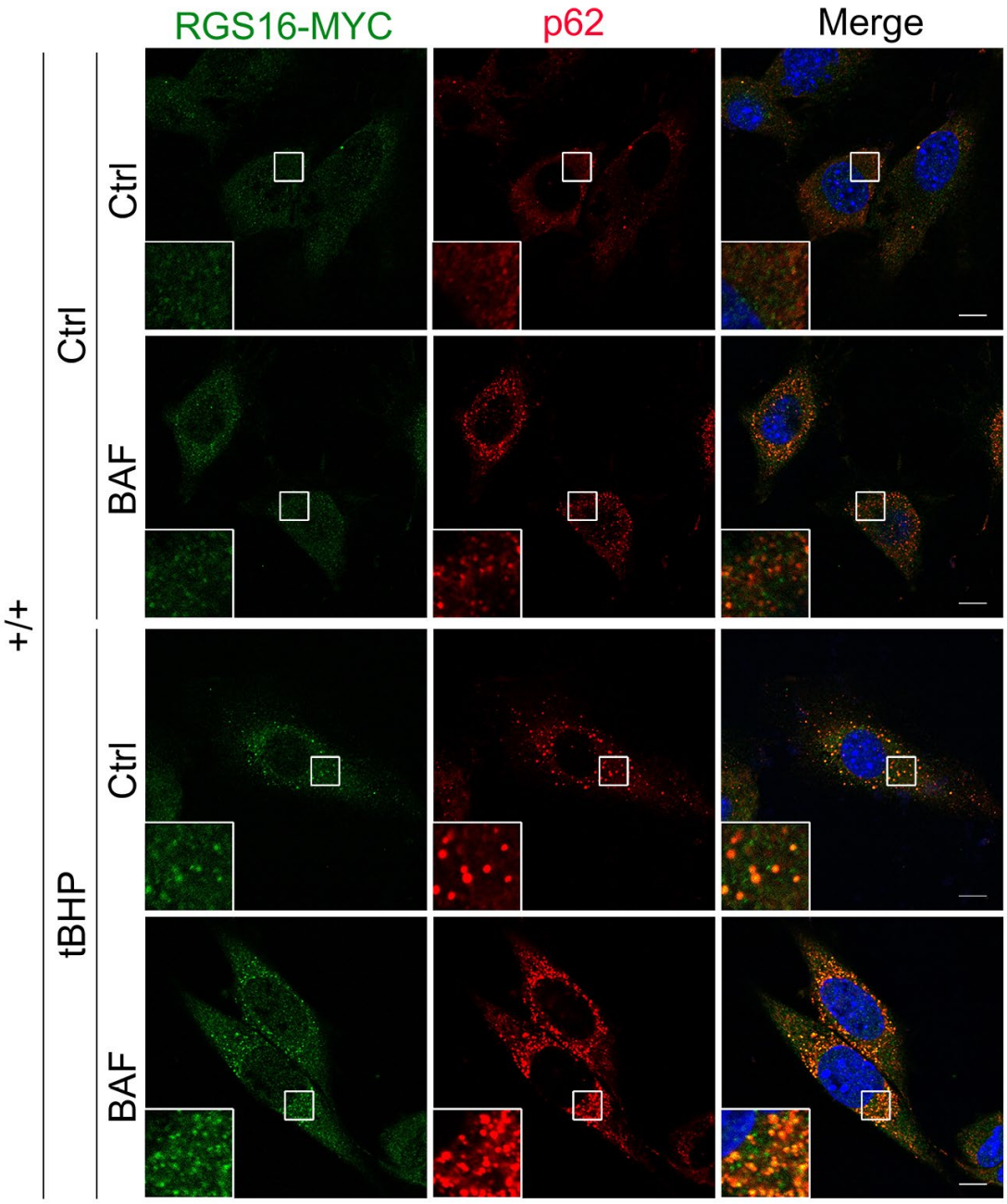

Figure 47. Oxidative stress induces autophagic targeting of RGS16. ICC of WT MEFs expressing RGS16^{MYC} and treated with treated with tBHP (250 µM, 6 h) and BAF (200 nM, 6 h). Scale bar, 10 µm.

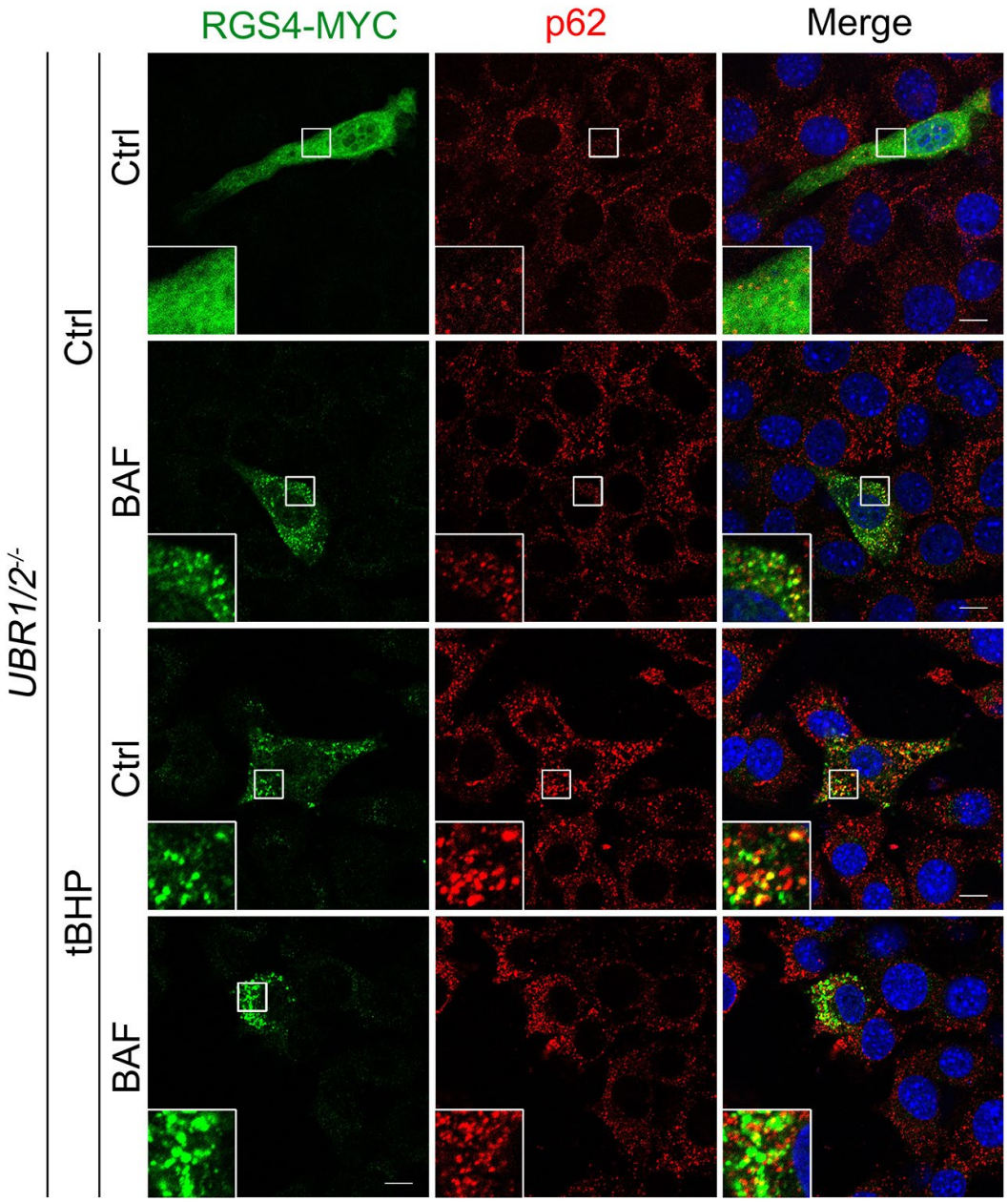

Figure 48. Depletion of the canonical N-recognin E3 ligase UBR1 and UBR2 still enables oxidative stress induced autophagic targeting of Nt-Cys substrates. ICC of *UBR1/UBR2*$^{-/-}$ MEFs expressing RGS4^{MYC} and treated with treated with tBHP (250 μM, 6 h) and BAF (200 nM, 6 h). Scale bar, 10 μm.

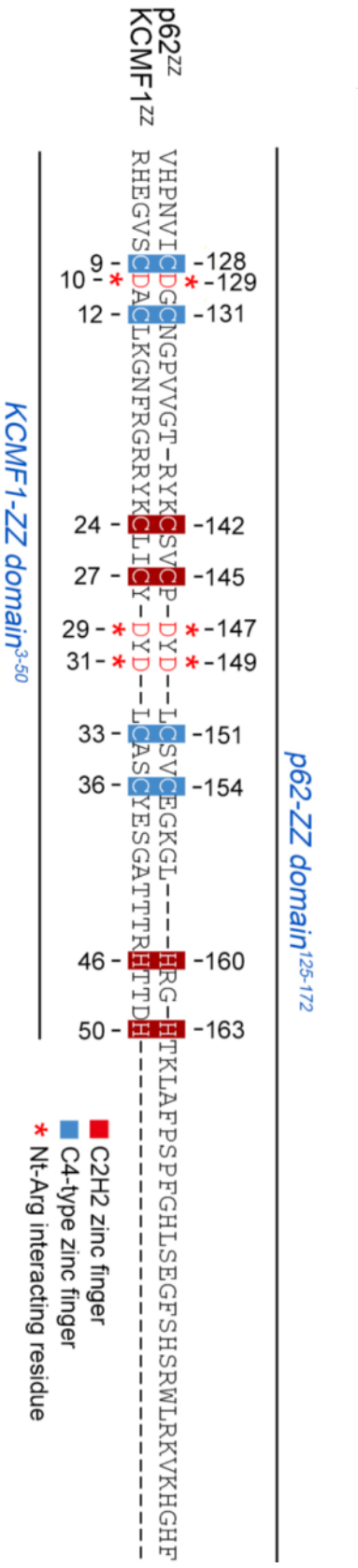

Figure 49. Sequence alignment of the ZZ domain of p62 and KCMF1.

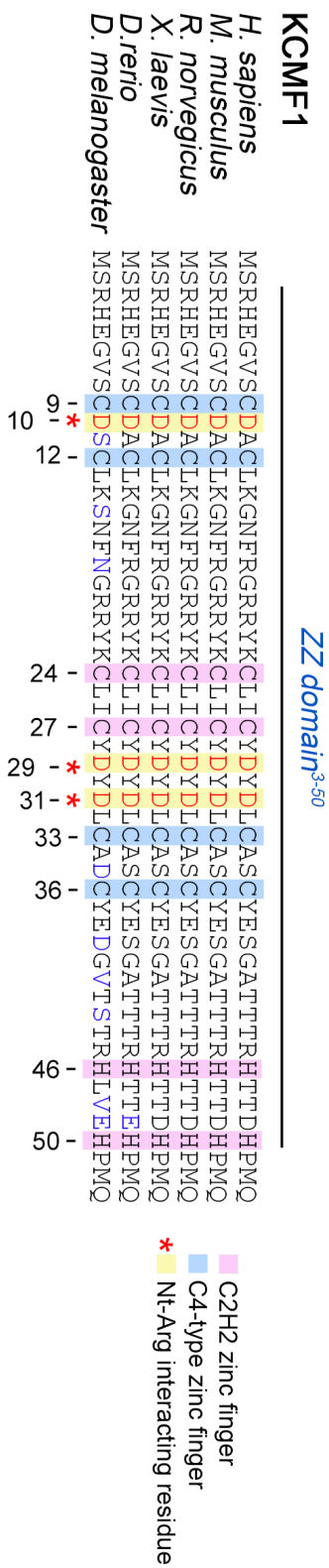

Figure 50. Sequence alignment of the evolutionarily conserved ZZ domain of KCMF1.

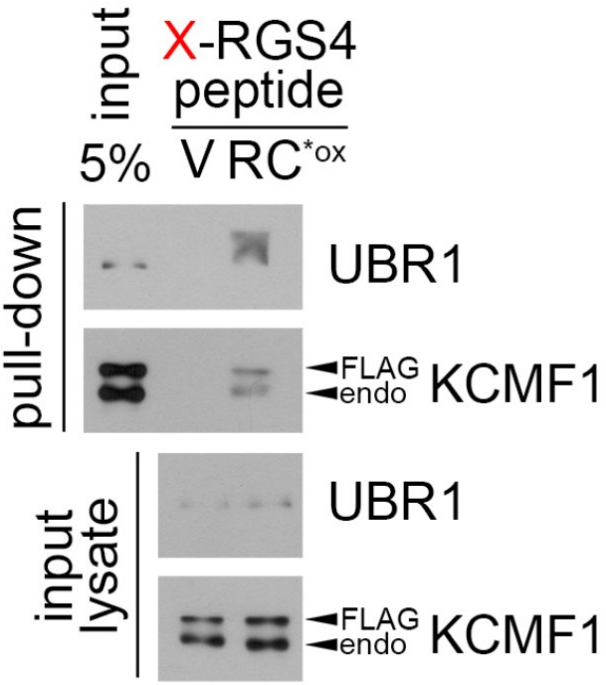

Figure 51. Nt-arginylated RGS4 peptide interacts with E3 ligase KCMF1. *In vitro* peptide pulldown assay of X-RGS4 (X = V, or RC^{O3}) 12-mer peptide using $KCMF1^{FLAG}$ transfected HEK293T cell lysates added with H_2O_2 (100 mM).

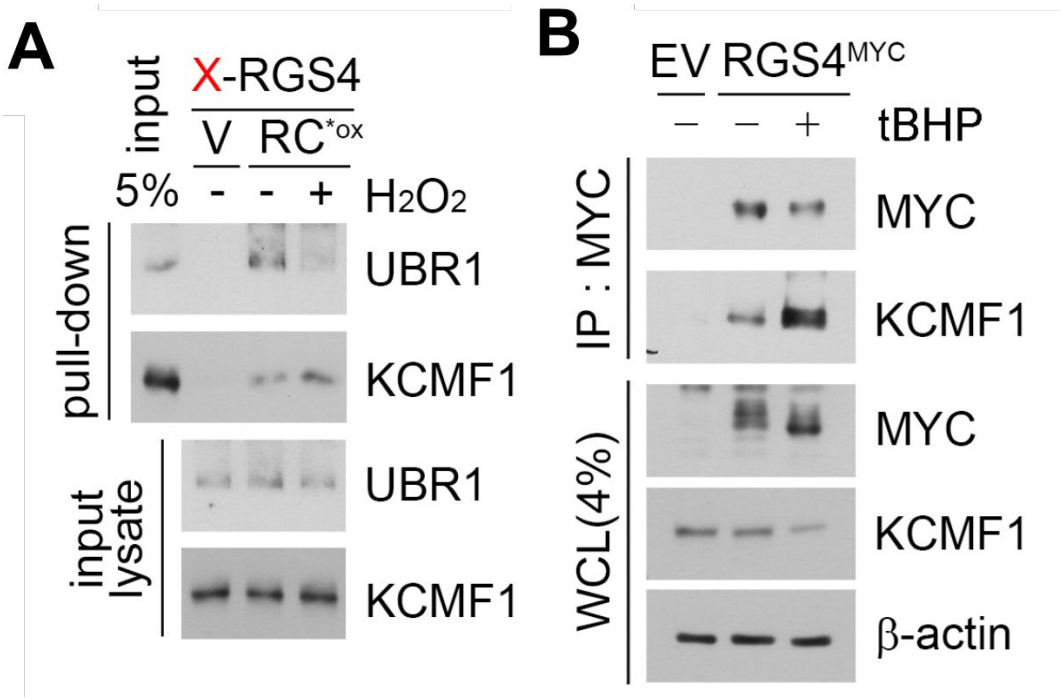

Figure 52. Nt-arginylated RGS4 strengthens its interaction with KCMF1 E3 ligase upon exposure to oxidative stress. (A) *In vitro* peptide pulldown assay of X-RGS4 (X = V, or RC^{O3}) 12-mer peptide using endogenous HEK293T cell lysates added with H_2O_2 (100 mM). **(B)** Co-IP of HEK293T cells expressing $RGS4^{MYC}$ treated with tBHP (250 μM, 6h).

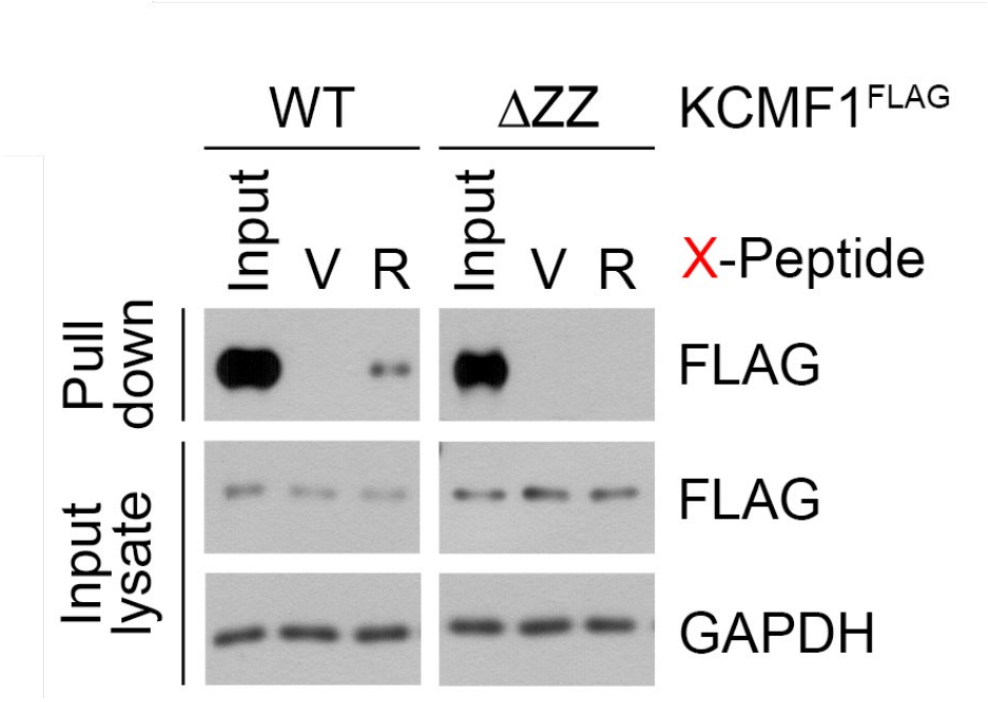

Figure 53. ZZ domain is required for interaction between RC^{O3}-RGS4 and KCMF1. X-RGS4 and (X=V, RC^{O3} or R) peptides were mixed with HEK293T cell lysates transfected with WT^{FLAG} and ZZ domain deficient mutant $KCMF1^{FLAG}$ to pull-out recombinant KCMF1 proteins.

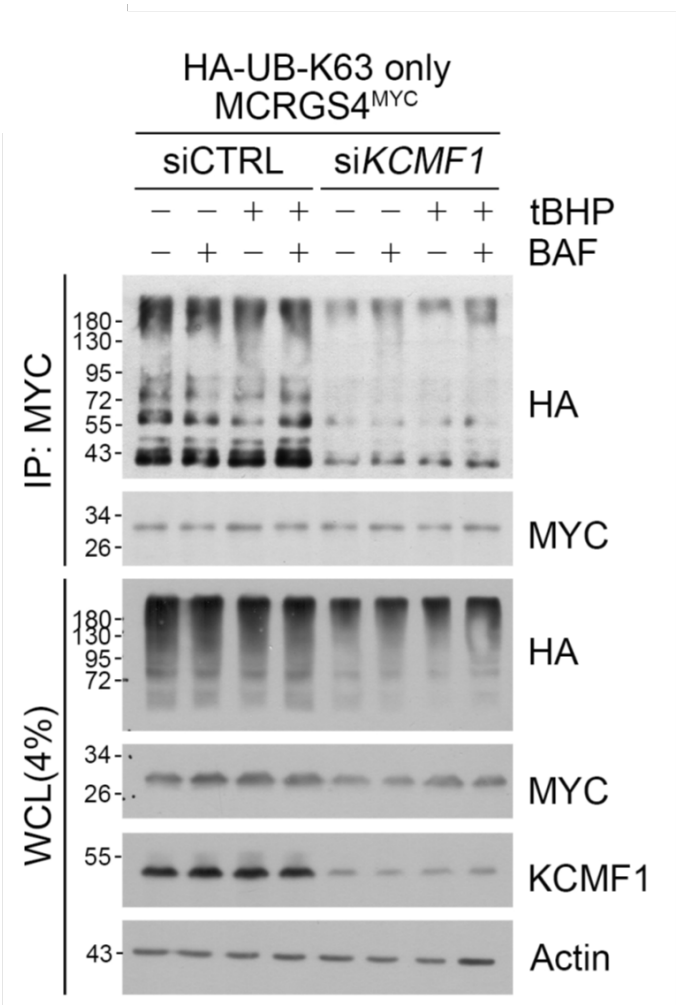

Figure 54. K63-linked ubiquitylation on Nt-Cys substrates under oxidative stress is mediated by KCMF1. Denaturation IP HEK293T cells expressing $RGS4^{MYC}$ and HA-Ub K63 only mutant with *KCMF1* siRNA (40 nM, 48 h) and treated with a combination of BAF (200 nM) and tBHP (250 μM) for 6 h.

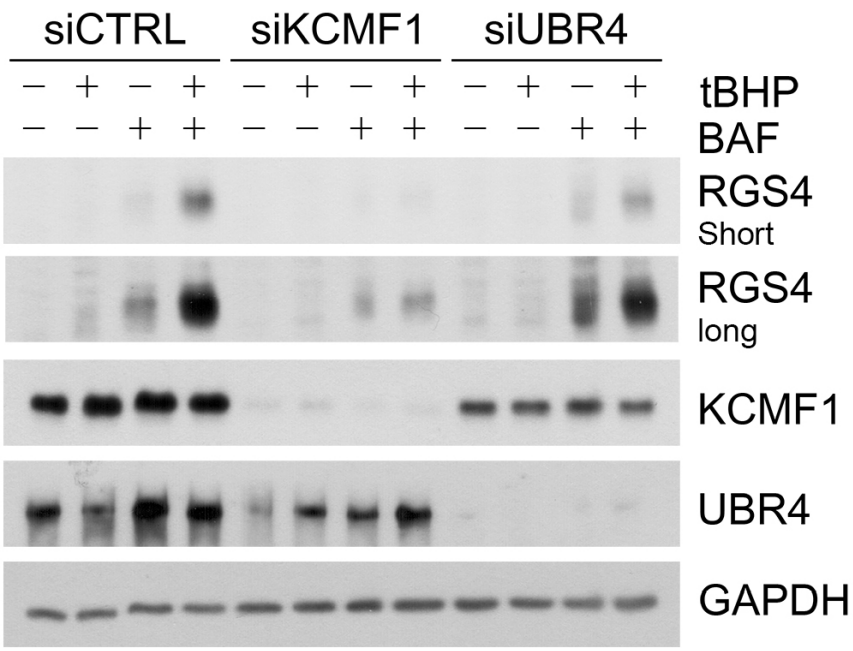

Figure 55. KCMF1 and UBR4 are responsible for autophagic degradation of the Nt-Cys substrate under oxidative stress. WB of SH-SY5Y cells transfected with *KCMF1* siRNA (40 nM, 48 h) or *UBR4* siRNA (20 nM, 48 h) and treated with a combination of BAF (200 nM) and tBHP (250 μM) for 6 h.

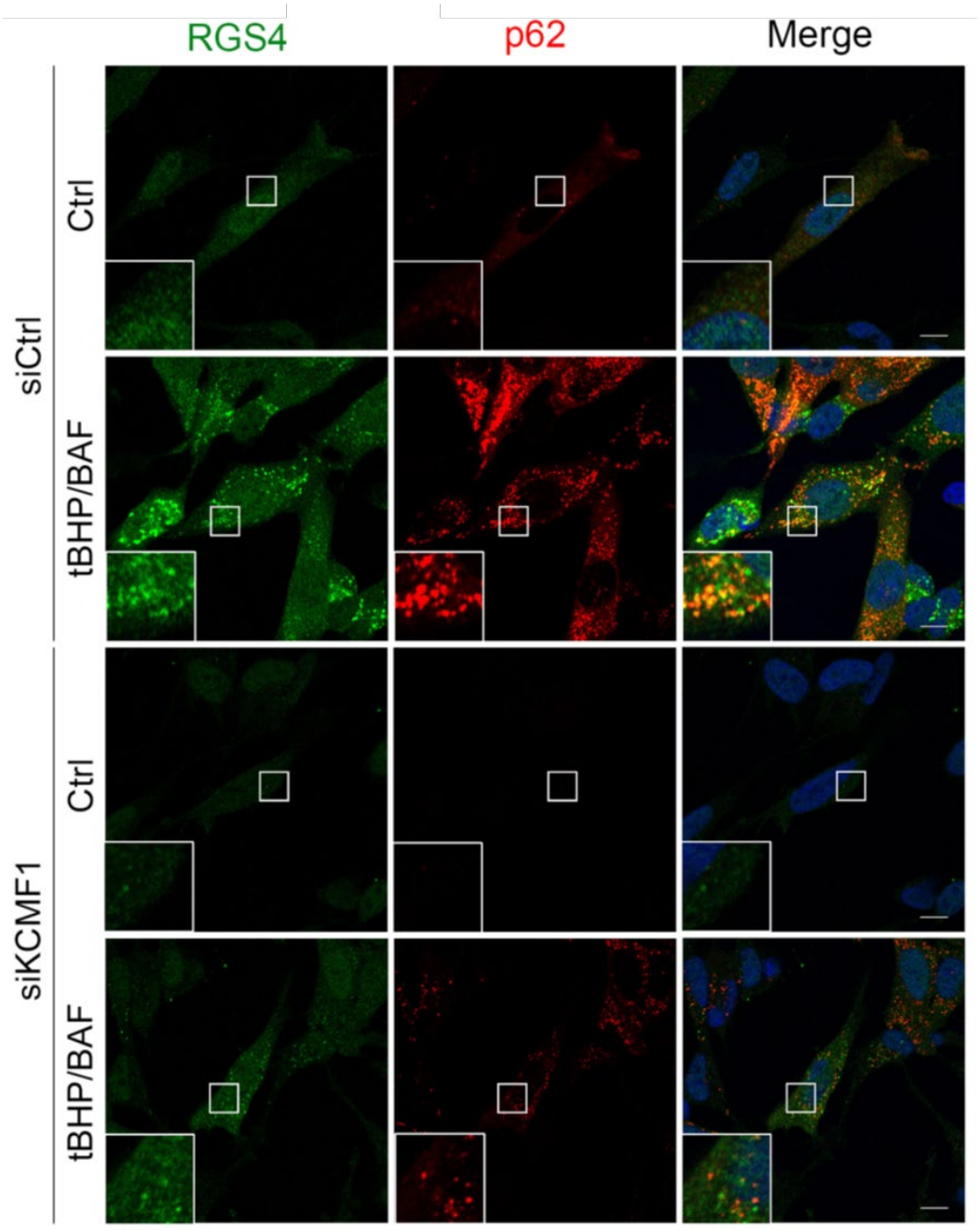

Figure 56. Genetic interference of KCMF1 interrupts oxidative stress induced autophagic targeting of Nt-Cys substrates. ICC of KCMF1-interfered SH-SY5Y cells treated with tBHP (250 μM, 6 h) and BAF (200 nM, 6 h). Scale bar, 10 μm.

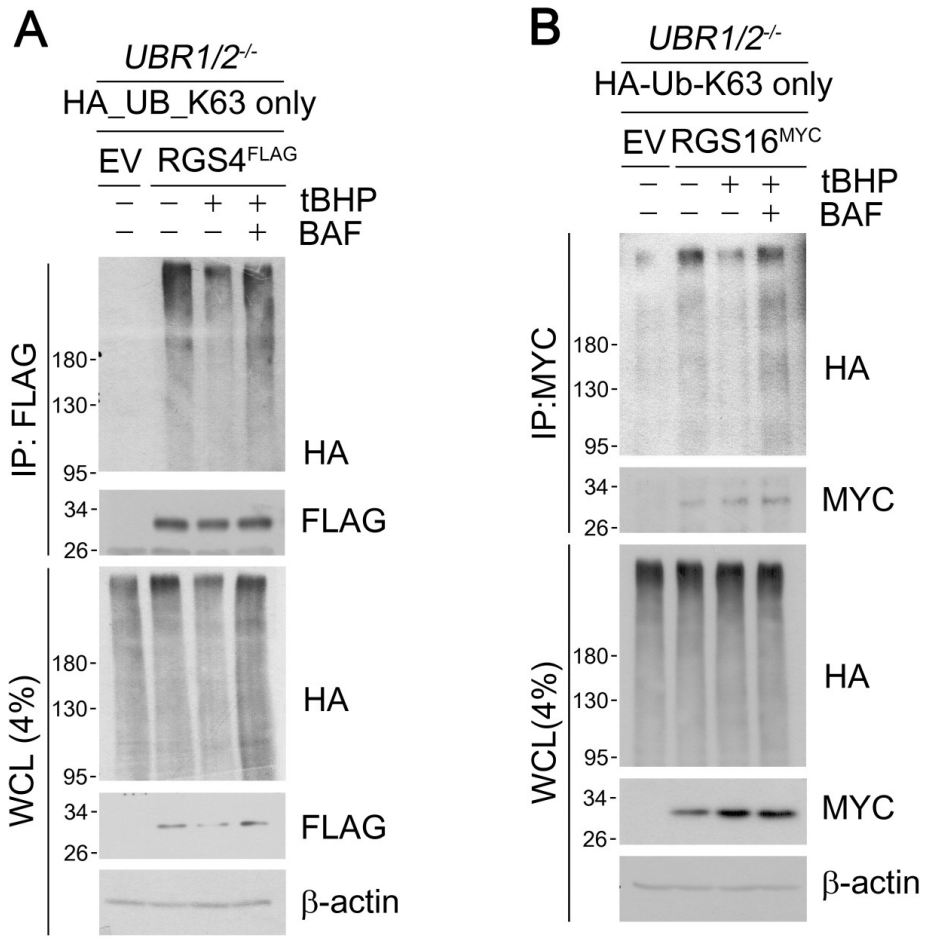

Figure 57. UBR1 and UBR2 is not responsible for ligating K63-linked ubiquitin chain on Nt-Cys substrates under oxidative stress. (A, B) Denaturation IP in *UBR1*$^{-/-}$ *UBR2*$^{-/-}$ MEF cells expressing HA-Ub-K63 only mutant and (**A**) RGS4^{FLAG} or (**B**) RGS16^{MYC} treated with combination of tBHP (250 μM, 6 h) and BAF (200 nM, 6 h).

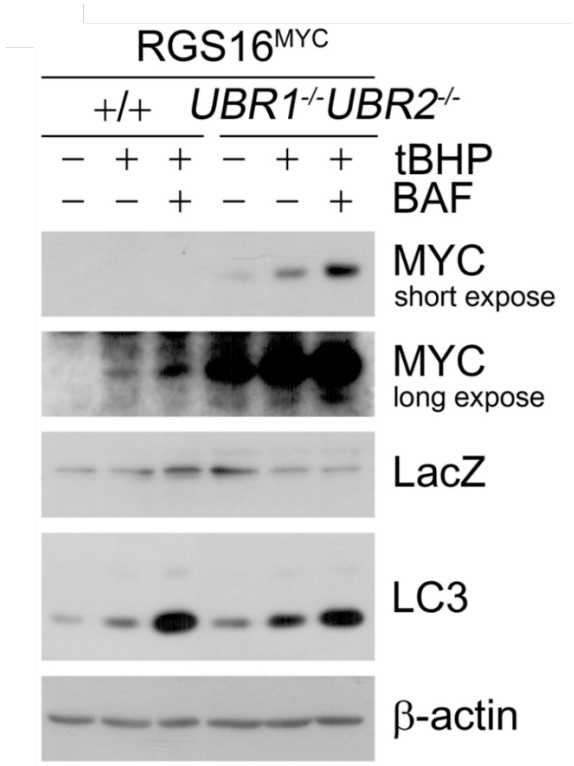

Figure 58. Oxidative stress induced autophagic degradation of Nt-Cys substrates is independent of UBR1 and UBR2. WB of RGS16^{MYC} expressing +/+ and *UBR1*$^{-/-}$ */UBR2*$^{-/-}$ MEF cells treated with a combination of BAF (200 nM) and tBHP (250 μM) for 6 h.

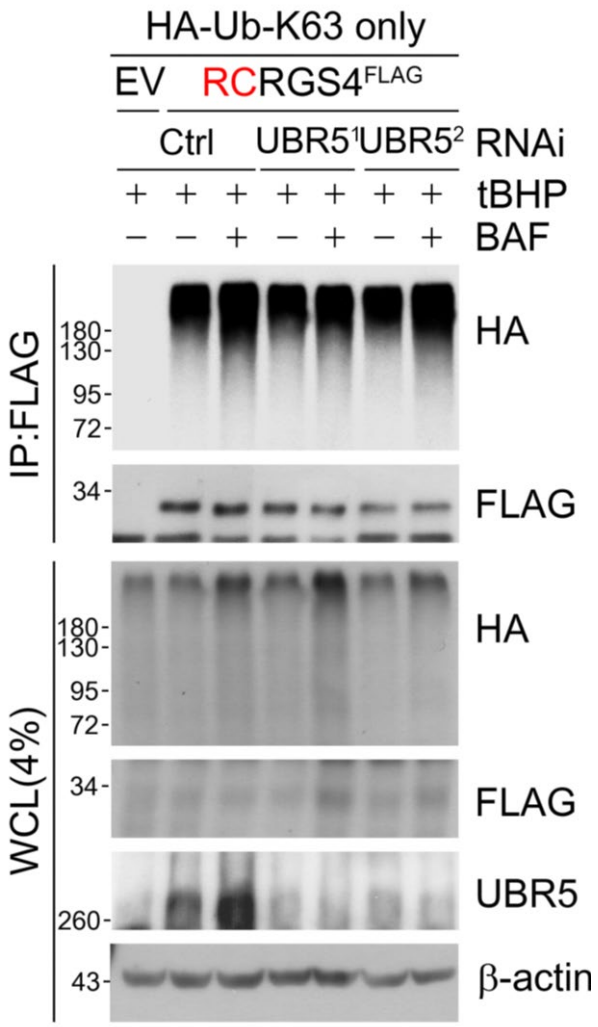

Figure 59. Oxidative stress induced K63-linked ubiquitylation of the Nt-Cys substrates does not require UBR5. Denaturation IP assay in RCRGS4^{FLAG} and HA-Ub-K63-only mutant-transfected HEK293T cells following *UBR5* interference and treatment with tBHP (250 μM, 6 h) and BAF (200 nM, 6 h).

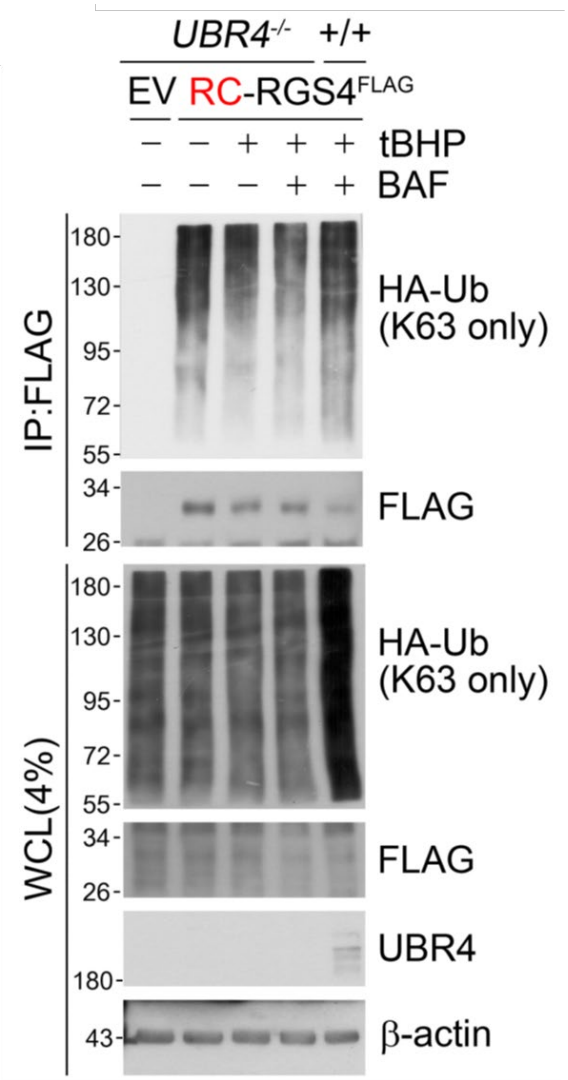

Figure 60. UBR4 is not responsible for ligating K63-linked ubiquitin chain on Nt-Cys substrates under oxidative stress. Denaturation IP in WT and *UBR4*$^{-/-}$ MEF cells expressing RCRGS4^{FLAG} and HA-Ub-K63 only mutant and treated with combination of tBHP (250 μM, 6 h) and BAF (200 nM, 6 h).

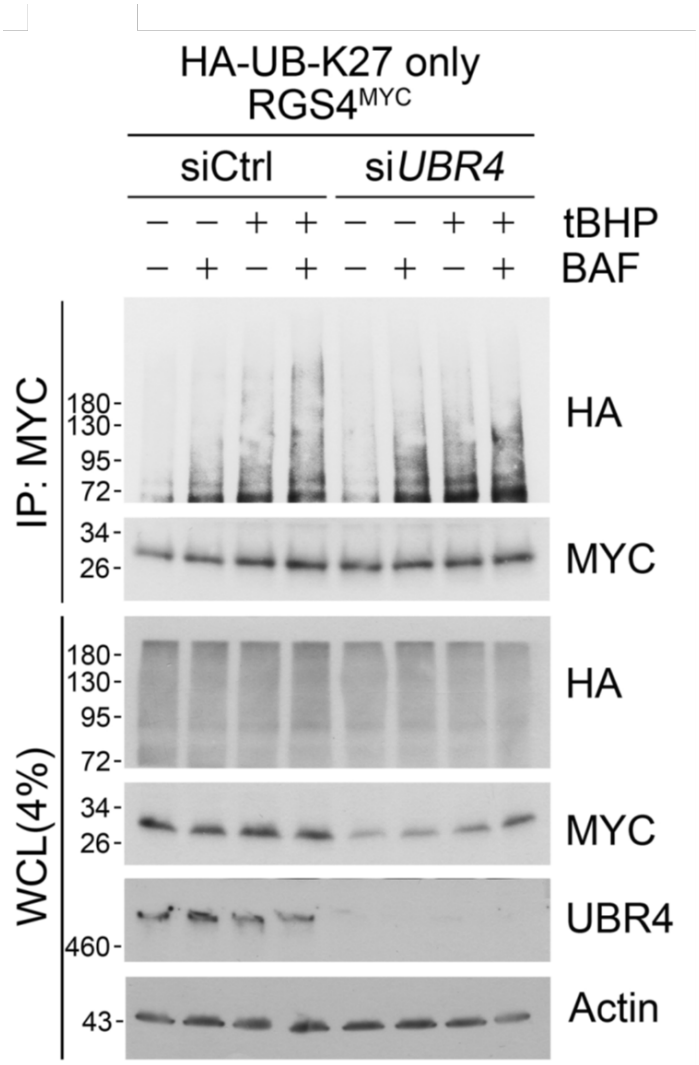

Figure 61. UBR4 is responsible for ligating K27-linked ubiquitin chain on Nt-Cys substrates under oxidative stress. Denaturation IP in WT and *UBR4*$^{-/-}$ MEF cells expressing RGS4^{MYC} and HA-Ub-K27 only mutant and treated with combination of tBHP (250 μM, 6 h) and BAF (200 nM, 6 h).

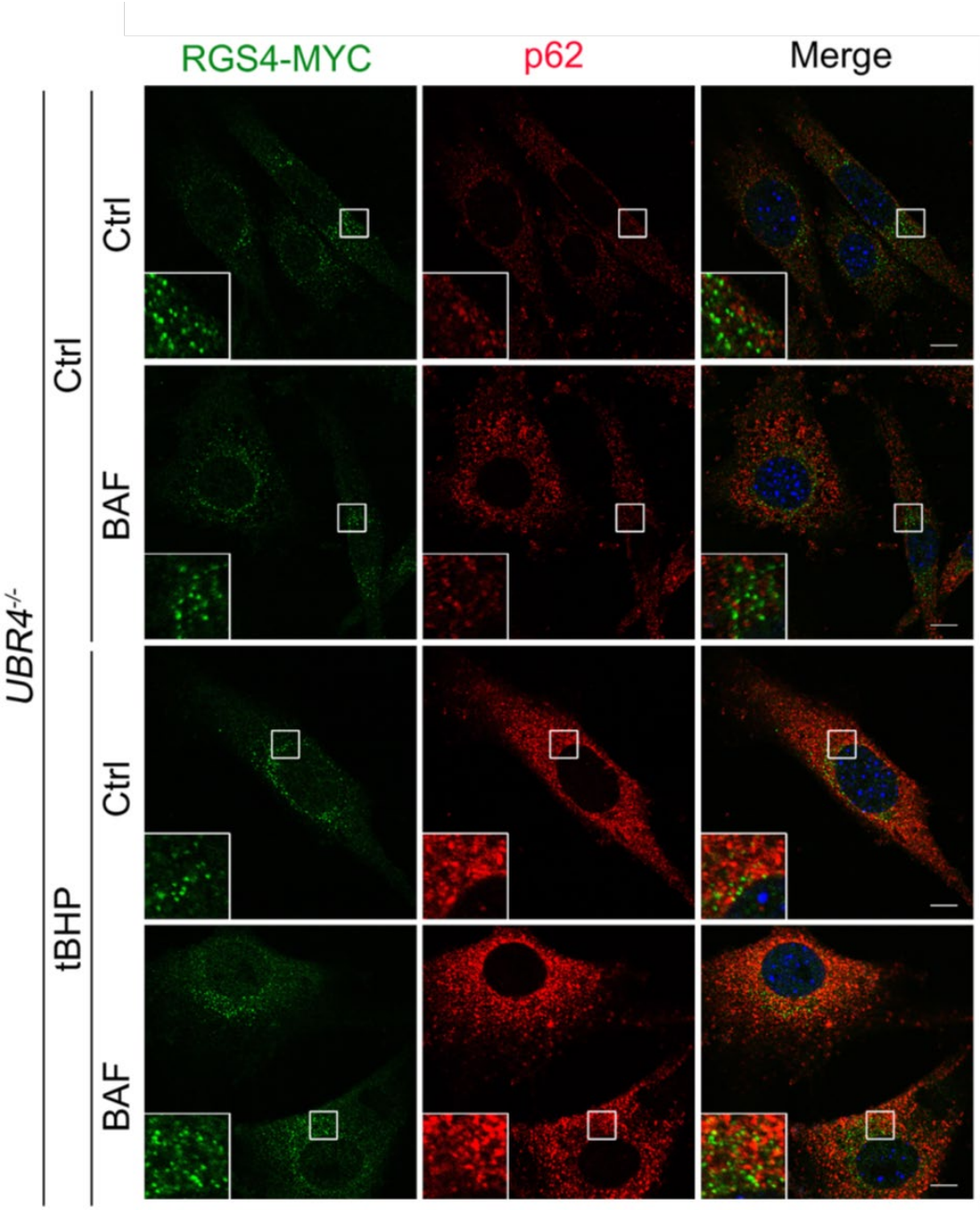

Figure 62. Oxidative stress induced autophagic targeting of RGS4 requires UBR4 N-recognin E3 ligase. ICC of *UBR4*$^{-/-}$ MEFs expressing RGS4^{MYC} and treated with tBHP (250 μM, 6 h) and BAF (200 nM, 6 h). Scale bar, 10 μm.

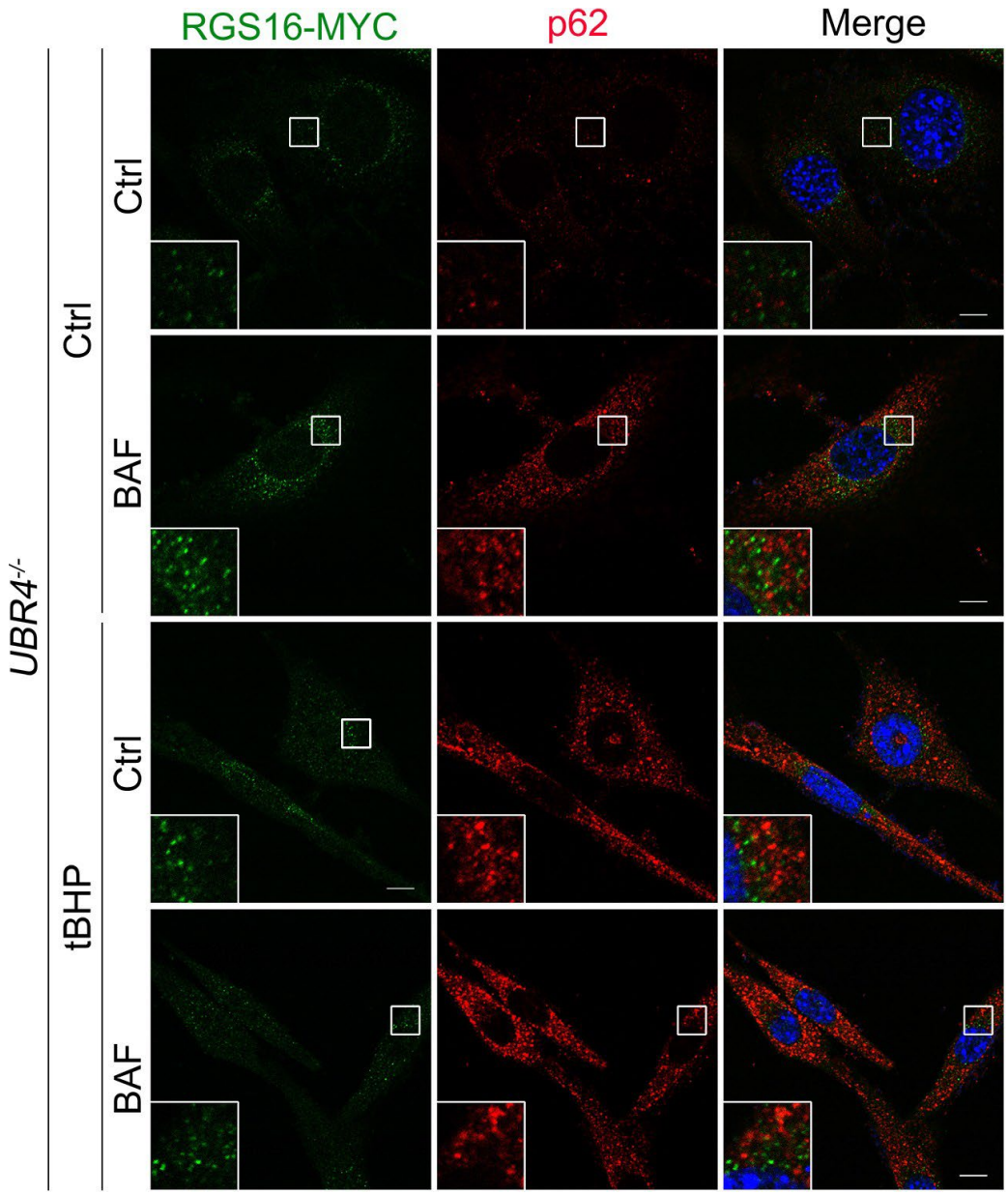

Figure 63. Oxidative stress induced autophagic targeting of Nt-Cys substrates requires UBR4 N-recognin E3 ligase. ICC of *UBR4*$^{-/-}$ MEFs expressing RGS16^{MYC} and treated with tBHP (250 μM, 6 h) and BAF (200 nM, 6 h). Scale bar, 10 μm.

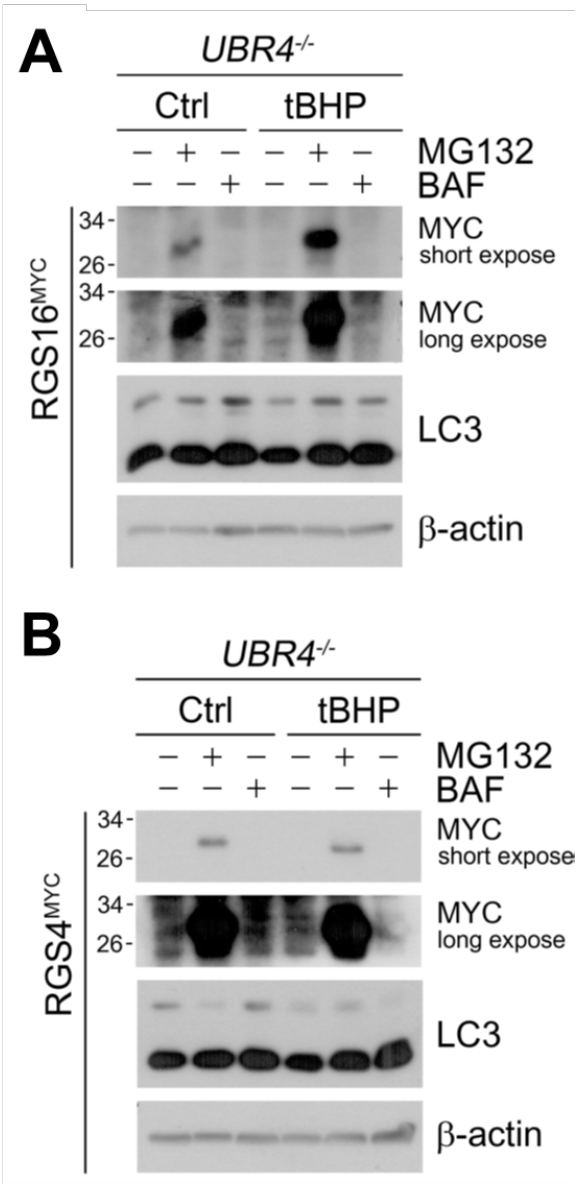

Figure 64. Depletion of UBR4 re-routes autophagy targeted Nt-Cys substrates to proteasome. (**A, B**) WB of (**A**) $RGS4^{MYC}$ and (**B**) $RGS16^{MYC}$ overexpressed in *UBR4*$^{-/-}$ MEF cells with tBHP (250 μM, 6h), MG132 (10 μM, 6 h), and BAF (200 nM, 6 h) treatment.

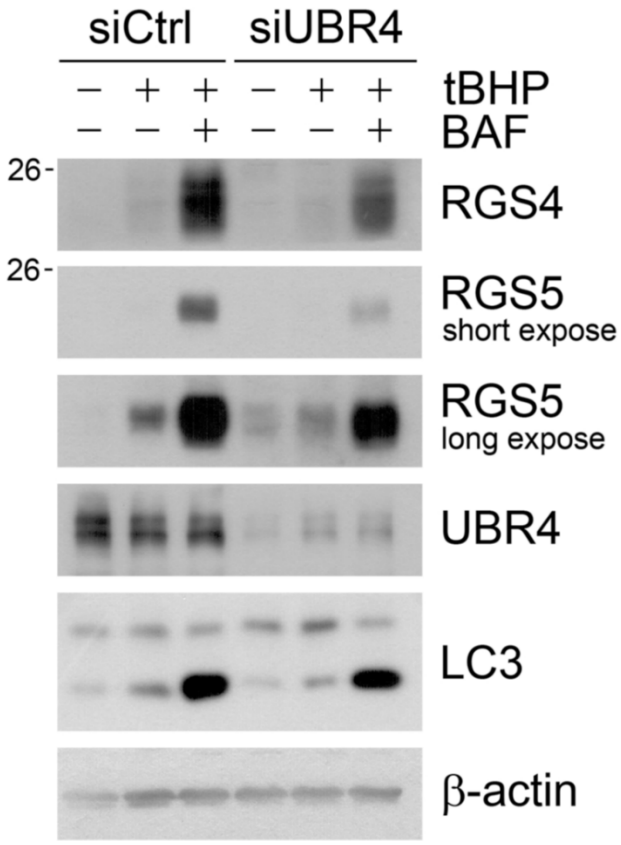

Figure 65. Genetic interference of UBR4 decreases autophagic flux of Nt-Cys substrates. WB of *UBR4* interfered SH-SY5Y cells with combination of tBHP (250 μM, 6h) and BAF (200 nM, 6 h) treatment.

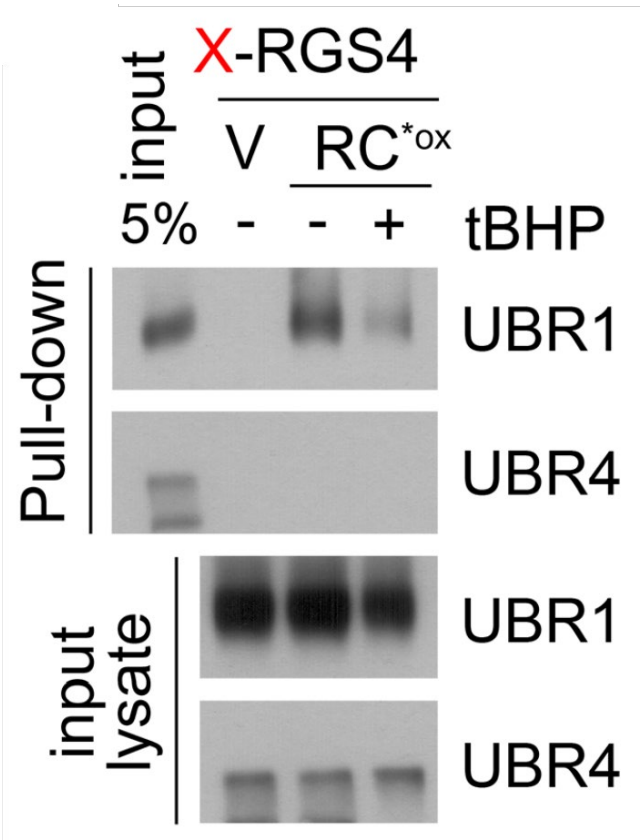

Figure 66. Nt-arginylated RGS4 does not directly bind to UBR4 under oxidative stress. *In vitro* peptide pulldown assay of X-RGS4 (X = V, or RC^{O3}) 12-mer peptide using endogenous HEK293T cell lysates added with tBHP (250 μM).

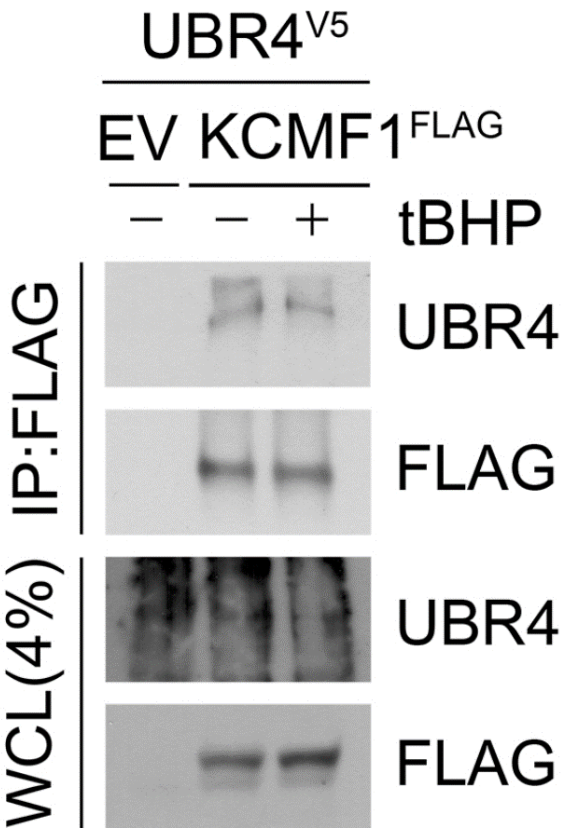

Figure 67. KCMF1 and UBR4 form a complex. Co-IP of HEK293T cells expressing $UBR4^{V5}$ and $KCMF1^{FLAG}$ treated with tBHP (250 μM, 6h).

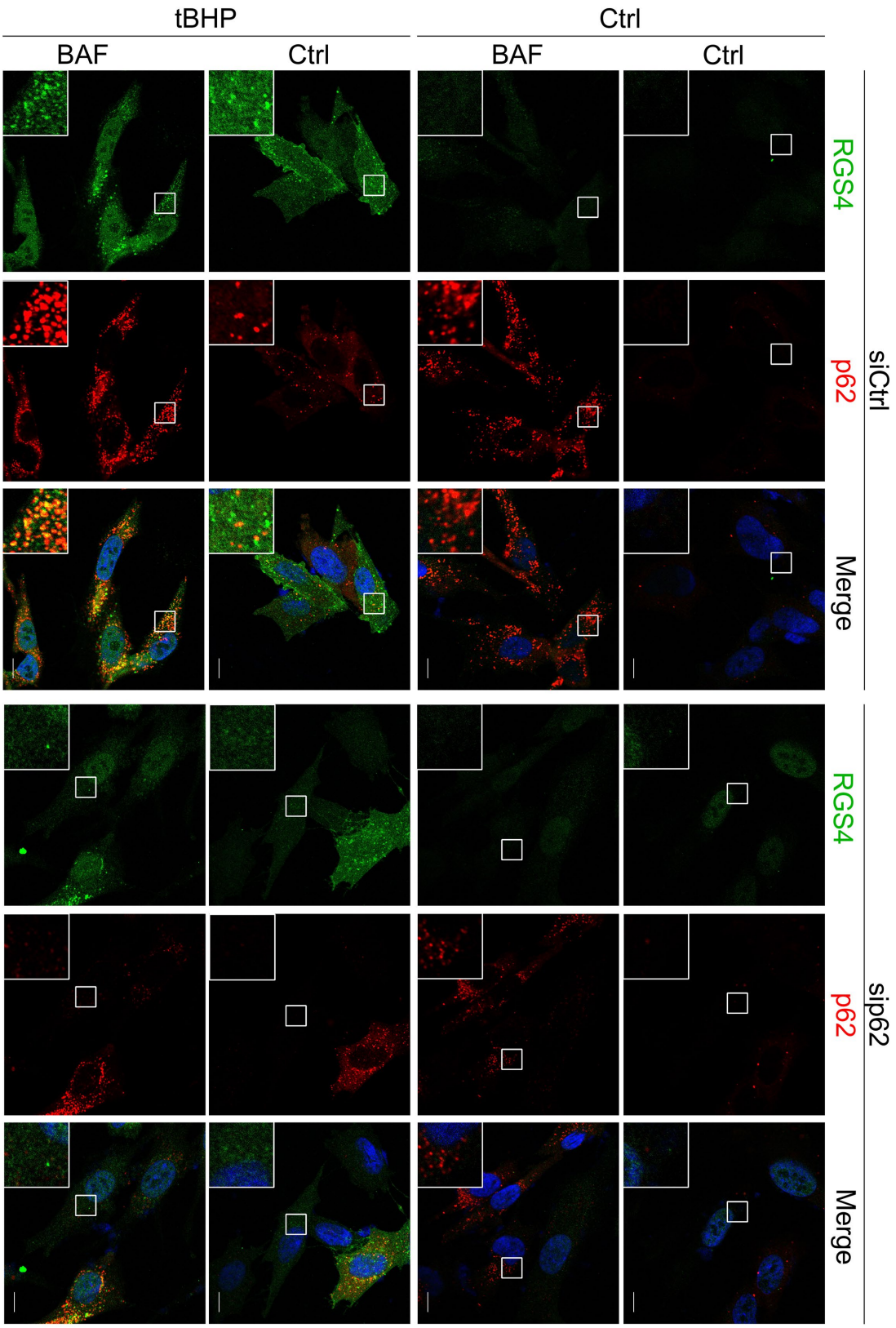

Figure 68. p62 is required for autophagic targeting of Nt-Cys substrates under oxidative stress. ICC analysis of SH-SY5Y cells under *p62* interference and treated with BAF(200 nM, 6 h), tBHP (250 μM, 6h) or both. Scale bar, 10 μm.

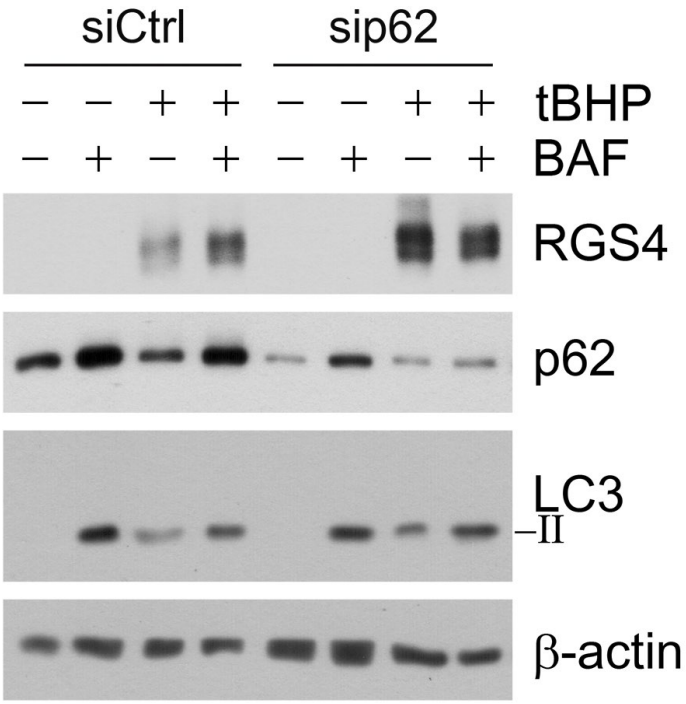

Figure 69. *p62* interference diminishes autophagic flux of Nt-Cys substrate under oxidiative stress. WB of SH-SY5Y cells under *p62* interference and treated with BAF(200 nM, 6 h), tBHP (250 μM, 6h) or both.

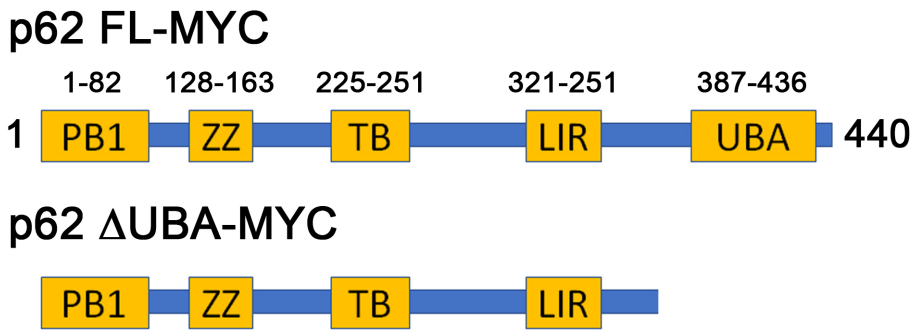

Figure 70. Graphical depiction of the p62 plasmid constructs.

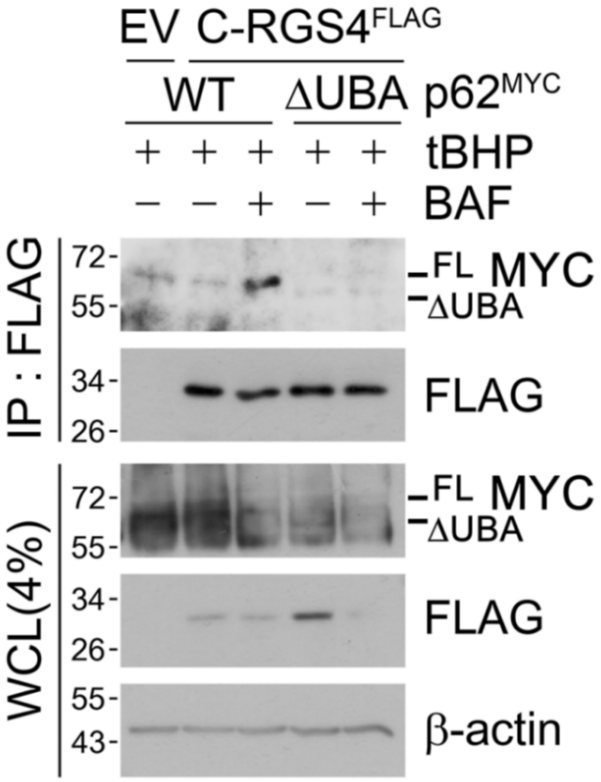

Figure 71. Nt-Cys substrate protein cannot binds to p62 without UBA domain. Co-IP of HEK293T cells expressing C-RGS4^{FLAG} and p62^{MYC} WT or p62^{MYC} ΔUBA and treated with tBHP (250 μM, 6h) with combination of BAF (200 nM, 6 h).

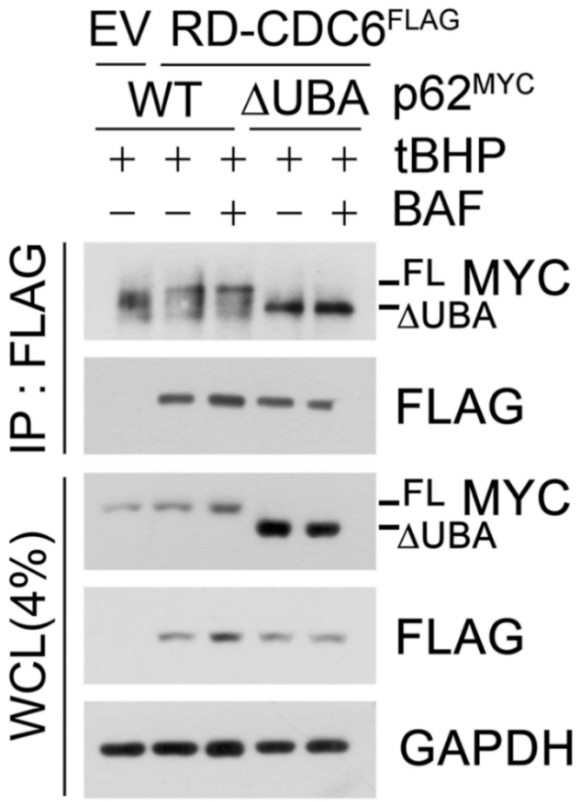

Figure 72. Autophagy targeted RD/N-degron substrate protein can bind to p62 even without UBA domain. Co-IP of HEK293T cells expressing RD-CDC6^{FLAG} and p62^{MYC} WT or p62^{MYC} ΔUBA and treated with tBHP (250 μM, 6h) with combination of BAF (200 nM, 6 h).

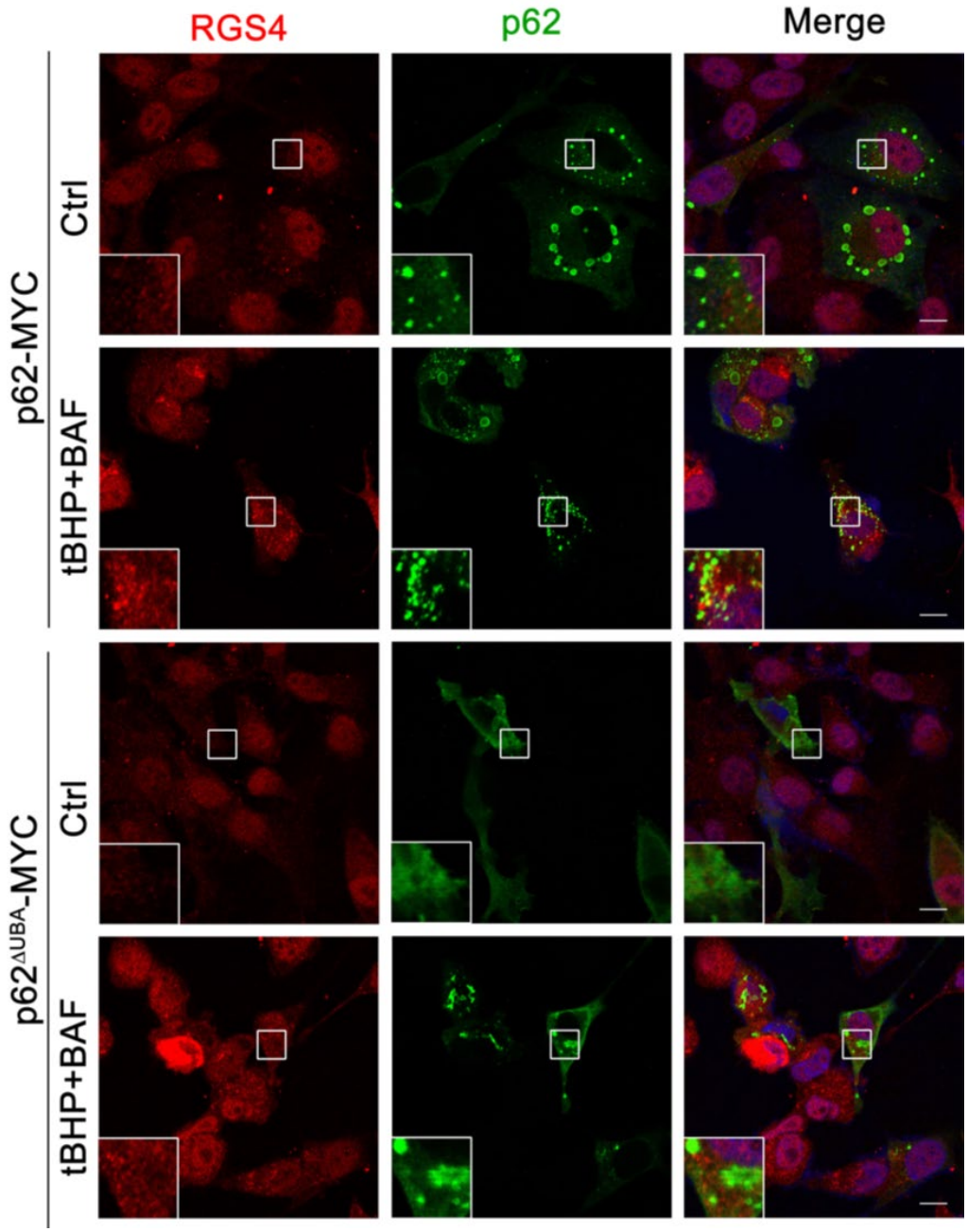

Figure 73. Autophagy targeted Nt-Cys substrate protein binds to p62 via UBA domain. ICC analysis of SH-SY5Y cells expressing $p62^{MYC}$ WT or $p62^{MYC}$ ΔUBA and treated with tBHP (250 μM, 6h) and BAF (200 nM, 6 h). Scale bar, 10 μm.

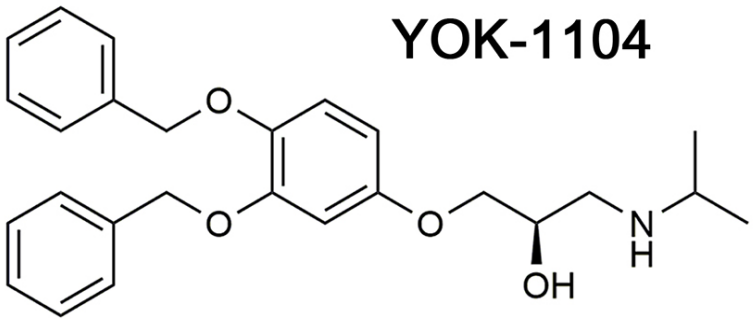

Figure 74. Chemical ZZ-ligand that mimics Nt-Arg. Chemical structure of the Nt-Arg mimic ZZ-ligand YOK-1104.

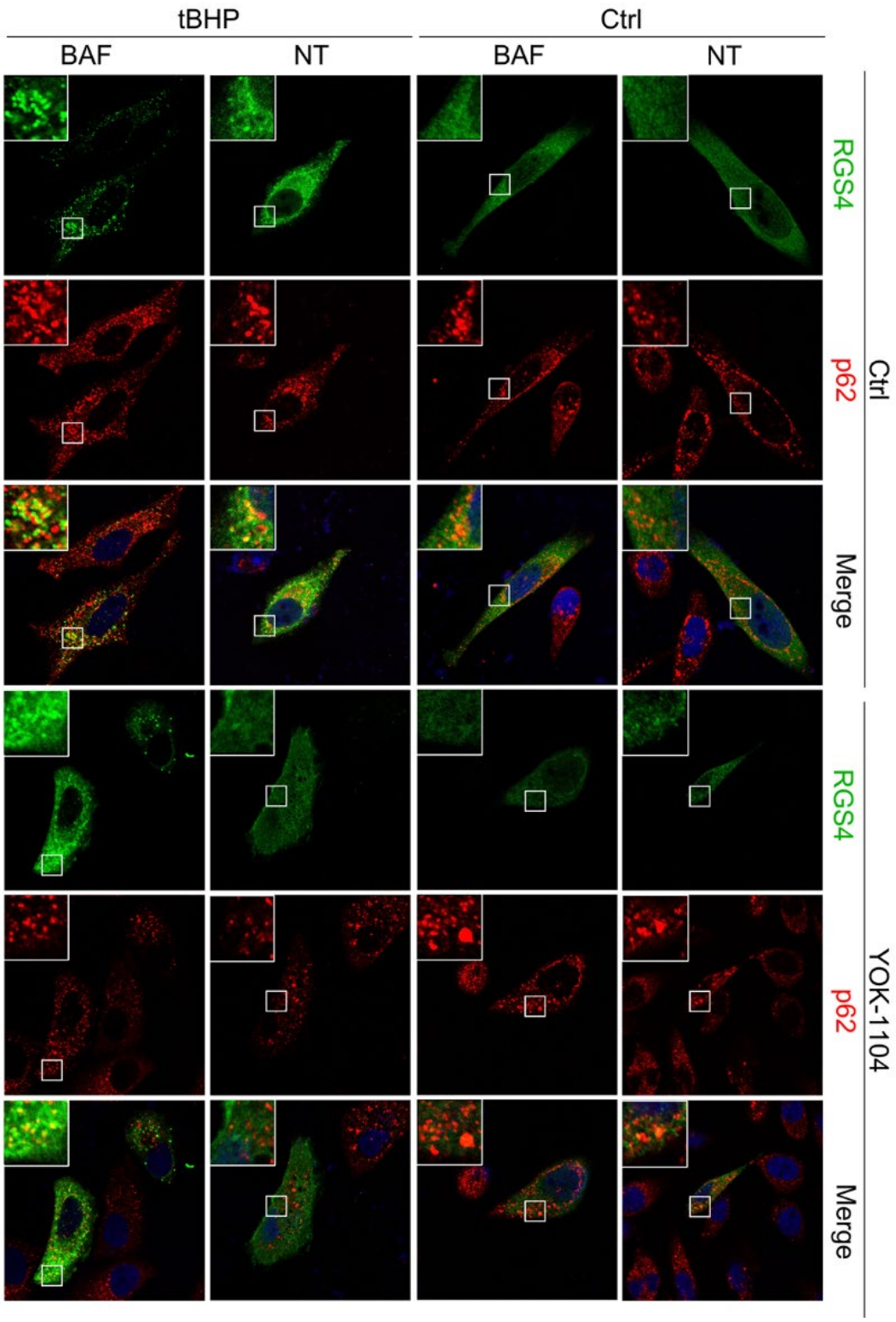

Figure 75. Chemical ZZ-ligand facilitates autophagic targeting of Nt-Cys protein under oxidative stress. ICC of SH-SY5Y cells treated with tBHP (250 μM, 6 h), BAF (200 nM, 6 h) and YOK-1104 (10 μM, 6 h).

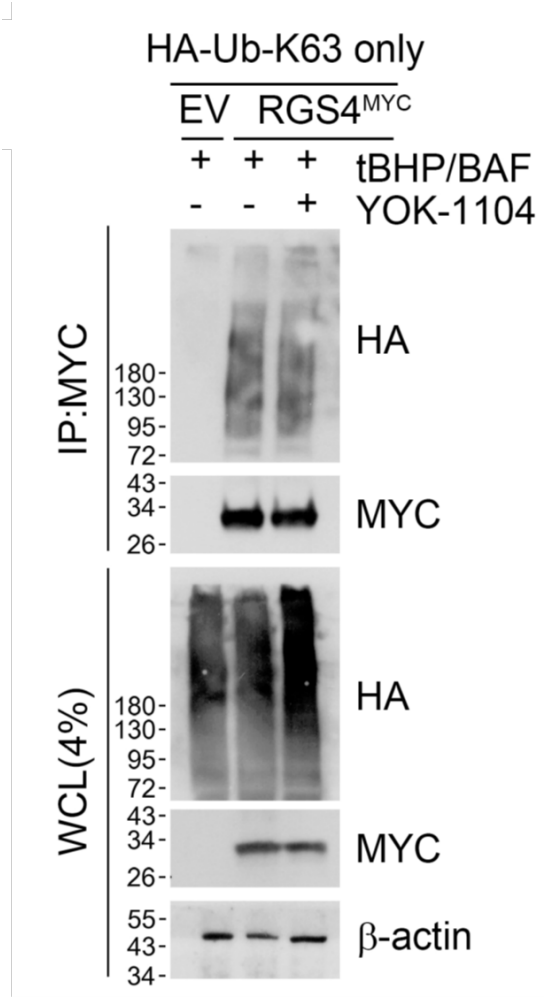

Figure 76. N-degron mimicking substrates do not alter KCMF1 activity.
Denaturation immunoprecipitation assay of the HEK293T cells transfected with RGS4MYC and HA-Ub-K63 only construct with co-treatment of tBHP (250 μM, 6 h) and BAF (200 nM, 6 h) and YOK-1104 (10 μM, 6 h).

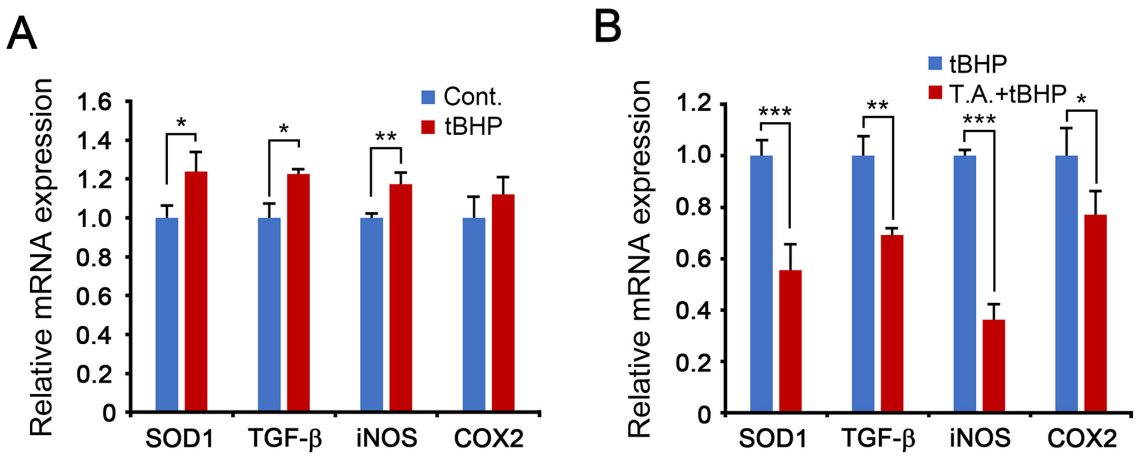

Figure 77. The Cys/N-degron pathway is required for cellular homeostasis in response to oxidative stress. (**A,B**) qRT assay of HEK293T cells treated with (**A**) tBHP(250 μM, 6 h), (**B**) in combination with tannic acid (35 μM, 24 h). **(C, D)** Same as **A** but exposed to **(C)** chronic hypoxia(1% O_2) **(D)** with combination of tannic acid (15 μM, 48 h).

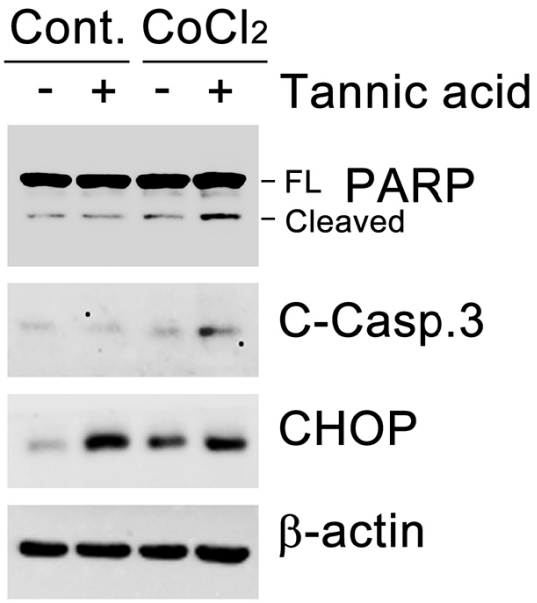

Figure 78. The Arg/N-degron pathway inhibition sensitizes cells to oxidative stress induced apoptosis. WB of HEK293T treated with $CoCl_2$ (250 μM) in combination of tannic acid (35 μM) for 24 h.

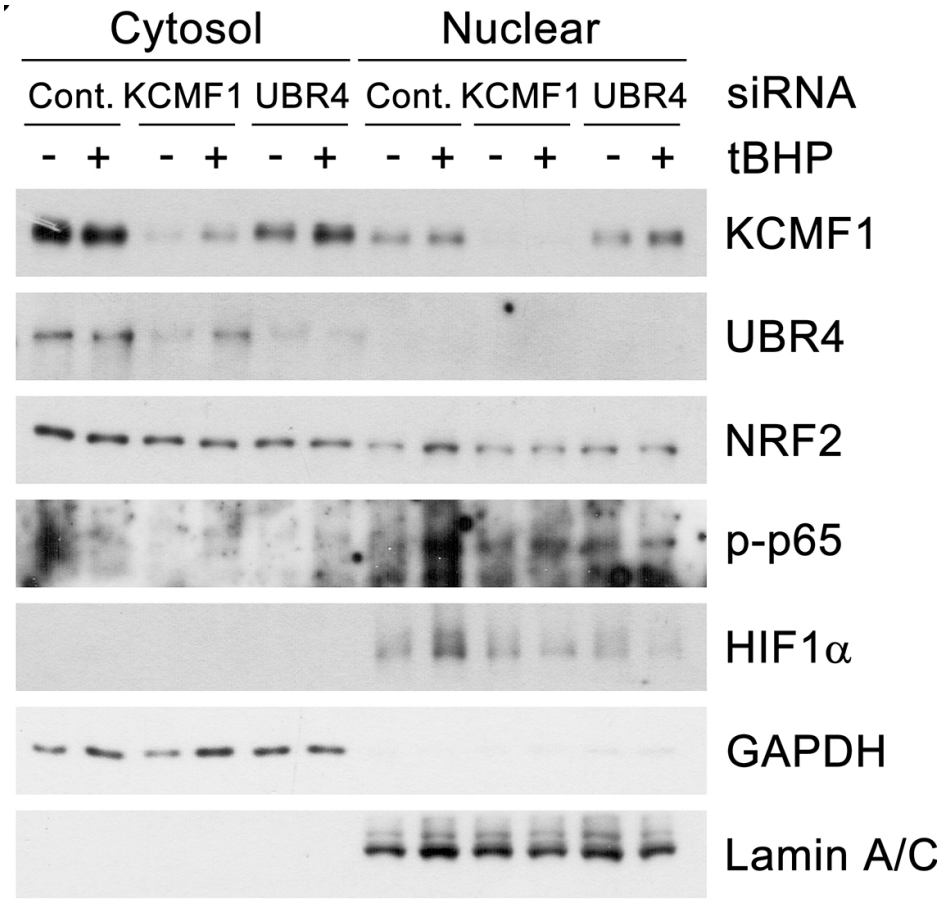

Figure 79. The Cys/N-degron pathway inhibition hinders nuclear translocation of the oxidative stress responsive transcription factor. Nuclear fractionation assay of HEK293T with *KCMF1* or *UBR4* interference treated with tBHP (250 μM, 6 h).

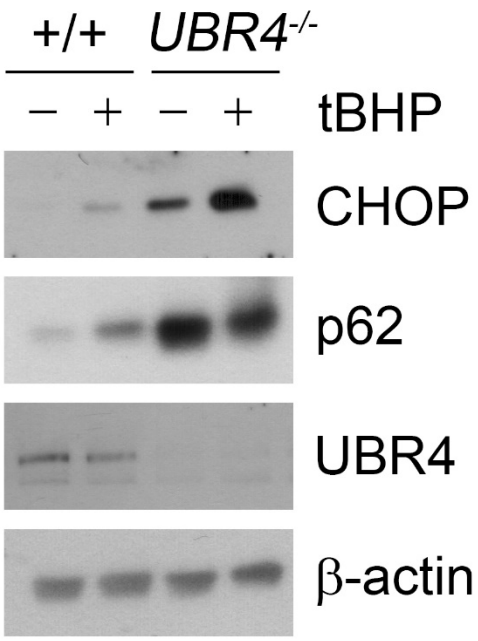

Figure 80. Genetic depletion of UBR4 sensitizes cells to oxidative stress. WB of WT or *UBR4*$^{-/-}$ MEFs treated with tBHP (250 μM, 6 h).

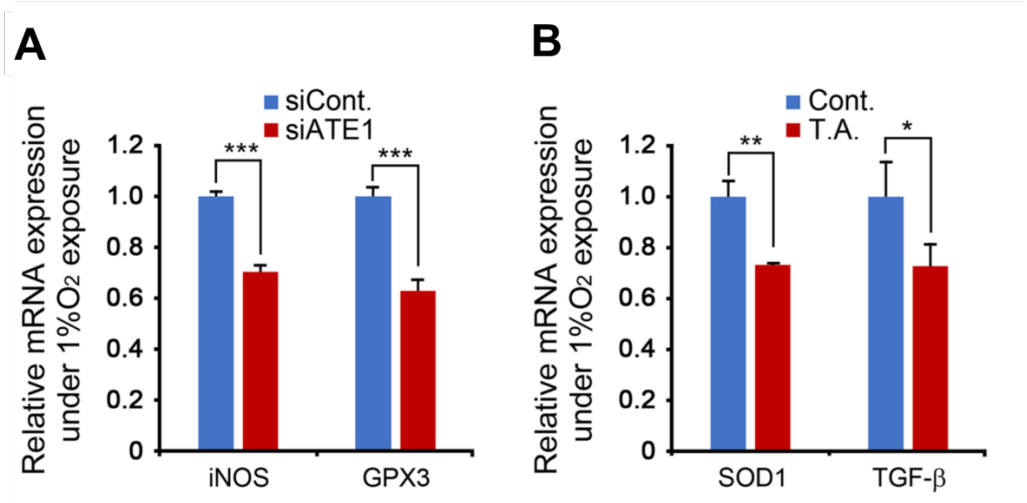

Figure 81. The Cys/N-degron pathway is required for cellular homeostasis in response to chronic hypoxia. (**A,B**) qRT assay of HEK293T cells treated with (**A**) chronic hypoxia (1% O_2, 48h) or (**B**) in combination of tannic acid (15 μM, 48 h).

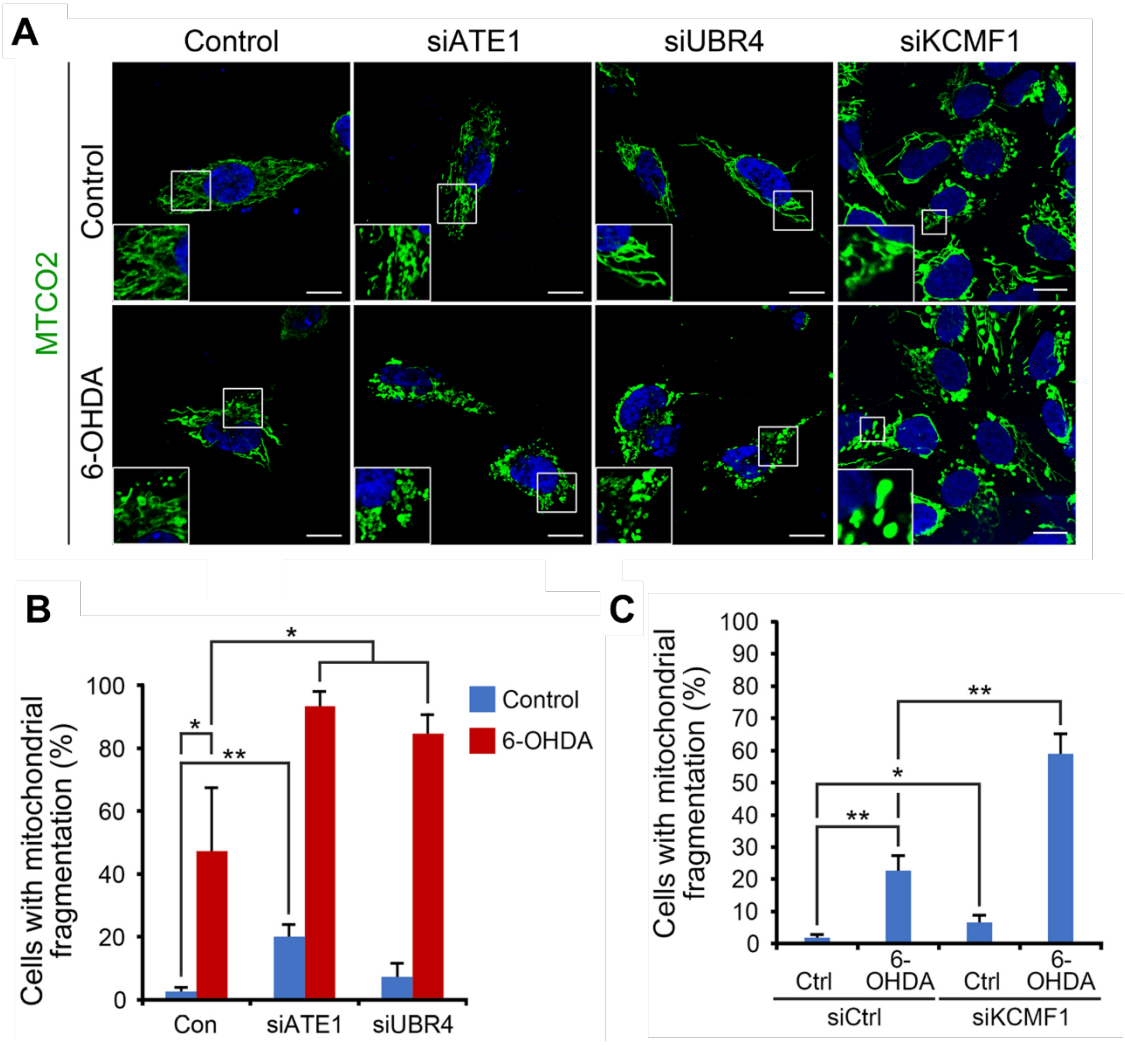

Figure 82. Genetic interference of Cys/N-degron pathway circuit sensitizes cells to oxidative stress induced mitochondrial fragmentation. (**A**) ICC of SH-SY5Y cells with *ATE1, UBR4,* and *KCMF1* interference followed by 6-OHDA treatment (50 µM, 6 h). Scale bar, 10 µm. (**B, C**) Quantification of **A** (n=50 or 100 cells, respectively).

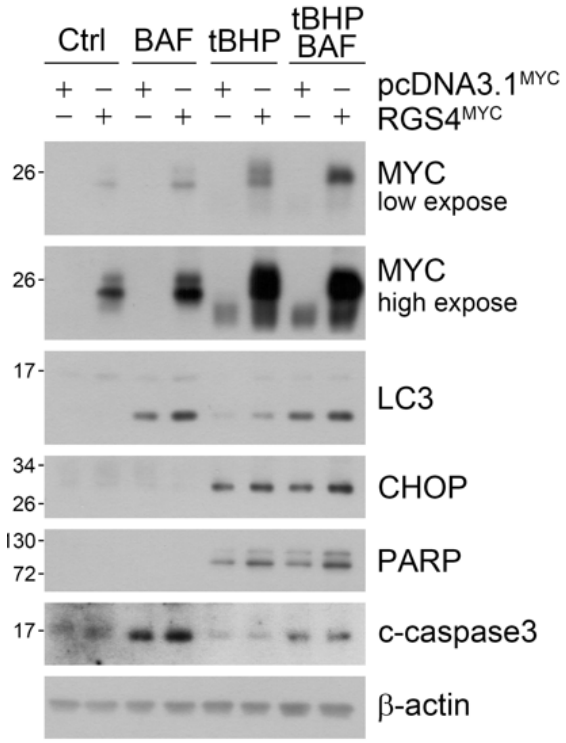

Figure 83. Accumulation of Cys/N-degron substrates sensitizes cells to oxidative stress induced apopotosis. WB of 293T cells with empty vector or $RGS4^{MYC}$ transfection followed by treatment of tBHP (250 μM, 6 h) and BAF (200 nM, 6 h).

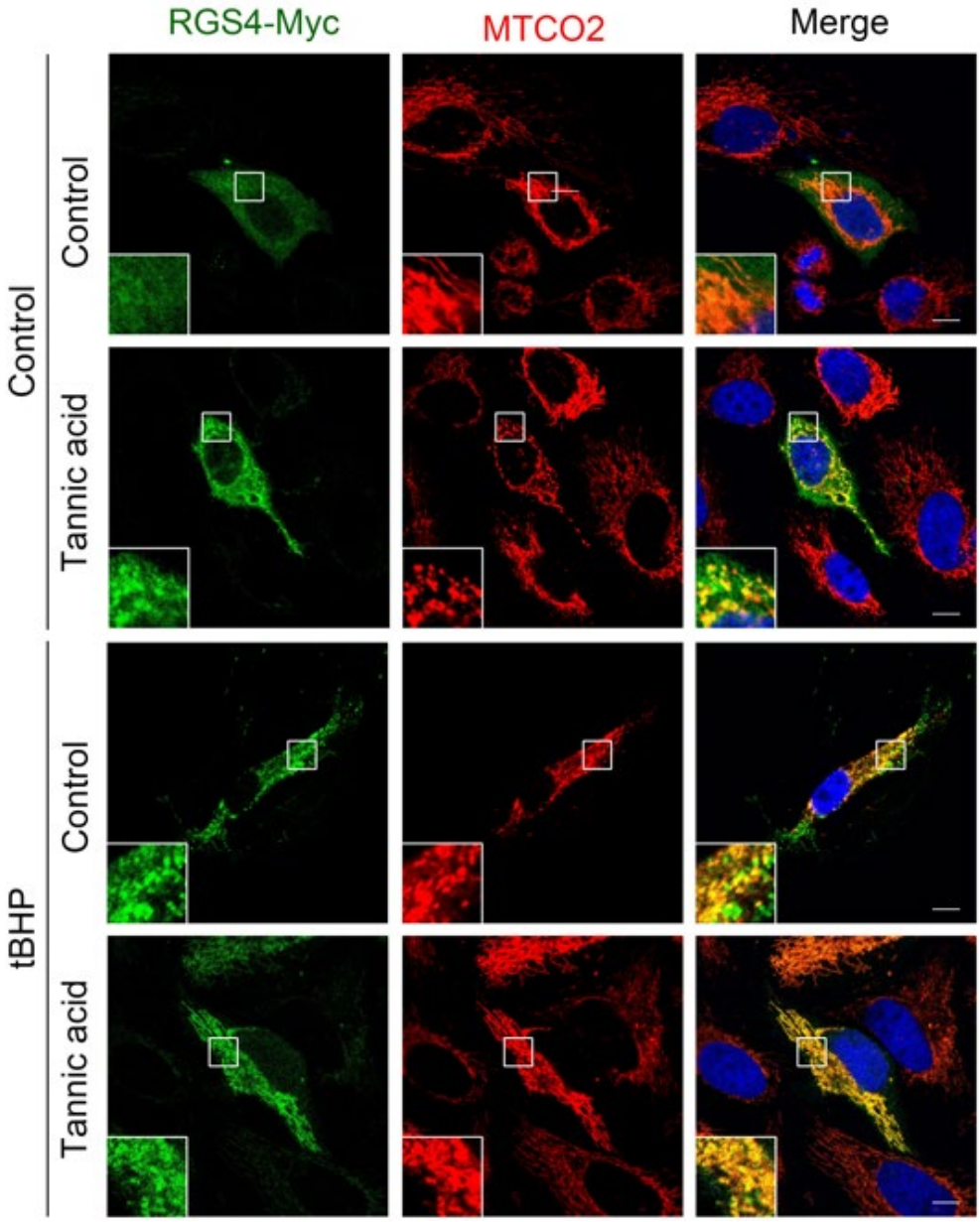

Figure 84. Inhibition of Arg/N-degron pathway leads to mitochondrial accumulation of Cys/N-degron substrates under oxidative stress. ICC of HeLa cells expressing $RGS4^{MYC}$ followed by treatment of tBHP (250 μM, 6 h), tannic acid (35 μM, 24 h) or both.

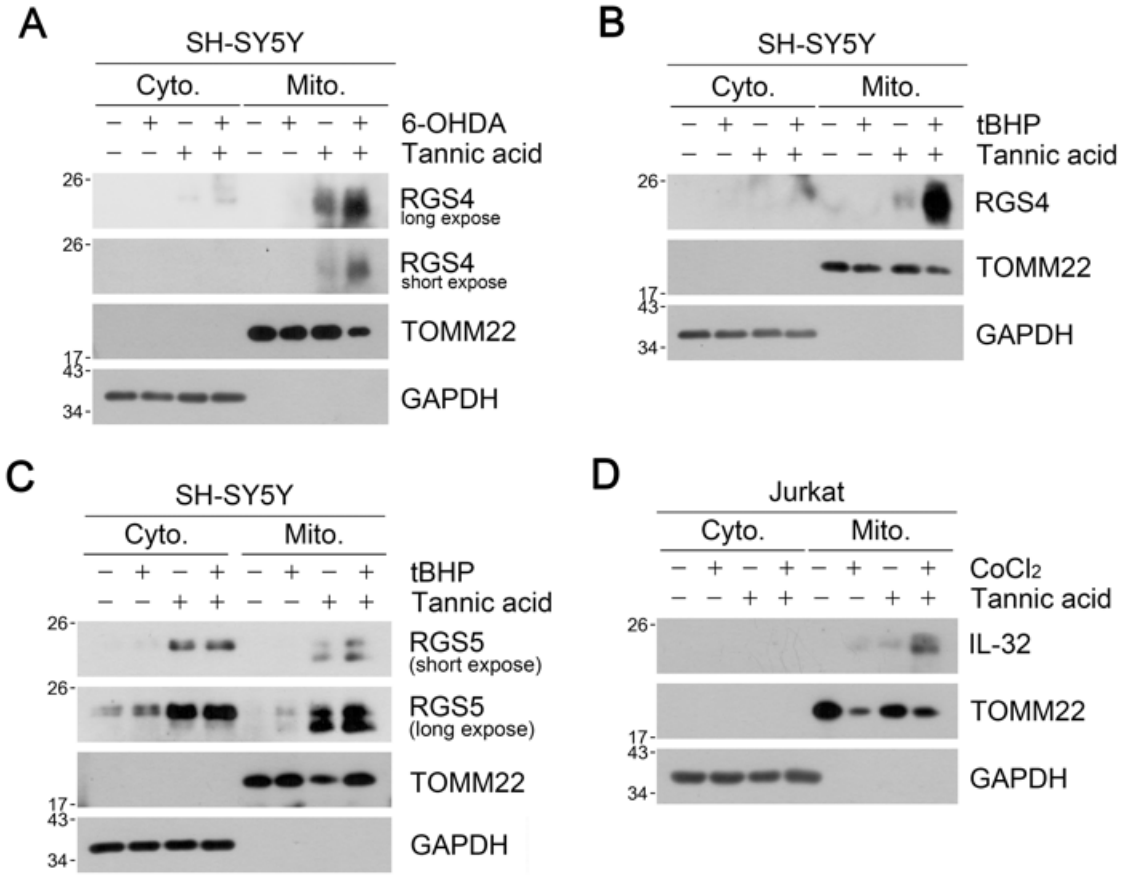

Figure 85. Inhibition of Arg/N-degron pathway leads to mitochondrial targeting of Cys/N-degron substrates under oxidative stress. (A) Mitochondrial fractionation of SH-SY5Y cells with treatment of 6-OHDA (50 μM, 6 h), tannic acid (35 μM, 24 h) or both. **(B, C)** Mitochondrial fractionation of SH-SY5Y cells with treatment of tBHP (250 μM, 6 h), tannic acid (35 μM, 24 h) or both. **(D)** Mitochondrial fractionation of Jurkat cells with treatment of $CoCl_2$ (250 μM, 6 h), tannic acid (35 μM, 24 h) or both.

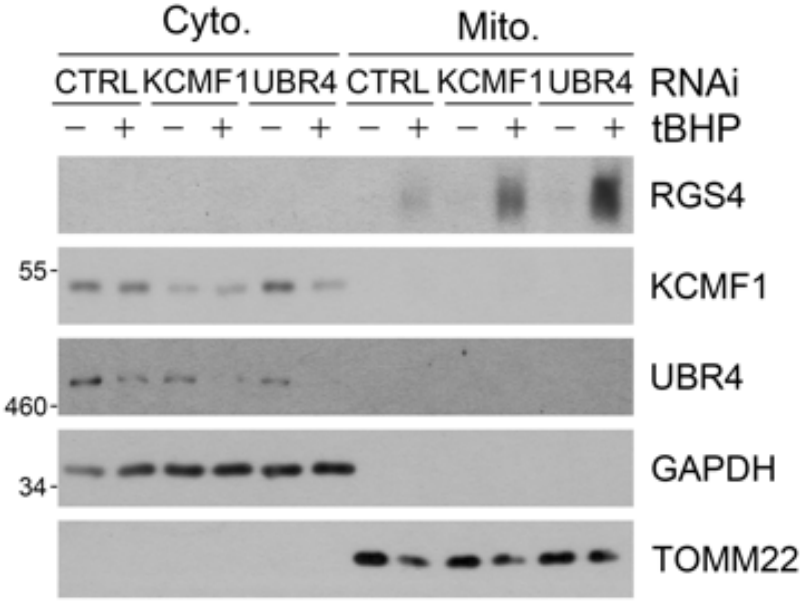

Figure 86. Inhibition of Cys/N-degron pathway circuit leads to mitochondrial targeting of Cys/N-degron substrates under oxidative stress. Mitochondrial fractionation of SH-SY5Y cells with *KCMF1* and *UBR4* interference followed by treatment of tBHP (250 μM, 6 h).

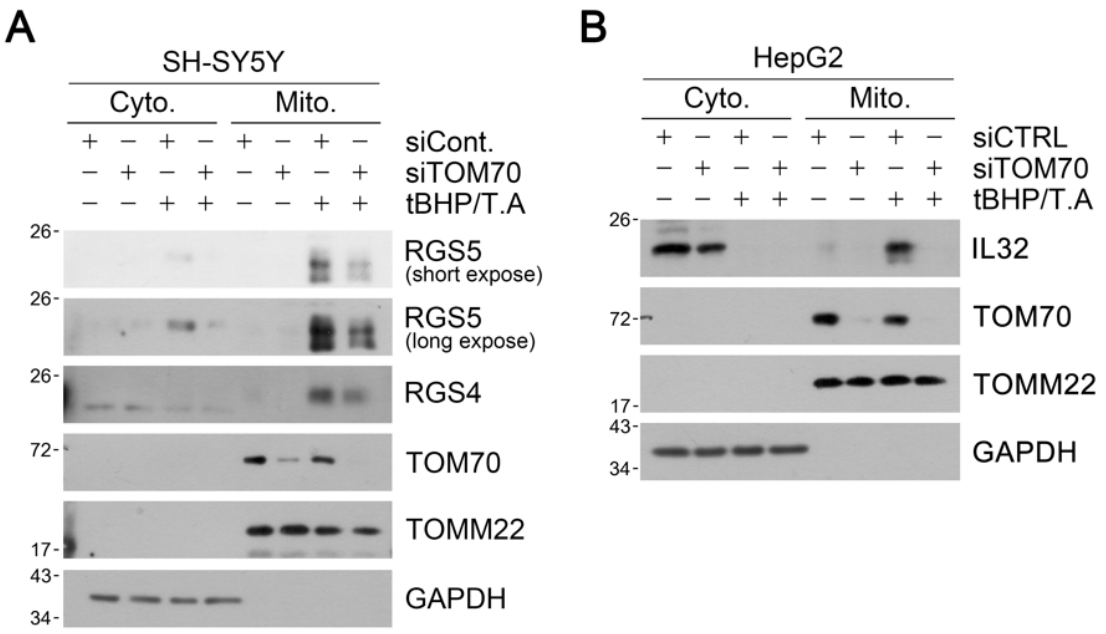

Figure 87. Cys/N-degron substrates targeting to mitochondria under oxidative stress is partly mediated by TOM70 transporter. (**A, B**) Mitochondrial fractionation of (**A**) SH-SY5Y cells or (**B**) HepG2 cells with *TOM70* interference followed by treatment of tBHP (250 μM, 6 h) and tannic acid (35 μM, 24 h).

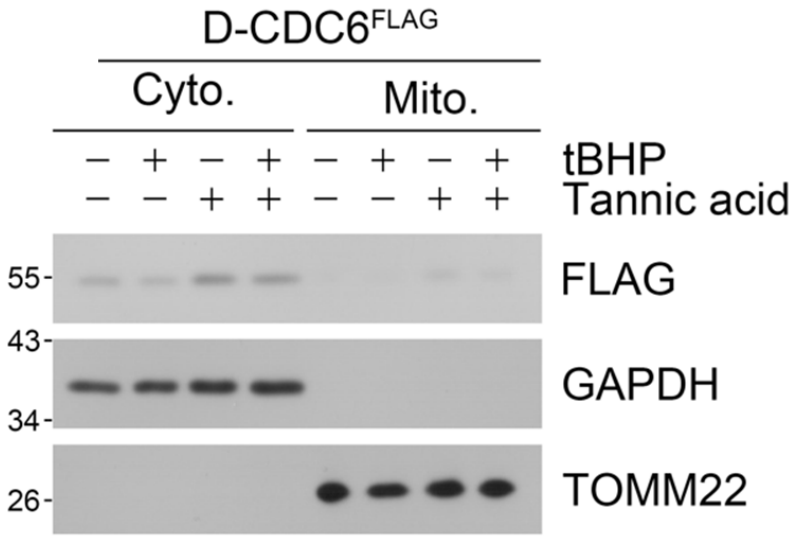

Figure 88. Inhibition of Arg/N-degron pathway does not target Asp/N-degron substrates to mitochondria under oxidative stress. Mitochondrial fractionation of 293T cells expressing D-CDC6^{FLAG} with treatment of tBHP (250 μM, 6 h), tannic acid (35 μM, 24 h) or both.

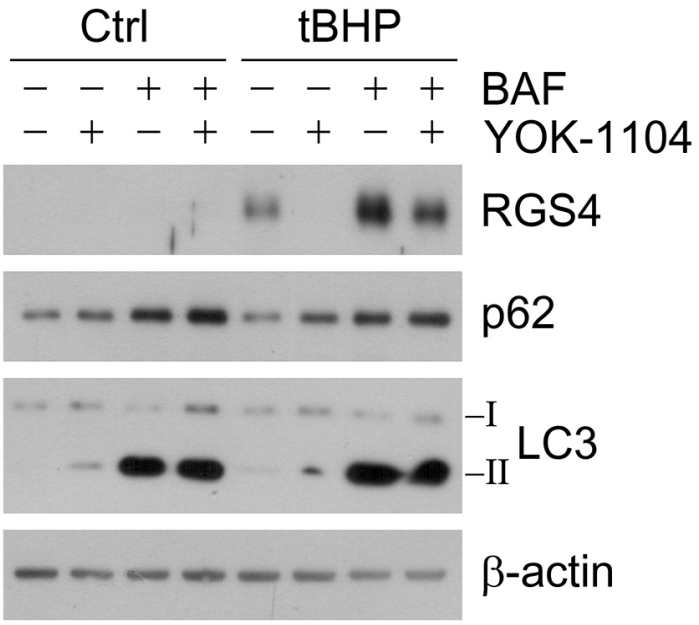

Figure 89. Activation of p62 via ZZ-ligand facilitates degradation of Cys/N-degron substrates under oxidative stress. (A) WB of SH-SY5Y cells treated with tBHP (250 μM, 6 h), YOK-1104 (10 μM, 6 h) and BAF (200 nM, 6 h).

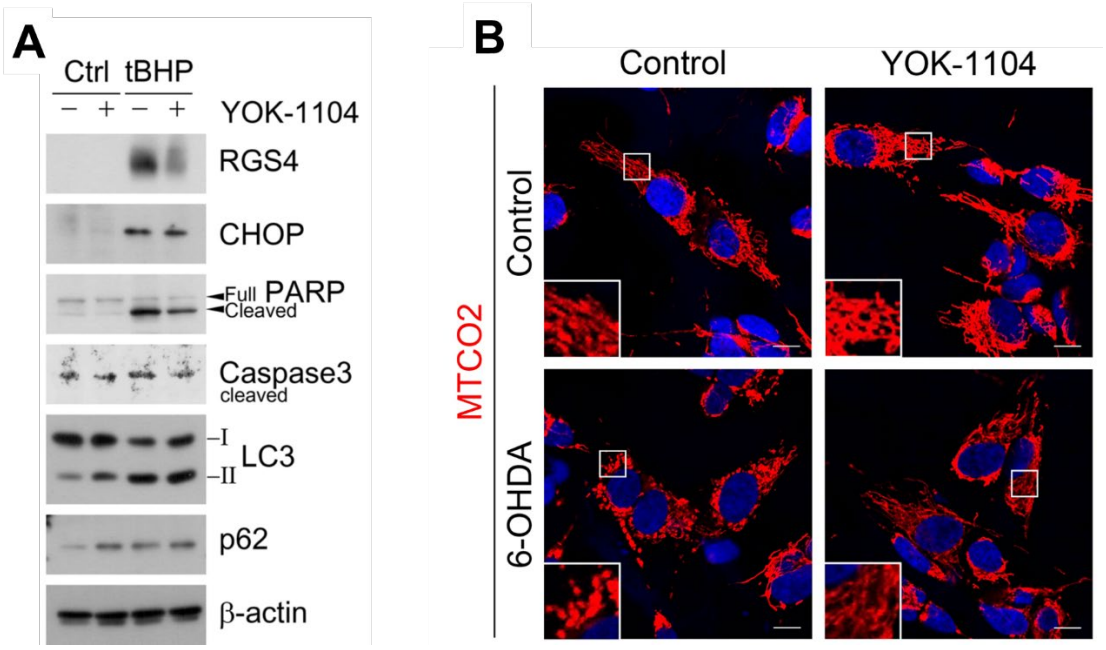

Figure 90. Facilitation of p62 via ZZ-ligand rescues cells from oxidative stress induced mitochondrial fragmentation and apoptosis. (A) WB of SH-SY5Y cells treated with combination of tBHP (250 μM, 6 h) and YOK-1104 (10 μM, 6 h) (**B**) ICC analysis with same conditions as **B** but with 6-OHDA (50 μM, 6 h). Scale bar, 10 μm.

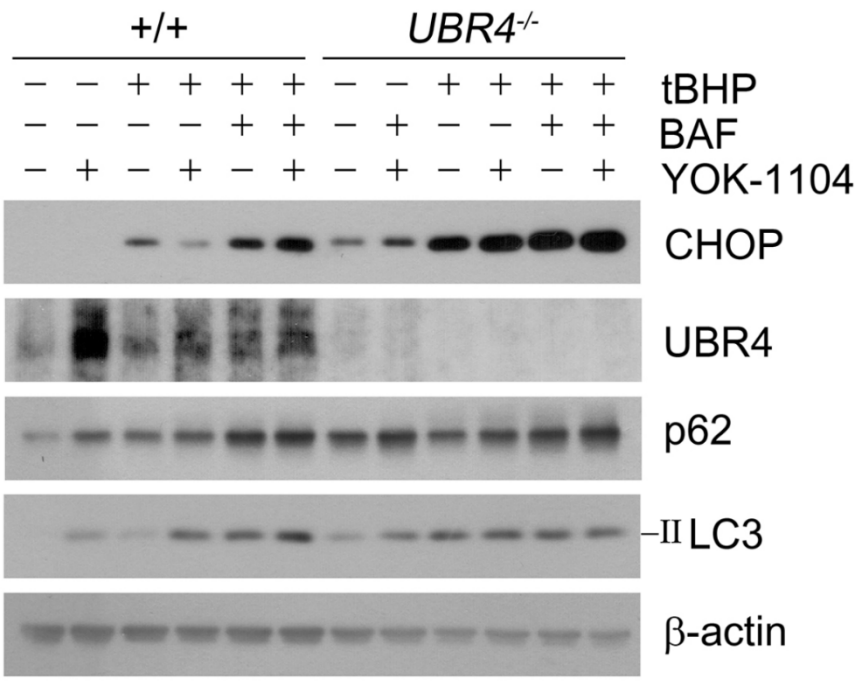

Figure 91. ZZ-ligand cannot rescue cells from oxidative stress induced apoptosis with defect on upstream Cys/N-degron circuit. WB of WT or *UBR4*$^{-/-}$ MEFs treated with a combination of treated with tBHP (250 μM, 6 h),YOK-1104 (10 μM, 6 h) and BAF (200 nM, 6 h).

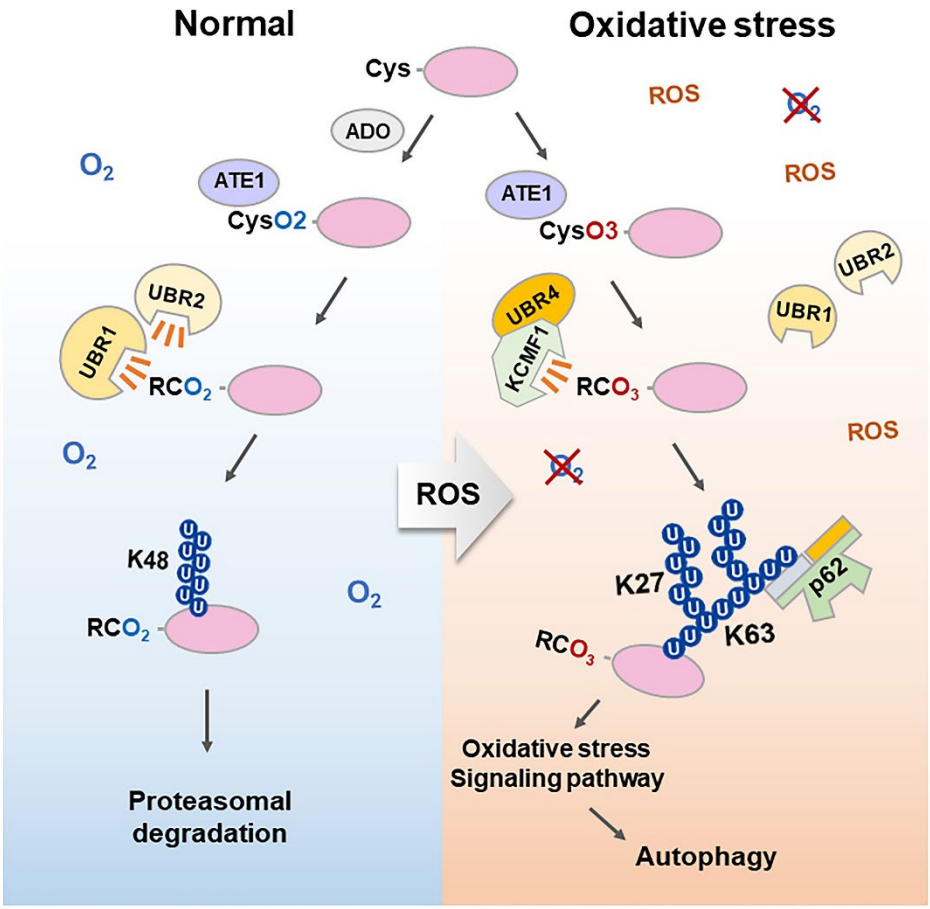

Figure 92. Schematic illustration of the Cys/N-degron-mediated cellular oxygen/oxidative stress sensing and signaling pathway.

	O_2		Reactive oxygen species	
	Normal Normoxia	Stress Hypoxia / Anoxia	Normal Low [ROS]	Stress High [ROS]
Oxidation status of Nt-Cys	CysO2 cysteine sulfinic acid	Cys → CysO3 Cysteine sulfonic acid	CysO2 cysteine sulfinic acid	CysO3 cysteine sulfonic acid
Mechanism of oxidation	Enzymatic	Nucleophilic	Enzymatic and nucleophilic	Nucleophilic
Stability	Short-lived (normal half-life)	Long-lived (degradation impaired, longer half-life)	short-lived (normal half-life)	Long-lived (longer half-life)
Fate of degradation	UPS	Autophagy	UPS	Autophagy
Ubiquitin chain	K48-linked	K63/K27-linked	K48-linked	K63/K27-linked

Figure 93. Mechanism of the oxygen homeostasis via the Cys/N-degron pathway. Summary of the post-translational modifications and degradation mechanisms of Cys/N-degron substrates in oxygen stress-induced versus basal conditions.

Discussion

Fluctuating levels of oxygen-containing molecules (e.g., O_2^- and H_2O_2). In this study, we show that the Cys/N-degron pathway functions as a sensor for both acute and chronic hypoxia as well as oxidative stress. In this bimodular sensing system, the Nt-Cys residues in the presence of O_2 is enzymatically oxidized by ADO1 and arginylated into the proteasomal N-degron R-CO_2, leading to acute proteolysis via K48-linked ubiquitylation. When cells encounter hypoxia, Cys/N-degron substrates cannot be readily oxidized and metabolically stabilized to adjust signaling pathways. However, if hypoxia is prolonged, the Nt-Cys residue is chemically oxidized by ROS to generate the autophagic N-degron R-CO_3 which enables cells to eradicate otherwise non-degradable substrates. Through this dual mechanism, the Nt-Cys residue acts as a common acceptor for O_2 and ROS in response to various O_2 dysregulations, generating two structurally distinct N-degrons that induce proteolysis via the UPS or autophagy, depending on the nature of O_2 stress and duration (Figure 92, 93).

In mammals, the HIF-1-based O_2 sensing system is known to regulate stress responsive pathways under hypoxia (39). In this O_2 sensing system, metabolically stabilized HIF-1 migrates into the nucleus to induce the transcription of hypoxia-responsive proteins. The resulting hnRNAs are processed into mRNAs, which in turn are transported back to the cytosol and used for translation on the ER. The nascent polypeptides discharged from the ribosome are folded, migrate to their designated sites to participate in cellular stress responses. However, this chronic sensor of hypoxia typically requires at least 2-4 hours for the cell to respond to hypoxia, one outstanding question had been how cells sense and react to rapidly changing O_2 levels. Our earlier work has identified the Cys/N-degron pathway as a sensor of O_2 and NO which modulates the half-life of RGS4 through Nt-Cys oxidation under basal condition (51,

52). In this mechanism, RGS4 is 'co-translationally' stabilized under hypoxia and migrates to the plasma membrane, exerting its functions in 2-3 min. There is now an increasing consensus that mammalian cells send O_2 through the Cys/N-degron pathway and the HIF signaling. In this study, we asked how metabolically stabilized RGS4 can be degraded if hypoxia is prolonged, despite the inability of its Nt-Cys to be oxidized. Our finding that the chemical oxidation of Nt-Cys by ROS under prolonged hypoxia and oxidative stress provides a comprehensive understanding on how cells adopt to the transition of transient hypoxia to chronic hypoxia. Given that the Met-Cys motif represents about 2% of the entire human proteome, the Nt-Cys degron may provide a wide-ranging means for cells to maintain O_2 homeostasis.

In mammals, proteins are mainly degraded by the UPS or autophagy. To date, little is known about selectivity in proteolytic flux into either of the two distinct degradative pathways. Our results show that in normoxia, the canonical N-recognins UBR1 and UBR2 preferentially bind the R-C^{O2}, inducing K48-ubiquitylation and proteasomal degradation (46, 49). However, under chronic hypoxia, the R-C^{O3} is selectively recognized by KCMF1, a novel N-recognin identified in this study. KCMF1 binds R-C^{O3} through its ZZ domain, which shares sequence similarity with the UBR box of UBR1 and the ZZ domain of the autophagic N-recognin p62. Upon binding to the R-C^{O3}, KCMF1 induces K63-ubiquitylation, followed by UBR4-mediated K27-ubiquitylation. Thus, reprograming of the Ub code from K48-ubiquititination by UBR1 and UBR2 to K63/K48-ubiquitylation by KCMF1 and UBR4 redirect Cys/N-degron substrates from the UPS to autophagy. One remaining question to be addressed concerns the topology of K27-, K63- and K48-linked Ub chains assembled on Cys/N-degron substrates. Given that UBR4 is known to assemble branched Ub chains (27, 30), K27-linked Ub chains may conjugate to already assembled K63-Ub chains ligated by KCMF1 as a branched chain conformation. Such possibility of a branched K63/K27-Ub

chain may explain our previous finding (48, 77) that p62 functions as an N-recognin only for Nt-Arg-Asp/Glu substrates but not for Nt-Cys substrates, which instead interact with the KCMF1-ZZ domain. It also remains to determine if the ZZ domain, in not only p62 and KCMF1 but also many other types of proteins, represents a generally applicable stress-specific N-recognin motif for cellular responses to said stresses.

Another possibility is that the sulfonic acid group, in contrast to the sulfinic acid group, on the Nt-Cys2 residue poses too much of a steric hindrance for the p62-ZZ domain. It will be interesting to investigate the structural and biological differences for Nt-Arg-binding ZZ domains and their substrate proteins depending on the identity of the secondary N-degron following Nt-Arg residue.

Maintenance of proteostasis, usually achieved by protein quality control systems such as ER-associated protein degradation (ERAD) or aggrephagy, is challenged by a variety of environmental stresses such as oxidative stress and the subsequent cellular responses(81). Specifically, oxidative stress is critically linked to the pathogenesis of neurodegenerative, cardiovascular, and metabolic disorders among others in part due to mitochondrial damage(82-86). A recent study showed that cytosolic and mitochondrial proteostasis are interlinked due to translocation of cytotoxic misfolded proteins and their aggregates to within the mitochondrial lumen, where they are degraded by mitochondrial proteases during a process termed MAGIC (mitochondria as a guardian in cytosol)(80). However, this protein quality control system acts as a double-edged blade in that excessive import of these pathological protein species can overload the mitochondrial degradation capacity. Given that ROS can not only directly destabilize mitochondria but also generate cytotoxic, mitochondria-translocated protein species, amelioration of oxidative stress is of paramount importance and a major therapeutic target (82). In this study, we show that the ATE1-KCMF1-UBR4 circuit promotes mitochondrial homeostasis and

cytoprotection under oxidative stress via degradation of Nt-$CysO_3$ substrates that are specifically accumulated within the mitochondrial lumen if un-oxidized/arginylated. Moreover, by using a synthetic ligand to the ZZ domain of p62 (YOK-1104) to accelerate the autophagic turnover of Nt-$CysO_3$ substrates, we rescued neuronal cells from oxidative stress-induced mitochondrial damage and subsequent apoptosis, which are the critical causes of various neurodegenerative disease including PD. Although the general efficacy of the p62-ZZ ligand requires further evaluation, it will be intriguing to test the therapeutic potential of synthetically accelerating the Cys-Arg/N-degron pathway for a myriad of mitochondrial deterioration and oxidative stress-related disorders, particularly in neurons where the damage is irreparable.

Chapter 2

The Arg/N-degron Pathway Regulates Oxidative Stress Induced Exocytosis

Introduction

For intercellular signaling, cell-to-cell communication via transfer of macromolecules to both adjacent and distant cells is essential. Stable proteins and chemicals, such as hormones, cytokines, and insulin can be directly secreted to distantly located cells via regulated exocytosis, which involves the fusion of intracellular secretory vesicles to the plasma membrane. Yet, to ensure stable delivery of the various types of the signaling molecule, cells also release a stable and protective vesicular envelop enclosing a wide variety of molecules including proteins, nucleic acids, amino acids, and metabolites via exocytosis (Figure 4).

Until recently, contributed by numerous studies regarding synaptic vesicle release, how to secrete protein and signaling molecules to extracellular space via regulated and constitutive exocytosis were major target for research. However, emerging interest for its clinical application such as diagnostic biomarkers and therapeutic cargo carriers, exosomes are getting attentions. Exosomes are part of extracellular vesicles released by cells from prokaryotes to eukaryotes. Enclosed by lipid bilayer membrane, exosomes are highly biocompatible and anti-immunogenic, which properties enabling the exosomes to become a highly effective vector system for covering long distance and large area of target cells.

Categorized by vesicular size, the distinct mechanisms of exocytosis are categorized into large plasma membrane-derived ectosome secretion or multivesicular body (MVB)-derived smaller sized exosome secretion, ranging up to 1 μm and 150 nm, respectively. Considered as originated by endocytic vesicles, exosome biogenesis is driven by the invagination of MVB membranes to generate intraluminal vesicles (ILV) encasing cytosolic proteins, nucleic acids and other signaling molecules. ILV generation can occur in an ESCRT (endosomal sorting complex required for transport)-dependent or

ESCRT-independent manner. Recent knowledge on ILV biogenesis and secretion is mainly focused on the role of the four distinct ESCRT complexes. First, ESCRT-0 forms a protein network on endosomal membranes (87, 88) then ESCRT-I binds to both ESCRT-0 and ESCRT-II for marking the site of nucleation for the ILV formation along with ESCRT-III recruitment (89, 90). Lastly, ESCRT-III, recruited by ESCRT-II, is responsible for physical membrane deformation induced by complex of Vps20, Snf7, Vps24, Vps22 and eventual vesicle abscission by AAA ATPase, VPS4 (91-94).

ILV formation is also mediated by ESCRT independent manner, especially in higher eukaryotes including mammalian cells. The ESCRT independent ILV formation is enabled by the difference in lipid composition of the membrane. Specifically, this non-cannonical pathway is known to be driven by the lysobiphosphatidic acid (LBPA) and ceramides, a critical component of lipid-raft formation, thereby enabling the physical inward deformation of the membrane to form vesicles inside MVB. Other than involvement of lipid component to this venting motion, this non-cannonical ILV forming mechanism is not elucidated in such detail. Moreover, the exact mechanisms and key players on how exosome release is stimulated under oxidative stress and which cue prompts biogenesis of ILV have not been investigated. Specifically, how, and why ILV containing MVBs are targeted to plasma membrane needs to be elucidated.

Results

Impaired Arg/N-degron pathway leads to failure on cellular synchronization for oxidative stress induced anti-inflammatory response

I then investigated how this intracellular oxidative stress response signaling impacted intercellular signaling. Among the four basic types of cell-to-cell signaling, namely paracrine, autocrine, endocrine and direct contact, the transfer of signaling molecules such as proteins occurs by exocytosis from the donor cell. Exocytosis is further canonically classified as constitutive or regulated, depending on calcium ion, cAMP, diacylglycerol, phospholipid, or ATP-induced trigger (95, 96). While the exact mechanisms and regulators mediating either constitutive or regulated exocytosis have been relatively well-identified, the same cannot be said for a third pathway, namely exosome release. Thus, given that the impairment of the Cys/N-degron pathway down-regulated expression of intracellular antioxidant genes, I hypothesized that the oxidative stress-induced transcriptional regulation of inflammation-associated genes and the subsequent cell-to-cell communication cascade would also be mediated by the Arg/N-degron pathway. As impaired Cys/N-degron pathway showed unconventional decrease of intracellular antioxidant gene expression, I also investigated inflammatory gene induction under oxidative stress.

As I expected, genetic knockdown of ATE1 upregulated the expression of pro-inflammatory cytokines IL6, IL8, IL32, and TNF-α not only under basal condition but also under oxidative stress (Figure 94). To directly test Cys/N-degron-dependent cell-to-cell communication via exosome release under oxidative stress, I purified exosomes from stressed donor cells and re-distributed to unstressed recipient cells. Surprisingly, while the expression levels of inflammatory genes within the recipient cells were down-regulated after treatment of exosomes purified from tBHP-treated cells, they were

drastically up-regulated by the same treatment but with donor cells under siRNA-mediated *ATE1* interference (Figure 95). To investigate whether this effect was induced by N-degron pathway dependent-exosome release, exosomes from donor cells under oxidative stress and genetic interference or chemical inhibition of ATE1 exhibited lower levels of Alix/Bro1 and TSG101/VPS23 (Figure 96A, 96B), the exosome lumenal marker proteins. Moreover, tBHP exposure resulted in greater levels of secreted Alix and TSG101 found in the exosome fraction, which was abolished by genetic interference of *ATE1* (Figure 97A, 97B). To confirm the functional role of ATE1-mediated Nt-arginylation in exosome secretion, secreted exosome luminal proteins were quantified upon transient expression of the ATE1 isoforms. Overexpression of the ATE1 isoforms, specifically ATE1^{1B7A}, increased both the secretion and the flux of exosome release of the Alix protein under oxidative stress (Figure 98A, 98B). These results suggest that ATE1-mediated Nt-arginylation mediates intercellular signaling via regulation of exosome release.

RILP is cleaved and arginylated under oxidative stress to mediate exosome secretion

To investigate the exact mechanisms by which ATE1-mediated Nt-arginylation regulated exosome release, a series of putative Nt-arginylation substrate candidates that could modulate exosome formation and/or release were examined. Rab interacting lysosomal protein (RILP), a Rab7 adaptor interacting with dynein-dynectin for negative-end directed movement of lysosomes, is an oxidative stress-activated inflammatory caspase-1 substrate. Recent studies indicated that RILP can mediate cellular trafficking upon caspase-1 mediated cleavage at D75. Similarly, I observed that treatment of inflammation-linked oxidative stress inducers such as tBHP and $CoCl_2$ induced cleavage of RILP (Figure 99). Considering that the P1 residue exposed upon caspase-1 mediated cleavage is Asp, a secondary N-degron, C-terminal RILP fragment was further tested for a putative substrate for arginylation. Indeed, tBHP induced cleaved C-terminal fragments

of RILP were further stabilized upon chemical inhibition of Nt-arginylation, indicating that RILP is indeed an Nt-arginylation substrate upon caspase-1 mediated cleavage (Figure 100).

To determine the role of the Nt-arginylated C-terminal fragment of cleaved RILP, the N-terminally arginylated form of the D75 cleaved RILP (RD-RILP), D75 cleaved RILP (D-RILP), and D75V cleaved RILP (V-RILP) were cloned into pcDNA3 vector using the ubiquitin fusion technique (Figure 33). While transiently expressed D-RILP was more stable than its Nt-arginylated form, RD-RILP (Figure 101A), it displayed heightened sensitivity to tannic acid-induced inhibition of Nt-arginylation (Figure 101B) and to MG132-induced proteasome inhibition as well (Figure 101C).

Loss-of-function analysis of RILP showed reduced exosome secretion upon oxidative stress exposure (Figure 102). In visualizing the function of the Nt-arginylated C-terminal fragment of RILP I performe dimmunocytochemistry analysis of the various URT recombinant species of full-length RILP ($RILP^{MYC,FLAG}$, $D\text{-}RILP^{FLAG}$, and $RD\text{-}RILP^{FLAG}$). I observed that while full-length RILP was found to aggregate around the MTOC, D- and RD-RILP were found evenly distributed throughout the cytosol (Figure 103). Notably, transient overexpression of caspase-1 increased the levels of Alix and TSG101 found in released exosomes (Figure 104), suggesting that RILP regulates exosome secretion upon oxidative stress in an Arg/N-degron-mediated manner.

Arginylated RILP mediates MVB trafficking toward plasma membrane with the association of ARL8B

Although a previous study reported that full-length RILP possesses N-terminal dynein-dynactin, a minus end-directed motor protein binding region (97), other studies have shown that RILP may interact with the small G protein ARL8 to link the lysosome with kinesin, the plus-end-directed motor protein in *Drosophila* (98). Thus, I expected

that the C-terminal fragment of cleaved RILP could function as an intermediate adaptor protein that interconnects intraluminal vesicles (ILV), containing MVBs, via kinesin motor protein interaction upon oxidative stress. HeLa cells transfected with full-length RILP and ARL8b showed mutually exclusive localization (Figure 105A) but showed co-localization for cleaved RILP and ARL8b (Figure 105B). Co-immunoprecipitation assay showed that RD-RILP binds to ARL8b while D-RILP could not (Figure 106A). Moreover, D-RILP interaction with ARL8b was strengthened upon tBHP exposure, whose interaction was diminished upon tannic acid-mediated inhibition of Nt-arginylation (Figure 106B). These results indicate that oxidative stress drives Nt-arginylation-dependent interaction of C-terminal RILP fragment with ARL8.

Additionally, immunocytochemistry assays showing co-localization of D-RILP with CD81 unaffected by *ATE1* interference confirmed that the D-RILP-positive punctate structure is indeed a MVB (Figure 107). This result indicates that the targeting of the MVB to the plasma membrane is mediated by stress-induced RILP cleavage and Nt-arginylation for subsequent exosome release.

Inhibition of ATE1 impairs ILV formation within MVB

To further examine the function of ATE1-mediated Nt-arginylation in exosome secretion, the morphology of MVB was examined via MVB membrane-localized cleaved D-RILP. Immunocytochemical analysis showed the formation of enlarged donut-like structured vesicular shapes positive for D-RILP upon genetic interference of *ATE1*, which was in stark contrast to the conventional puncta structure in the control group (Figure 108A, 108B). Moreover, transmission electron microscopic images of *ATE1*$^{-/-}$ MEF cells and *ATE1*-interfered A549 cells clearly showed both the increased size of MVBs and diminished numbers of ILV contents within (Figure 109, 110). Enlarged MVBs with reduced numbers of ILVs imply that excess membrane supply was provided by impaired

ILV biogenesis. Furthermore, immunoprecipitation assay showing Nt-Arg-specific interaction of RD-RILP with VPS22, an MVB-localized ESCRT-II protein, suggested a possibility of Nt-arginylated RILP dependent formation of the ILV via ESCRT machinery (Figure 111). Collectively, these results indicate that ATE1-mediated Arg/N-degron pathway regulates exosome secretion via modulation of the ILV biogenesis and MVB trafficking.

Arg/N-degron pathway exacerbates cancer metastasis via exosomal secretion of Annexin A1

To elucidate the physiological substrates of the Arg/N-degron pathway-dependent exosome secretion, mass spectrometry analysis was performed on purified exosomes secreted from donor cells under oxidative stress and genetic interference of *ATE1*. As expected, mass spectrometry analysis confirmed our previous findings of accelerated exosome secretion upon exposure to oxidative stress (Figure 112A). However, ATE1 depletion under the same conditions drastically abolished and even inhibited exosome secretion (Figure 112A). Specifically, I identified Annexin A1 (ANXA1), an immune-modulating protein that mediates proliferation signaling and is a marker of increased metastasis (99). Secreted levels of ANXA1 were increased upon exposure to tBHP, which was largely counteracted by genetic interference of *ATE1* in quantitative mass spectrometry analysis (Figure 112B), immunoblotting analysis (Figure 113) as well as qPCR analysis of the anti-inflammatory gene IL-6 expression (Figure 114). This result is consistent with my previous data indicating increased inflammatory gene expression in recipient cells upon treatment of exosomes secreted from *ATE1*-knockdown donor cells (Figure 95). To further characterize the physiological effect of reduced ANXA1 secretion via exosomes, wound healing assay was performed. While non-stressed recipient cells with treatment of isolated exosomes from tBHP-treated donor cells displayed faster

closure of the wound scratch, the same treatment but from *ANXA1*- or *ATE1*-interfered cells exhibited significantly slower wound closure (Figure 115, 116). In sum, the exosomal release of ANXA1 gene via ATE1-dependent exocytosis circuit could possibly influence cancer metastasis.

Pathogenic hTau-P301L mutant proteins are propagated via Arg/N-degron pathway mediated exosomal secretion

Neurodegenerative disease is also an epitome of proteopathy which condition is largely induced by propagation of the pathogenic mutant proteins to the other cells. To further evaluate the physiological function of the Arg/N-degron pathway mediated exocytosis in a pathogenic context, mutant tau protein, an archetypic pathogenic protein seeded via exosomal secretion, was investigated. Exosomes secreted from SH-SY5Y cells consistently expressing hTau-P301L were purified and analyzed upon chemical inhibition of ATE1. Surprisingly, tannic acid treatment induced reduced hTau-P301L contents in the exosomal fraction (Figure 117). Moreover, Tau-dimer, a primary unit of pathogenic tau propagation in between neuronal cells (100), was further reduced upon genetic interference of *ATE1* (Figure 118) suggesting that the Arg/N-degron mediated propagation of the pathogenic neurodegenerative protein.

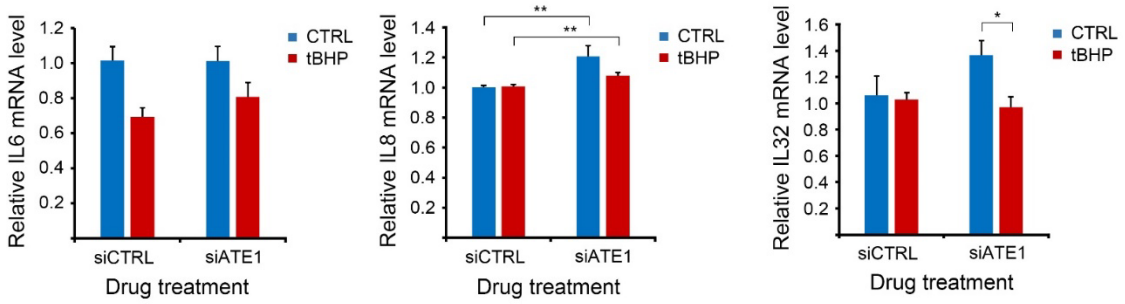

Figure 94. Genetic interference of *ATE1* reduces intracellular inflammatory genes under oxidative stress. (A, B, C) qPCR analysis of the A549 cells treated with tBHP (250 μM, 6 hr) under *ATE1* interference compared to control (40 nM, 72 hr).

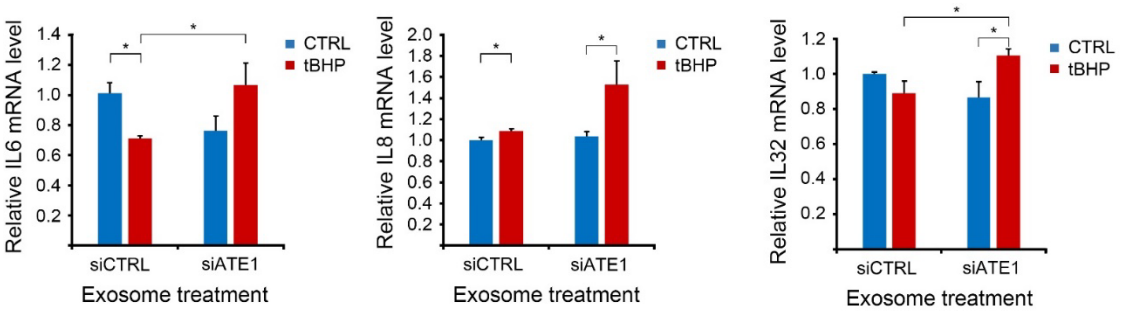

Figure 95. Genetic interference of *ATE1* reduces intercellular signaling regulating inflammatory genes under oxidative stress. qPCR analysis of the A549 cells treated with tBHP (250 μM, 6 hr) under *ATE1* interference compared to control (40 nM, 72 hr). A549 cells were treated with gathered exosomes for 24hr.

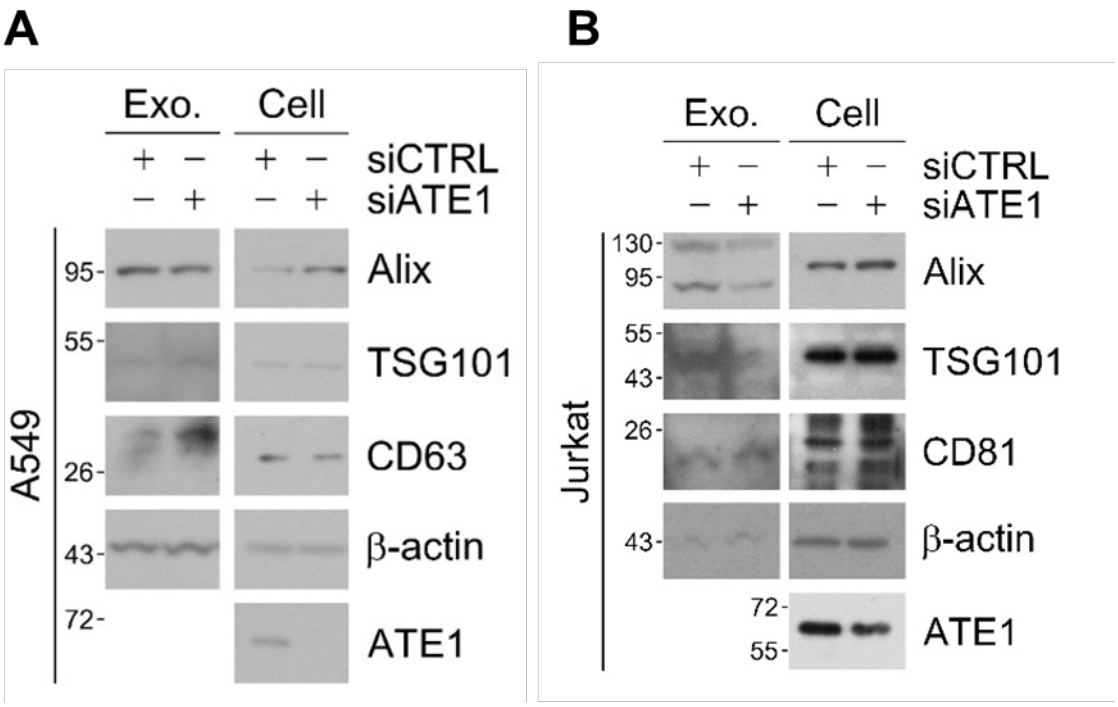

Figure 96. Genetic interference of ATE1 reduces exosome release. (A) WB of A549 cells and responsible exosomes purified from identical cells transfected with siATE1 RNA (40 nM, 48 hr). **(B)** WB of Jurkat cells and responsible exosomes purified from identical cells transfected with siATE1 RNA (40 nM, 48 hr).

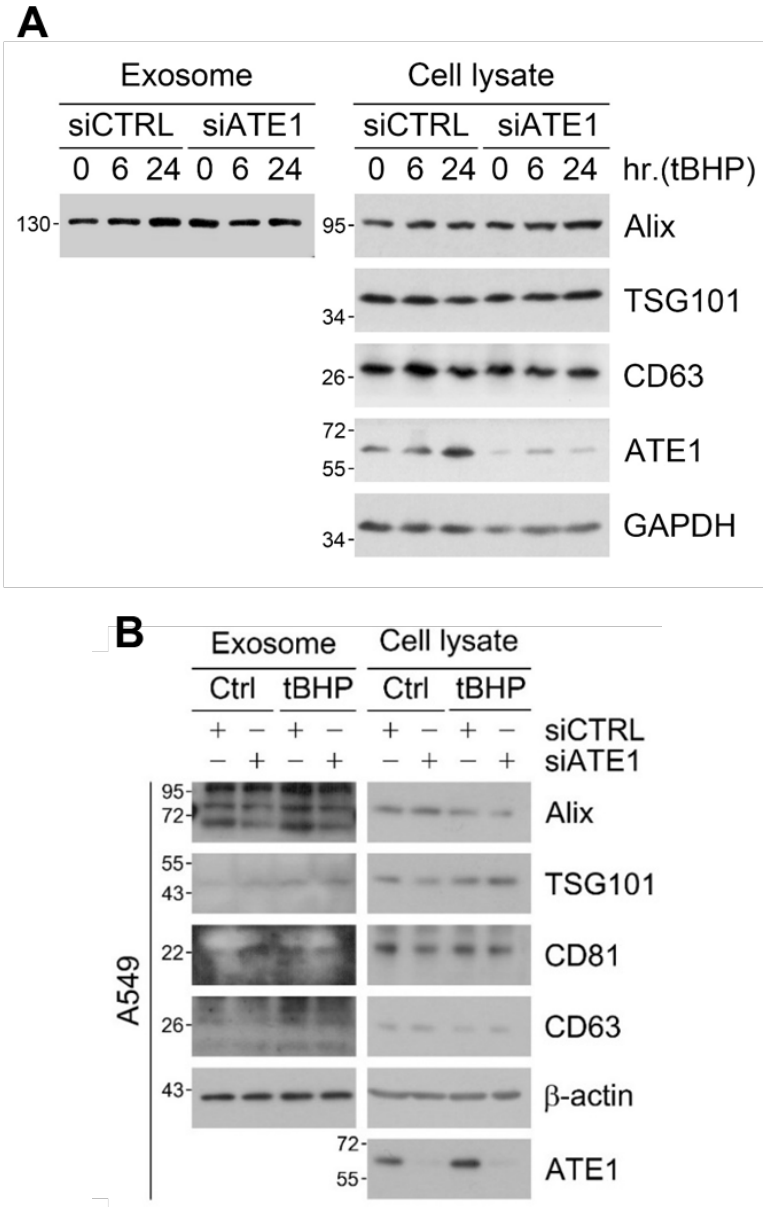

Figure 97. Genetic interference of ATE1 reduces oxidative stress induced exosome release. (A) WB of A549 cells and responsible exosomes purified from identical cells transfected with siATE1 RNA (40 nM, 48 hr) and treated with tBHP (250 μM) for indicated time. **(B)** WB of A549 cells and responsible exosomes purified from identical cells transfected with siATE1 RNA (40 nM, 48 hr) and treated with tBHP (250 μM, 6 hr).

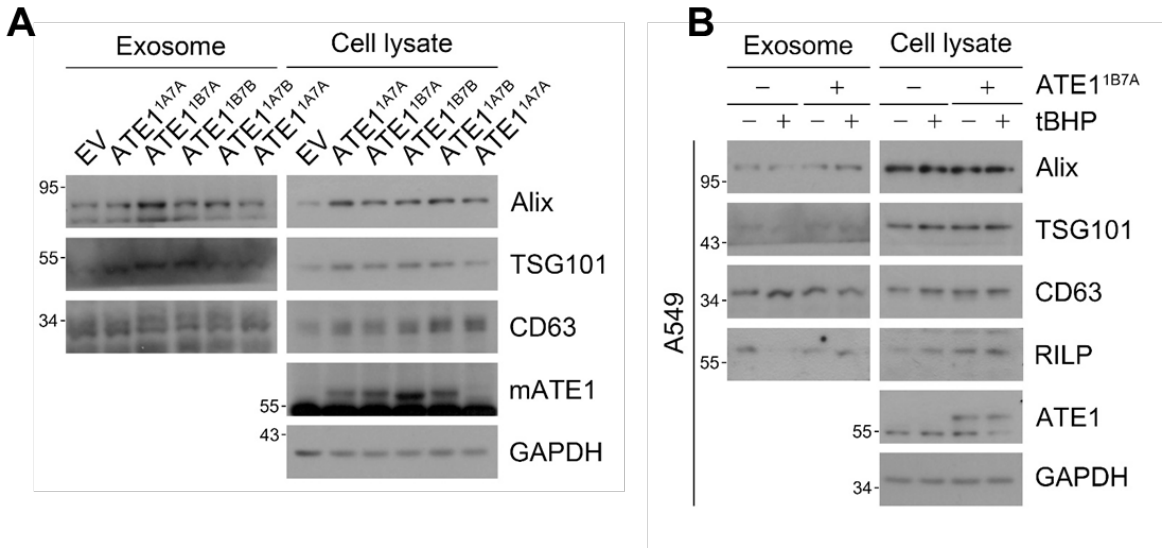

Figure 98. ATE1 overexpression inhanced exosome release. (A) WB of A549 cells and exosomes released from identical cells transfected with indicated ATE1 isoforms (24 hr). **(B)** WB of A549 cells and exosomes released from identical cells transfected with ATE1^{1B7A} isoform and treated with tBHP (250 μM, 6 hr).

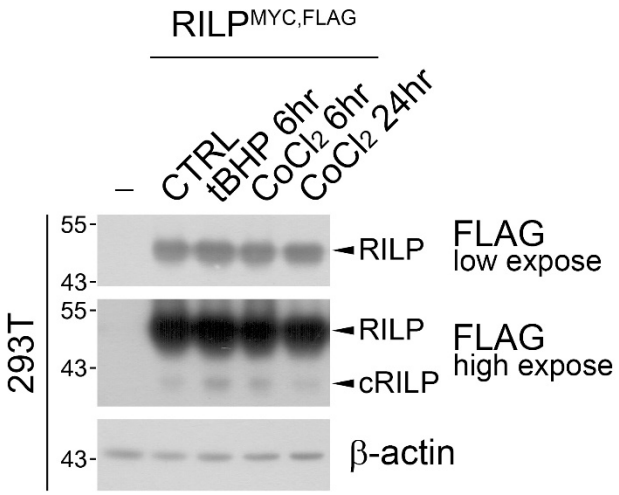

Figure 99. RILP is cleaved under oxidative stress. WB of 293T cells transfected with full-length $RILP^{FLAG}$ with tBHP (250 μM), $CoCl_2$ (250 μM) for indicated time.

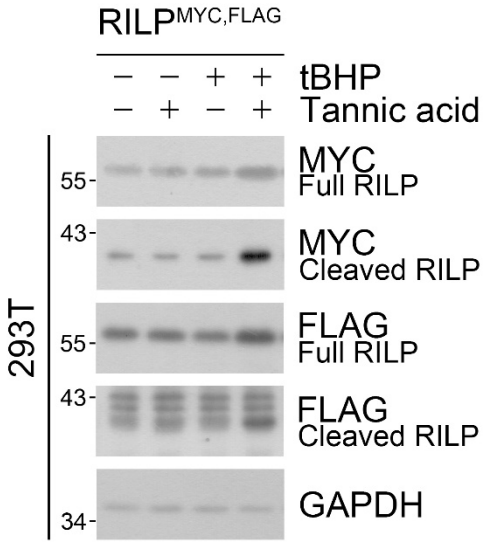

Figure 100. ROS-cleaved RILP is stabilized by ATE1 inhibitor treatment. WB of 293T cells transfected with full-length $RILP^{MYC,FLAG}$ with tBHP (250 μM, 6 hr) and tannic acid (35 μM, 24 hr).

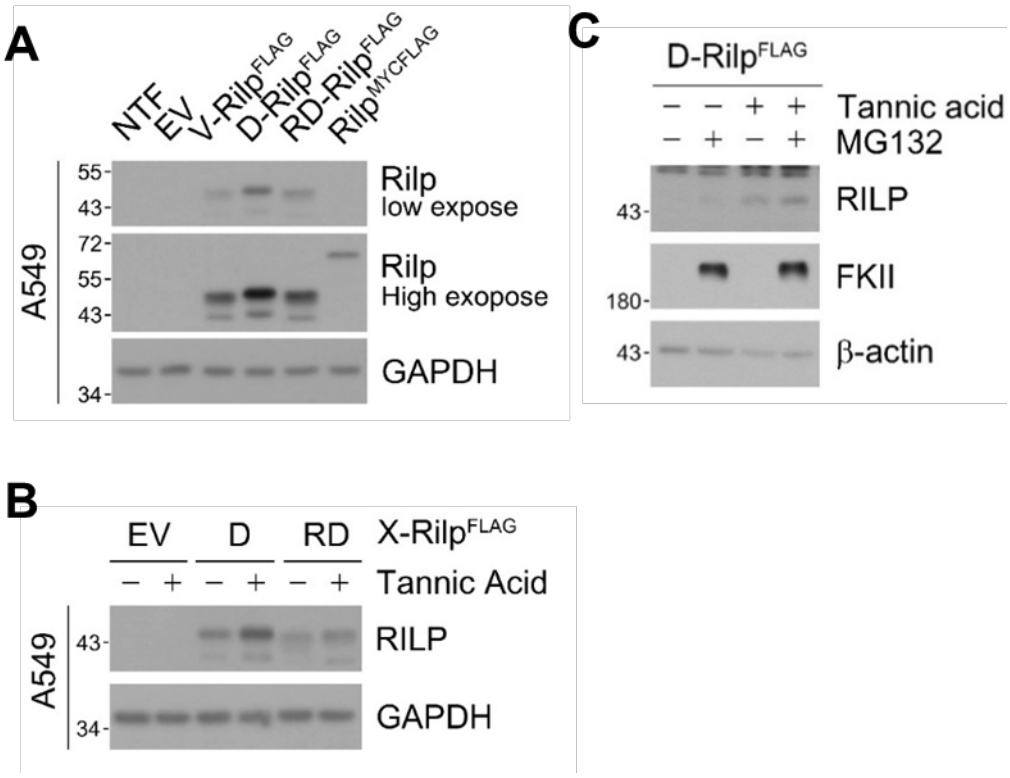

Figure 101. Cleaved RILP is a putative substrate of the Arg/N-degron pathway. (A) WB of A549 cells transfected with full-length or X-RILP^{FLAG} (X=RD, D or V). **(B)** WB of A549 cells transfected with X-RILP^{FLAG} (X=RD or D). **(C)** WB of 293T cells transfected with D-RILP^{FLAG} with MG132 (10 μM, 6 hr) and tannic acid (35 μM, 24 hr).

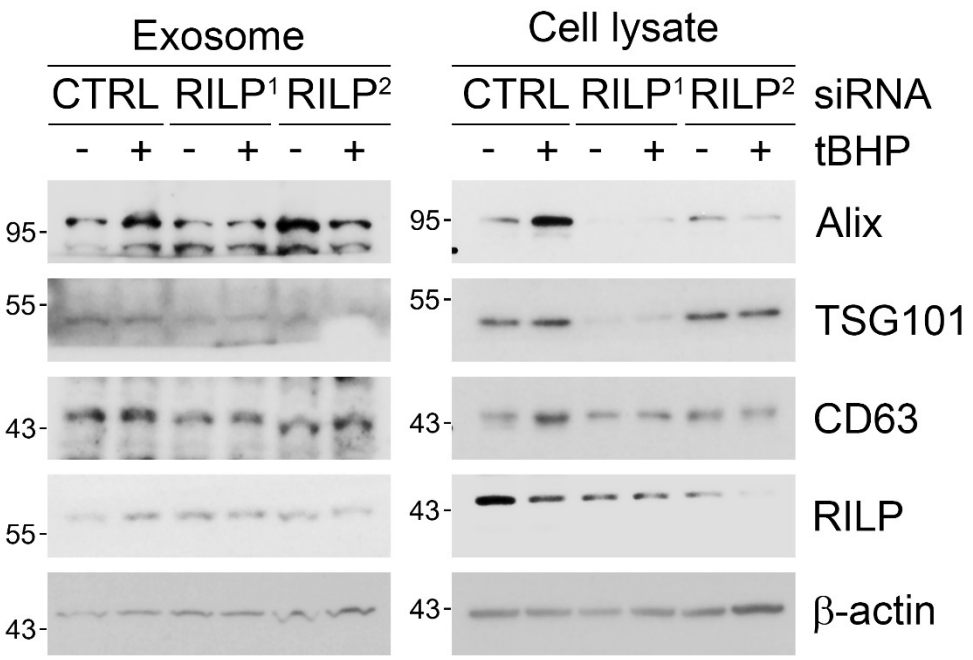

Figure 102. Genetic interference of RILP reduces oxidative stress induced exosome release. WB of A549 cells transfected with siRILP RNA (60 nM, 48 hr) and treated with tBHP (250 μM, 6 hr).

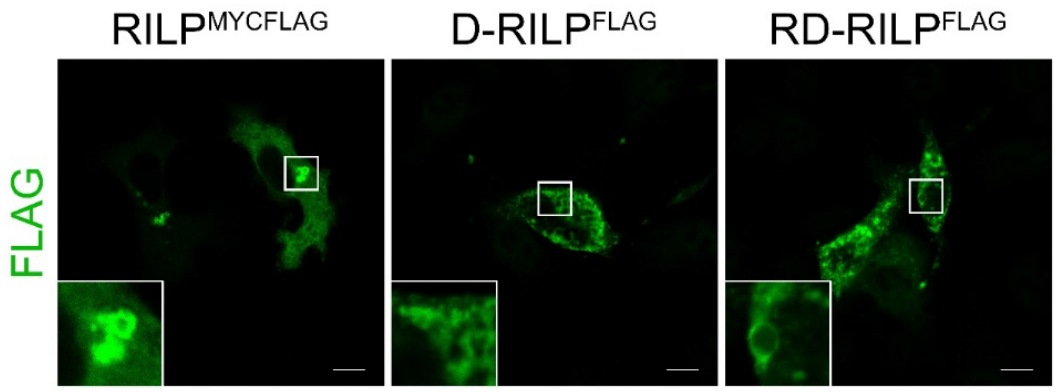

Figure 103. RILP cleavage distributes RILP positive vesicles from perinuclear aggregates. ICC of A549 cells transfected with full-length RILP^{MYCFLAG}, D-RILP^{FLAG}, or RD-RILP^{FLAG}. Scale bar, 10 μm.

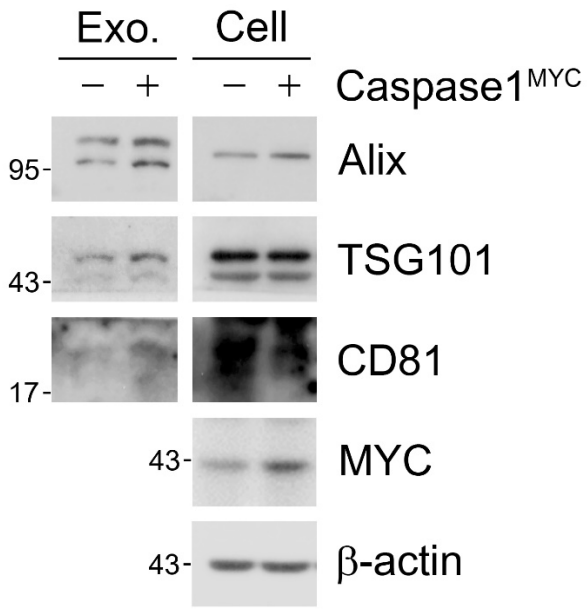

Figure 104. Caspase 1 increases secretion of the exosome. WB of A549 cell lysates and exosomes gathered from identical cells transiently expressing human Caspase 1.

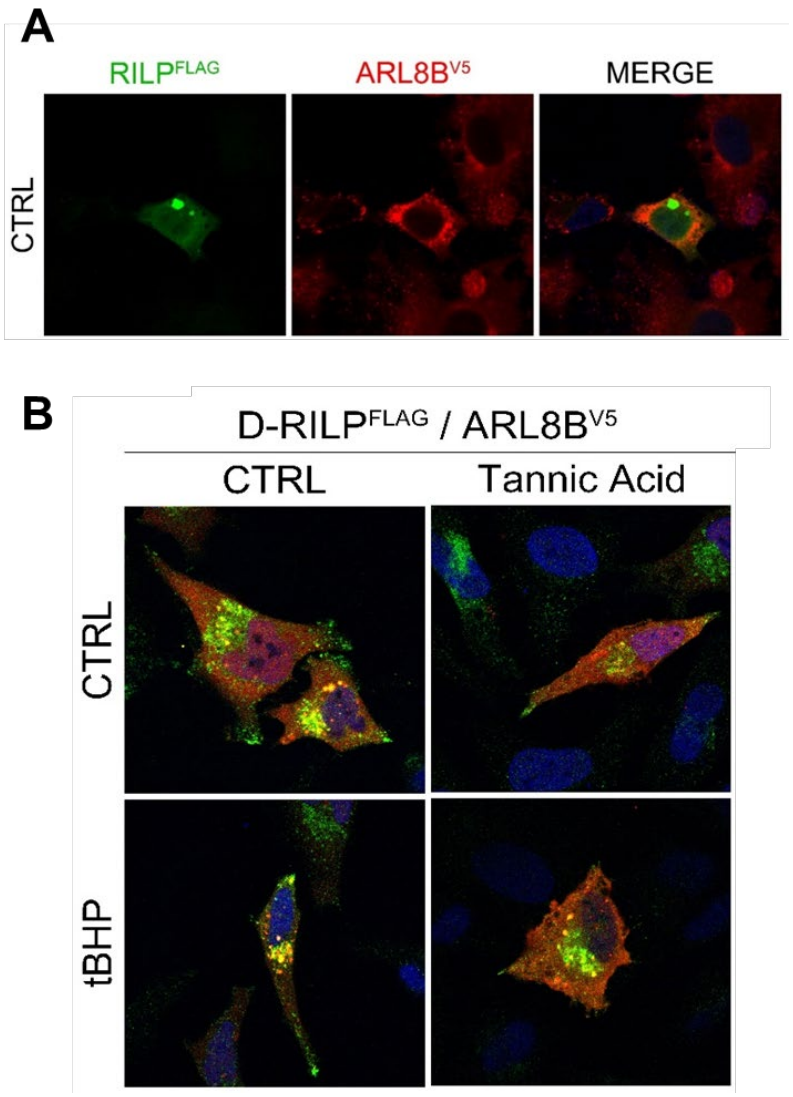

Figure 105. Cleaved RILP interacts with ARL8B upon Nt-arginylation. (A) ICC of HeLa cells transfected with full-length $RILP^{FLAG}$ and $ARL8B^{V5}$. **(B)** ICC of HeLa cells with co-transfection of D-$RILP^{FLAG}$ and ARL8B followed by the treatment of tannic acid (35 μM, 24 hr), tBHP (250 μM, 6 hr) or both. Scale bar, 10 μm.

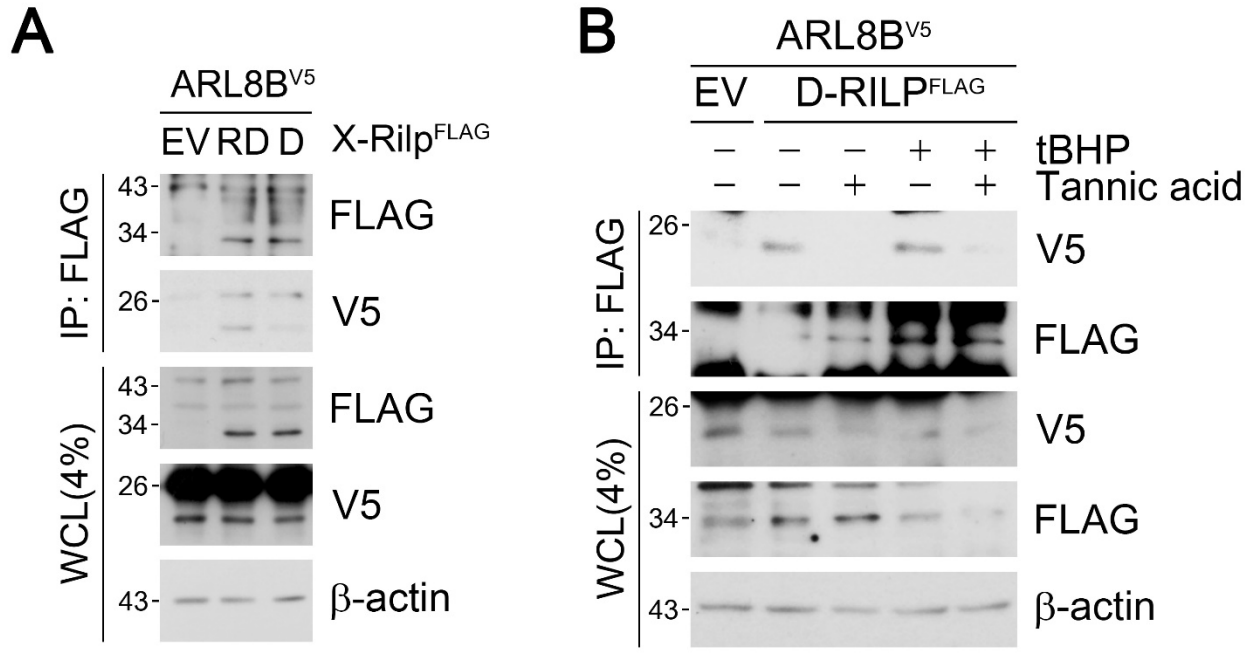

Figure 106. RD-RILP interacts with ARL8B. (A) Co-IP assay in HEK293T cells expressing X-RILP^{FLAG} (X=RD or D). **(B)** Co-IP assay in HEK293T cells expressing D-RILP^{FLAG} and ARL8B^{V5} and treated with tBHP (250 μM, 6 h), tannic acid (35 μM, 24 h), or both.

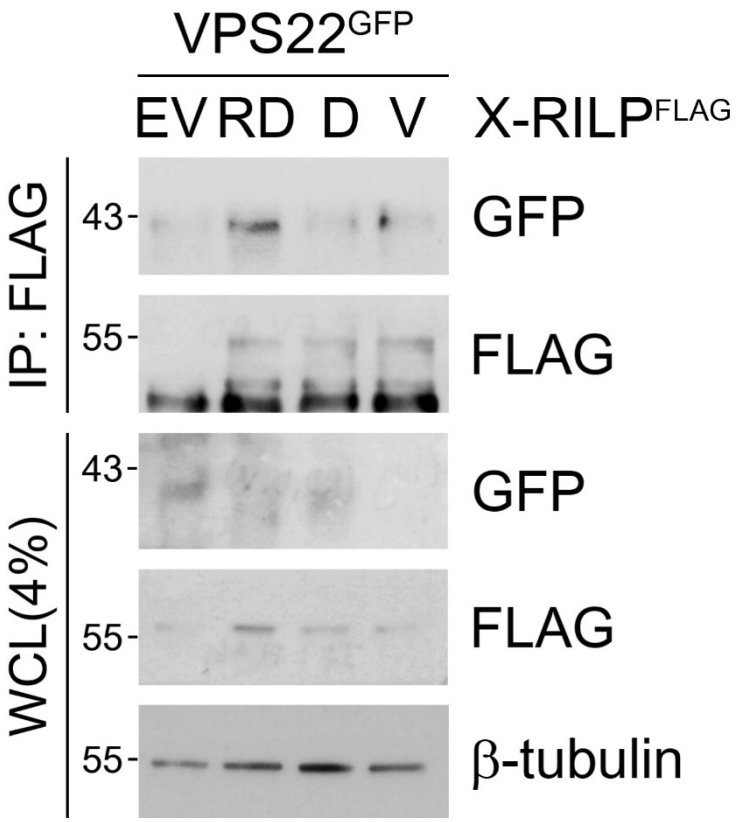

Figure 107. RD-RILP interacts with VPS22. Co-IP assay in HEK293T cells expressing X-RILP^{FLAG} (X=RD, D or V) and VPS22^{GFP}.

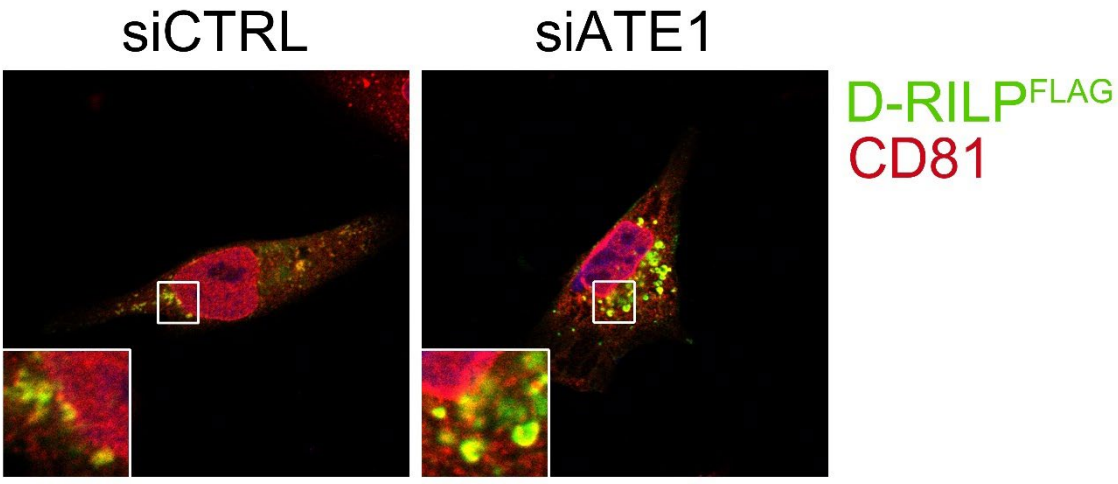

Figure 108. Genetic interference of *ATE1* induced formation of RILP positive enlarged MVB. (A) ICC of HeLa cells transfected with either negative control (40 nM, 72 h) or ATE1 siRNA (40 nM, 72 h), followed by D-RILP^{FLAG} transfection. Scale bar, 10 μm.

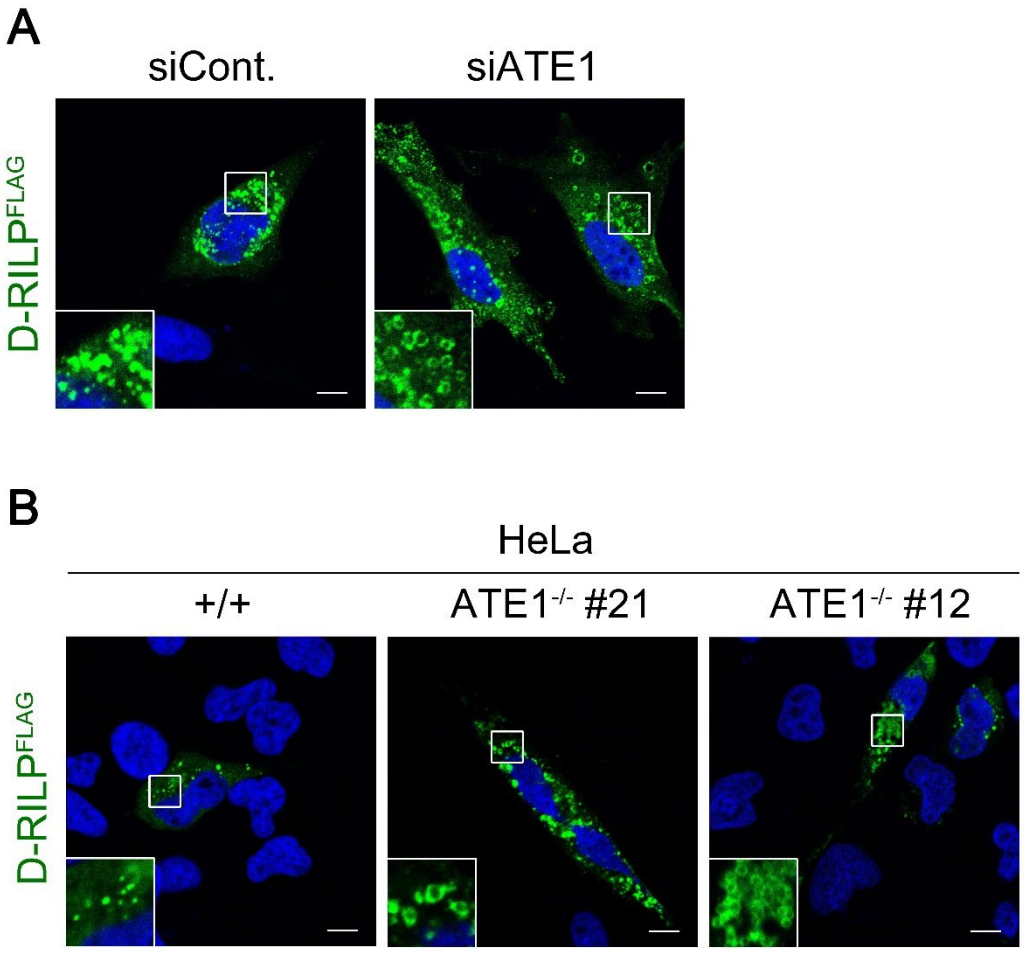

Figure 109. Genetic depletion of ATE1 promotes formation of enlarged RILP positive MVB. (A) ICC of HeLa cells transfected with either negative control (40 nM, 72 h) or ATE1 siRNA (40 nM, 72 h), followed by D-RILP^{FLAG} transfection. **(B)** ICC of Crispr-Cas9 mediated +/+ and ATE1$^{-/-}$ HeLa cells with transfection of D-RILP^{FLAG}. Scale bar, 10 μm.

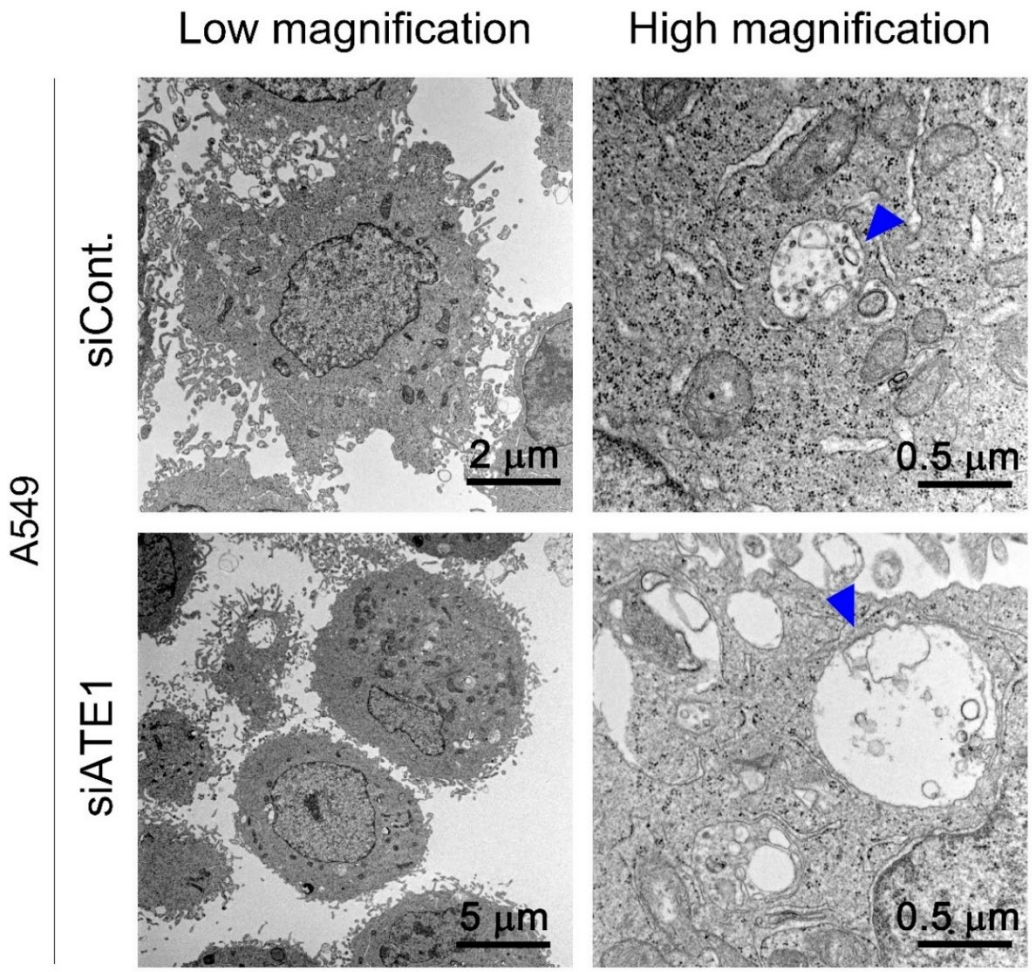

Figure 110. ATE1 interference impedes formation of ILVs inside MVB. TEM of A549 cells transfected with either negative control (40 nM, 72 h) or ATE1 siRNA (40 nM, 72 h). MVB with ILV inclusion is indicated by arrows.

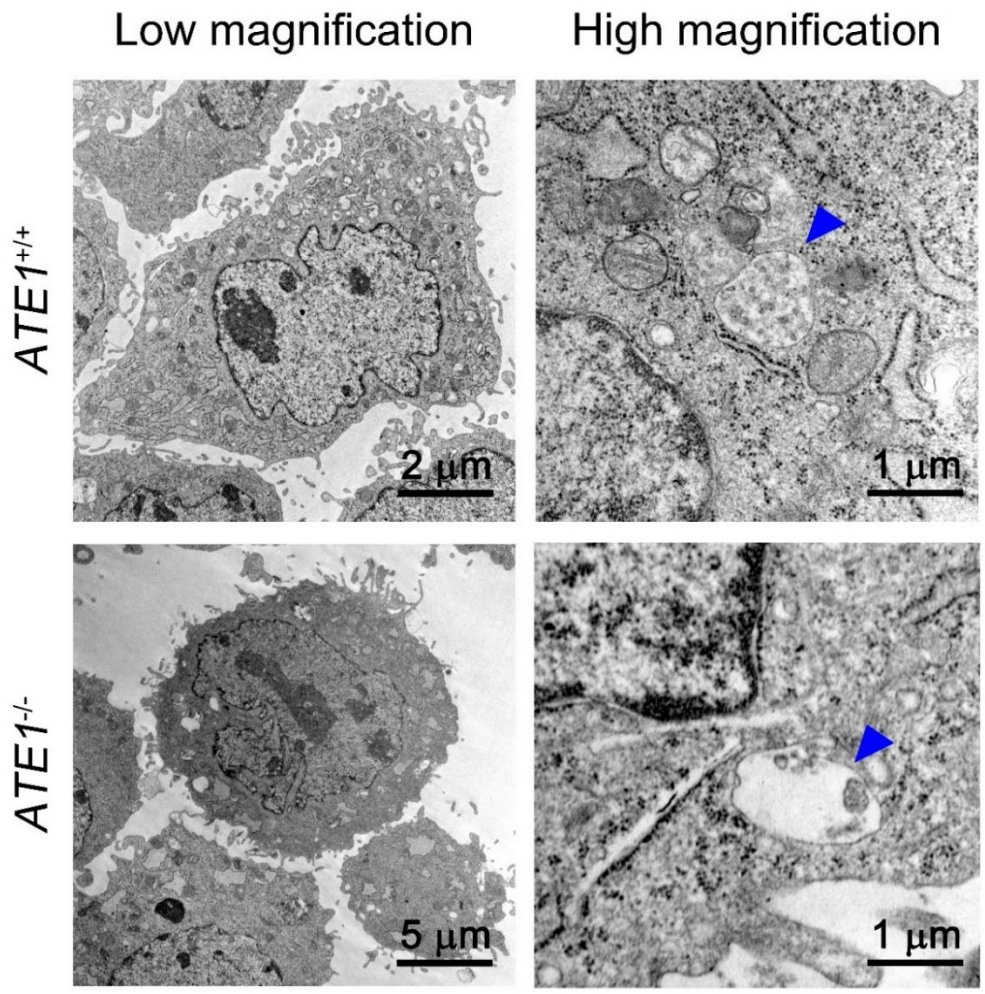

Figure 111. Genetic depletion of ATE1 obstructs formation of ILVs inside MVB. TEM of A549 cells transfected with either negative control (40 nM, 72 h) or ATE1 siRNA (40 nM, 72 h). MVB with ILV inclusion is indicated by arrows.

A

	CTRL	tBHP
siCTRL	4.54μg	4.78μg
siATE1	7.44μg	7.04μg

B

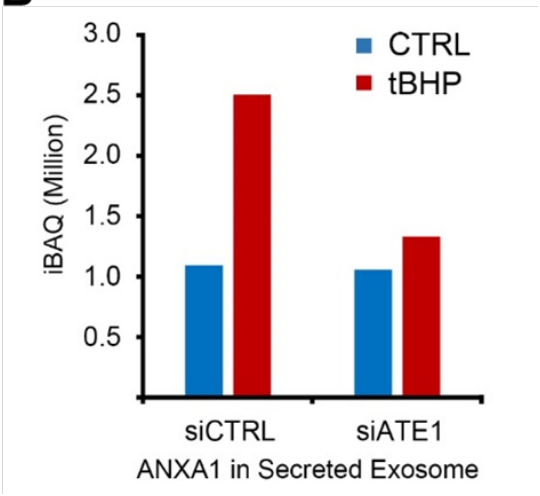

Figure 112. ATE1 interference reduces oxidative stress induced release of exosomal contents, specifically ANXA1. (A) Mass spectrometry analysis of total purified proteins from exosome gathered from donor A549 cells treated with 6 hrs of tBHP (250μM) with ATE1 interference (40 nM, 72 hr) compared to that of the negative control **(B)** Quantitative analysis of the exosomal ANXA1 contents of A549 cells gathered from donor A549 cells treated with 6 hrs of tBHP (250μM) with ATE1 interference (40 nM, 72 hr) compared to that of the negative control.

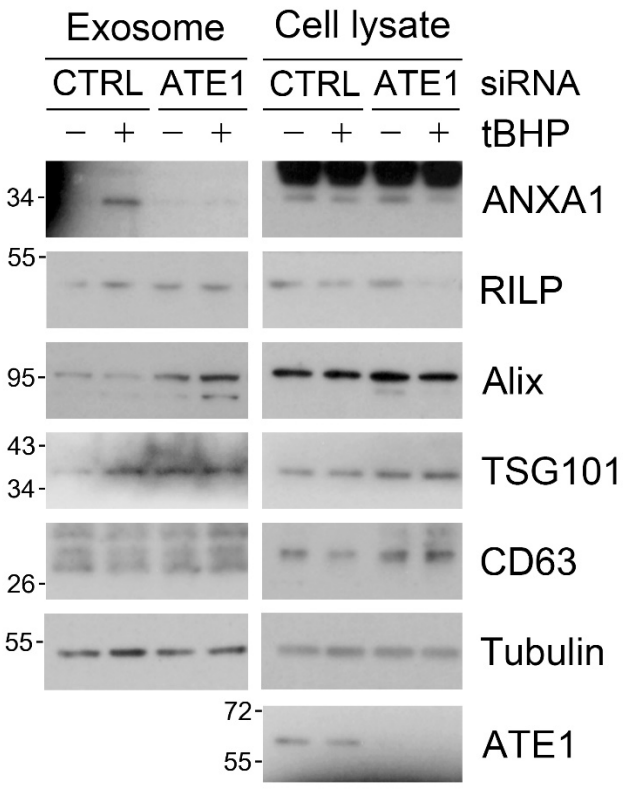

Figure 113. ATE1 interference reduces exosomal release of ANXA1. IB of exosomal protein contents of A549 cells treated with 6 hrs of tBHP (250μM) with *ATE1* interference (40 nM, 72 hr) compared to that of the negative control.

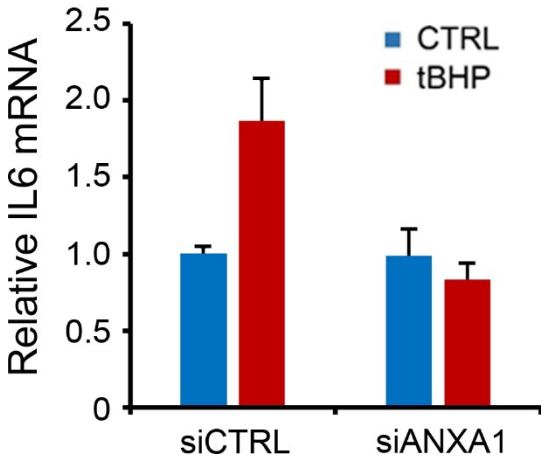

Figure 114. ANXA1 interference mediates exosome mediates anti-inflammatory signaling. A549 cells were treated with exosomes from cells treated with tBHP (250 μM, 24 hr) under ANXA1 interference compared to control (72 hr). Exosomes were gathered with PEG exosome isolation kit. (Invitrogen 4478359) (18 hr) A549 cells were treated with gathered exosomes for 24hr.

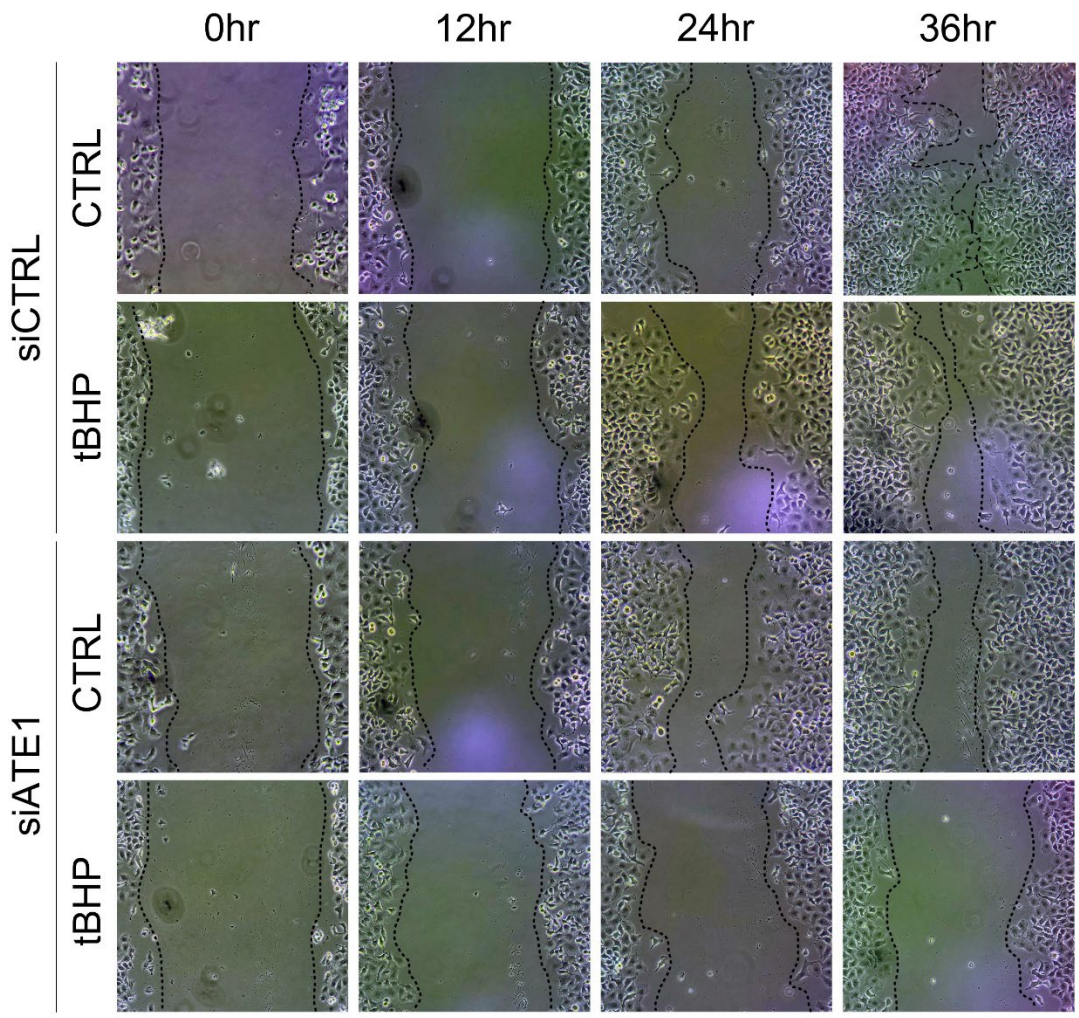

Figure 115. ATE1 mediates exosome release supporting cancer cell migration. Wound healing assay of A549 cells treated with exosomes purified from cell with either of negative control or ATE1 siRNA transfection (40 nM, 72 hr) followed by 6 hrs of tBHP treatment.

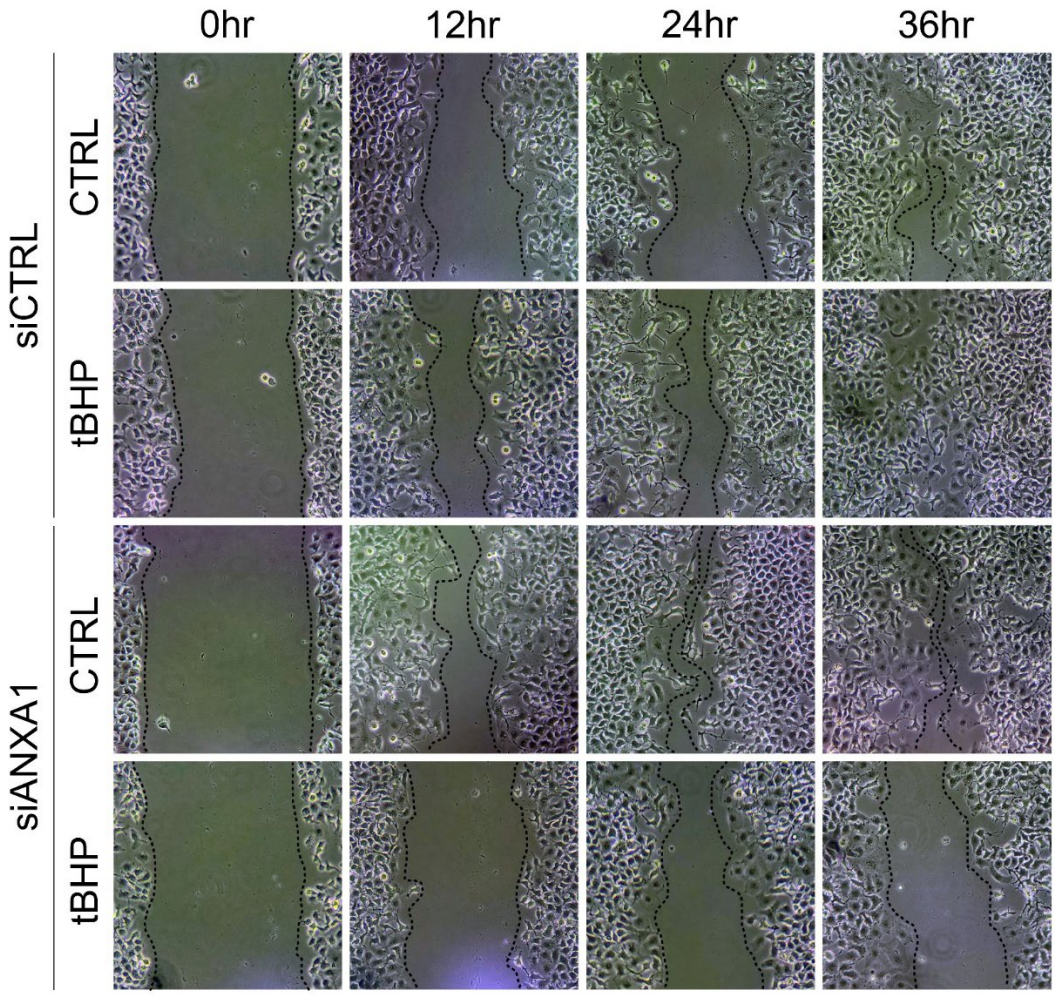

Figure 116. Exosomal ANXA1 mediates cancer cell migration. Wound healing assay of A549 cells treated with exosomes purified from cell with either of negative control or ANXA1 siRNA transfection (40 nM, 72 hr) followed by tBHP (250 μM, 6 hr) treatment.

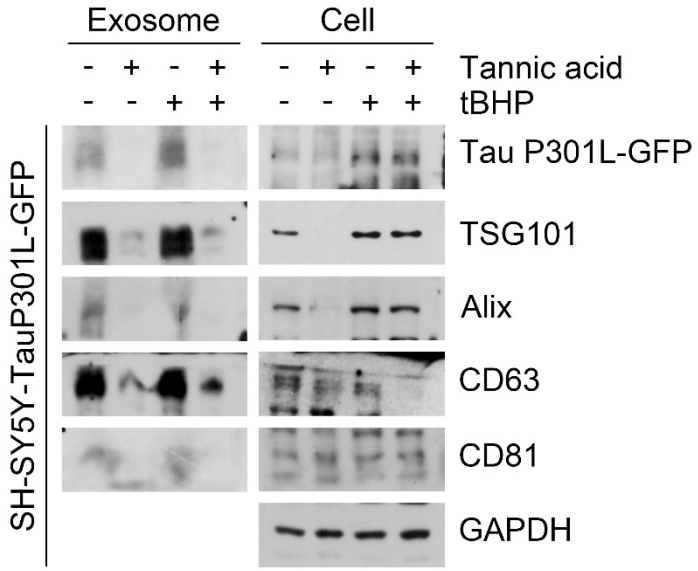

Figure 117. Exosomal Tau-P301L is released via Arg/N-degron pathway. Exosomes purified from SH-SY5Y cells stably expressing hTau-P301L-GFP with either of control or tannic acid (30 μM, 24 hr) followed by tBHP (250 μM, 3 hr) treatment.

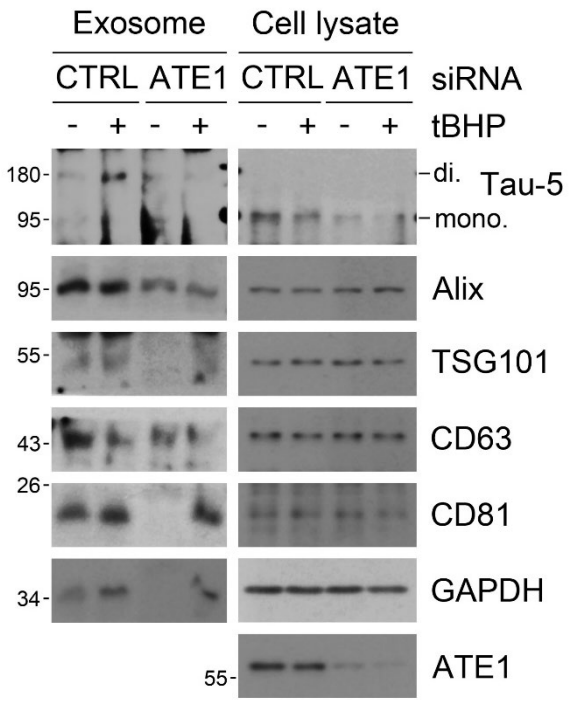

Figure 118. Tau-P301L dimer unit is propagated via Arg/N-degron pathway.
Exosomes purified from SH-SY5Y cells stably expressing hTau-P301L-GFP with either of control or tannic acid (30 μM, 24 hr) followed by tBHP (250 μM, 3 hr) treatment.
.

Discussion

As part of the global signal transduction pathway throughout the organism, cells communicate via transfer of signaling molecules to maintain cellular homeostasis against oxidative stress. These signaling molecules ready cells facing imminent oxidative stress to prepare antioxidant proteins in advance to minimize cellular damage for organismal level risk-management. Thus, preparing and transferring intercellular signaling molecules to other cells is one of the primary interests to the cells. However, how to select and convey the molecules to transfer and what signal and mechanisms cells use to prepare stress-resisting exosome biogenesis and release have not been investigated in detail.

In this study, I have demonstrated that the Arg/N-degron pathway mediates both biogenesis and release of exosomes, potentially also modulating their sorting mechanism. The mechanism of action involving the Arg/N-degron pathway is a multi-layer process in which the aforementioned processes manipulate mutually exclusive Arg/N-degron regulatory substrates. While this study presents the general principles of the Arg/N-degron-mediated exosome release pathway, further delineation of how ATE1-mediated Nt-arginylation regulates ILV biogenesis yet remains. Furthermore, several inflammatory interleukins, which are directly released via secretory vesicle-mediated exocytosis in response to oxidative stress, are putative Cys/N-degron substrates. Thus, it will be interesting to see if an additional layer of anti-oxidative stress intercellular signaling pathway may also be regulated by Arg/N-degron pathway.

As previous research identified UBR4 as a regulatory factor of the endosome biogenesis (101) and that multivesicular body is originated from endosomes, it will be relevant to identify a possible the linkage between UBR4 and exosomal protein secretion. Furthermore, primary cellular function of the Arg/N-degron pathway is quality control of the misfolded and aggregated cytosolic proteins, intracellular

proteotoxic aggregates which cannot be processed could be dumped out to extracellular region as a form of cytoprotective machinery.

MATERIALS & METHODS

Plasmids and other reagents

The Myc tagged RGS4 plasmid was constructed using pcDNA 3.1/myc-His A vector (Invitrogen) at EcoRI/XhoI sites. Human RGS16 gene were cloned from cDNA of 293T cell. Then cloned RGS16 gene were inserted into pCMV14/3xFLAG vector using HindIII/BamHI sites. C-RGS4 and D-RILP genes are sub-cloned into previously established pcDNA3 plasmid URT construct (102) and subjected to site-directed-mutagenesis to generate RC/V-RGS4^{FLAG} and RD/V-RILP^{FLAG} mutant.

Plasmid mentioned above are transfected to indicated cell lines using Lipofectamine 2000 reagent (HEK 293T, PC-12, HeLa and A549), Lipofectamine LTX reagent (MEFs), and Lipofectamine 3000 reagent (SH-SY5Y) from Thermo Fisher Scientific. All the chemicals other than mentioned are purchased from Sigma Aldrich.

RNA interference analysis

Cells were cultured in 6-well plate (1.2 x 106 per well) and transfected with either negative control siRNA (Bioneer, 4390843), or sip62 (Bioneer), siATE1(Invitrogen, s21887), siUBR4(Invitrogen, s23628), siUBR3 (Bioneer), siUBR6 (Bioneer), siUBR7(Invitrogen, s30283), siADO (Bioneer), siTOM70 (Bioneer), siKCMF1 (Bioneer) using Lipofectamine RNAiMAX reagent (Invitrogen, 13778150). Final concentrations of siRNAs except for siUBR4 were 40nM, and that of siUBR4 was 20nM. 48h after transfection, cells were treated for indicated chemicals or harvested for immunoblotting and immunocytochemistry. The sequences of pre-designed siRNAs are as follows: sip62 (sense, 5'-GUGAACUCCAGUCCCUACA-3'; antisense, 5'-UGUAGGGACUGGAGUUCAC-3'), siATE1 (sense, 5'-ACCCACCAUCUUUGUUUCCACCAAA-3'; antisense, 5'-

UUUGGUGGAAACAAAGAUGGUGGGU-3'), siUBR4 (sense, 5'-GCCUGUUCGAAAGCGCAAA-3'; antisense, 5'-UUUGCGCUUUCGAACAGGC-3') siUBR3 (sense, 5'-CCGUCUUUGAAAGAUUUAA-3'; antisense, 5'-UUAAAUCUUUCAAAGACGG-3'), siUBR6 (sense, 5'-GCAGACUGGAGGAAUAUAU-3'; antisense, 5'-AUAUAUUCCUCCAGUCUGC-3'), siUBR7 (sense, 5'-GCAAGAGACCUUAUCCUGA-3'; antisense, 5'-UCAGGAUAAGGUCUCUUGC-3'), siRILP (sense, 5'-GAUCAAGGCCAAGAUGUUA-3'; antisense, 5'- UAACAUCUUGGCCUUGAUC-3'), siANXA1 (sense, 5'-UGACCGAUCUGAGGACUUU-3'; antisense, 5'-AAAGUCCUCAGAUCGGUCA-3').

Antibodies

Following list of antibodies were used for this study: rabbit polyclonal anti-RGS4 (Merck, ABT-17, 1:2000), rabbit polyclonal anti-RGS5 (Bioworld, BS5897, and Sigma Aldrich, HPA001821, both in 1:1000), rabbit polyclonal anti-RGS16 (Bioworld, BS70592, 1:1000), rabbit polyclonal anti-UBR4 (Abcam, ab86738, 1:3000), rabbit polyclonal anti-KCMF1 (Thermo Scientific, PA5-56453, 1:2000), polyclonal anti-LC3 (Sigma Aldrich, L7543, 1:20000), mouse monoclonal anti-p62(Abcam, ab56416, 1: 10000), mouse monoclonal anti-b-actin (Sigma Aldrich, A1978, 1:10000), mouse monoclonal b-tubulin (Santa Cruz, SC-55529, 1:1000), rabbit polyclonal anti-GAPDH (Bioworld, AP0063, 1:20000), mouse monoclonal anti-FK2 (Enzo, BML-PW8810, 1:3000), rabbit polyclonal anti-K48 linkage specific ubiquitin (Abcam, ab140601, 1:2000), rabbit polyclonal anti-K63 linkage specific ubiquitin (Abcam, ab179434,1:3000), anti-K27 linkage specific ubiquitin (Abcam, ab181537, 1:3000), rabbit polyclonal anti-Myc (Cell signaling, 2278S, 1:1000), mouse monoclonal anti-FLAG M2 (Sigma, F1804, 1:1000), rabbit polyclonal anti-FLAG (Sigma, F7425, 1:10000), rabbit polyclonal anti-PARP (Cell signaling, 9542,

1:3000), mouse monoclonal anti-CHOP (Cell signaling, 2895, 1:2000), rabbit polyclonal anti-cleaved caspase3 (Cell signaling, 9661,1:1000), rabbit anti-p38 MAPK (Cell signaling, 9212, 1:1000), rabbit anti-phospho p38 MAPK (Cell signaling, 9211, 1:1000), mouse anti-MTCO2 (Abcam, ab110258, 1:2000), rabbit anti-TOMM22 (Sigma Aldrich, , 1:2000), rabbit anti-RILP (Invitrogen, PA5-34357, 1:3000), mouse anti-V5 (Invitrogen, MA5-15253, 1:5000), anti-FLAG M2 affinity gel agarose beads (Sigma), anti-Myc affinity gel agarose beads (Thermo Scientific).

Following list of secondary antibodies were used: alexa fluor 488 goat anti-rabbit IgG (Invitrogen, A11034, 1:400), alexa fluor 488 goat anti-mouse IgG (Invitrogen, A11029, 1:400), alexa fluor 555 goat anti-rabbit IgG (Invitrogen, A32732, 1:400), alexa fluor 555 goat anti-mouse IgG (Invitrogen, A32727, 1:400), alexa fluor 633 goat anti-rabbit IgG (Invitrogen, A21071, 1:400), alexa fluor 633 goat anti-mouse IgG (Invitrogen, A21052, 1:400), anti-rabbit IgG-HRP (Jackson ImmunoResearch, 111-035-003, 1:10000), and anti-mouse IgG-HRP (Jackson ImmunoResearch, 115-035-003, 1:10000).

Cell culture and immunoblotting

HeLa and HEK293T cells were purchased from ATCC (American Type Culture Collection). SH-SY5Y and PC-12 cells were obtained from Korean Cell Line Bank. Wild type and 62-/- MEF cells were obtained from Keiji Tanaka's laboratory (Tokyo Metropolitan Research Institute, Tokyo, Japan) with the permission of T. Ishii. The constructions of MEFs were previously mentioned; *ATE1*$^{-/-}$ (55), *UBR1*$^{-/-}$*UBR2*$^{-/-}$ (102), *UBR4*$^{-/-}$ (101). Cells were resuspended at PBS and lysed using 2× Laemmli sample buffer (1610747; Bio-Rad, [277.8 mM Tris-HCI, pH 6.8, 4.4% LDS, 44.4% (v/v) glycerol]) with 10% beta-mercaptoethanol. Then whole cell lysates were separated by SDS/PAGE and transferred onto polyvinylidene difluoride (PVDF) membranes. The membranes were blocked with 5% skim milk in PBST (PBS and 0.1% Tween 20) for 30 min at room

temperature. Subsequently, the membranes were incubated with primary antibodies and washed 3 times with PBST for 10 min. Then, membranes were incubated with host-specific secondary antibodies conjugated with HRP for 1 h and washed for 3 times as mentioned above. For detection, a mixture of SuperSignal West Pico Chemiluminescent Substrate (34080; ThermoFisher) or SuperSignal West Femto Maximum Sensitivity Substrate (34095; ThermoFisher) were used to visualize immunoreactive proteins on to X-ray films (AGFA).

Immunocytochemistry

Cells were cultured on coverslips coated with poly-L-Lysine in 24-well plate followed by fixation with 4% paraformaldehyde in PBS (pH7.4) for 15 min and washed with PBS for 5 min three times. Subsequently, the cells were permeabilized with 0.5% Triton X-100 in PBS for 15 min followed by washing three times with PBS for 5 min. After blocked with 2% BSA in PBS for 1 hr, the cells were incubated with primary antibodies overnight at 4 °C. The cells were washed for 10 min three times and incubated with Alexa Fluor conjugated secondary antibodies for 30 min at room temperature. Then, washing three times, the coverslips were mounted on slide glasses using VECTASHIELD hard set mounting medium with DAPI (H-1500). Confocal images were taken using laser scanning confocal microscope 510 Meta (Zeiss) and analyzed by Zeiss LSM Image Browser (Blue edition, ver. 4.2.0.121). Subsequently, for puncta counting analysis, cells were counted as showing significant co-localization if more than ten clear puncta structures of the proteins in question showed association and/or co-localization. Quantification results are shown as mean +/- S.D. of at least three independent experiments.

Co-immunoprecipitation

Co-immunoprecipitation assay was performed to demonstrate physical interaction of the proteins of interest. Cells were harvested by scraping and centrifuged using ice-cold PBS. Cell pellets were resuspended in lysis buffer (50 mM Tris-HCl pH 7.5, 150 mM NaCl, 0.5% Triton X-100, 1 mM EDTA, 1 mM PMSF and protease inhibitor cocktail) and incubated on rotator for 30 min at 4°C. After incubation cell debris were removed by centrifugation at 13000 rpm for 10 min. Supernatant were subjected to pre-clearing using normal mouse IgG and A/G agarose bead (Santa Cruz) overnight on rotator at 4°C. After incubation, samples were centrifuged at 13000 rpm for 10 min to remove non-specific protein bound IgG and bead. Pre-cleared supernatant was incubated with anti-FLAG M2 affinity agarose beads (Sigma) or anti-c-Myc affinity agarose beads (Thermo) for 3 h on rotator at 4°C. Next, incubated anti-FLAG M2 beads were precipitated and washed four times with identical lysis buffer. Then bound proteins were eluted at 2X Laemmli sample buffer by heating 10 min at 95 °C, separated by SDS PAGE, and immunoblotted using antibodies of interests.

Denaturation-ubiquitylation assay

Ubiquitylation status of substrate proteins were investigated under denaturation immunoprecipitation. Either WT or selective Lys (K48 or K63) only remained ubiquitin coding plasmid were transfected to cells of interests. Cells were harvested using ice-cold PBS by scraping. Harvested pellets were lysed using 100 ml of N-ethylmaleimide (NEM)-based buffer (1% SDS, 1 mM NEM in PBS) and heated at 100°C for 10 min. Then lysates were 1/10 diluted using lysis buffer (50 mM Tris-HCl pH 7.5, 150 mM NaCl, 0.5% Triton X-100, 1 mM EDTA, 1 mM PMSF and protease inhibitor cocktail) and following steps are identical to the method used in co-IP.

***In vitro* peptide pull-down assay**

A set of 12-mer peptides corresponding N-terminal 11mer sequences reflecting MetAP cleavage and post translational modification of RGS4 and Lys at the C-terminal for biotinylation was synthesized. A set of X-RGS4 peptides (X-KGLAGLPASCLK-biotin) was composed of Arg-Cys^2_{ox}(Cys^2_{ox} reflects tri-oxidized second Cys residue), Cys^2(native), Val^2(Cys^2-to-Val^2 mutant). 400 mg of synthesized peptides were mixed to 1 ml of high -capacity streptavidin agarose resin (20361; Thermo) and conjugated at 4 °C overnight. Streptavidin resin were washed 5 5imes with PBS. Harvested cells were resuspended in hypotonic buffer [10 mM KCl, 1.5 mM MgCl2, and 10 mM HEPES (pH 7.9)] with a protease inhibitor mix (P8340; Sigma) and lysed by repetitive freezing and thawing process. Protein lysates were centrifuged at 13000 rpm for 10 min. for removal of cellular debris. Supernatant were quantified by BCA protein assay kit (23227; Thermo). 600 mg of protein lysates were mixed with 50 ul of peptide conjugated resin and binding buffer [0.05% Tween-20, 10% glycerol, 0.2 M KCl, and 20 mM HEPES (pH 7.9)] was added up to 300ul. The mixture of lysates and resin were incubated at 4 °C for 4 hr on a rotator. Protein-bound bead were washed for 5 times with binding buffer and resuspended in 35 ml of 2X Laemmli sample buffer. Samples were heated for 10 min at 95 °C, separated by SDS PAGE, and immunoblotted.

Digitonin based mitochondria fractionation

Cells were harvested via centrifugation at 1500xg for 5min. The plasma membranes of the harvested cells were resuspended using digitonin based lysis buffer (0.01% digitonin, 110 mM potassium acetate, 25 mM HEPES in pH7.2, 2.5 mM sodium acetate and 1mM EGTA) and incubated on ice for 15 min. Mitochondria were pelleted by centrifugation at 1000xg for 5 min. Resulting cytosolic supernatant was transferred to new tube and re-centrifuged at 15000xg for 15min for complete removal of contaminating organelle

portion. Mitochondria containing pellet was washed for three times using identical lysis buffer following centrifugation at 15000 xg for 5 min. Laemmli sample buffer was added to cytosolic portion and 0.01% digitonin-insoluble pellets which were resuspended by PBS. Samples were heated for 10 min at 100°C, separated by SDS PAGE, and immunoblotted.

Cycloheximide based protein degradation assay

Either WT or C2V mutant RGS4 coding plasmids were transfected to selected cell lines using indicated lipofectamine reagent mentioned above. After 24 h or transfection, oxidative stress was induced by indicated chemicals for 6 h. Then, media was exchanged into the mixture of media with either 10 mM cycloheximide (CHX) alone or in combination with oxidative stress inducing chemicals. From the point of CHX treatment, cells were harvested at indicated time point and subjected to analyzation using SDS-PAGE and immunoblotting.

Quantitative real-time PCR analysis

Upon treatment of oxidative stress inducing chemicals for indicated time, mRNA of treated cells was extracted using Trizol reagent (Invitrogen). 2 mg of extracted RNA were used to synthesize cDNA via using PrimeScript 1st strand cDNA synthesis kit (Takara, 6110). Synthesized cDNAs are 1/4 diluted using 60 μl D.W. and 2 μl of the cDNA were used to run quantitative RT PCR. 2X Fast Q-PCR master mix with SYBR (SMOBIO, TQ1210) were used to measure the expression of the gene of interest. Following sequences are the primer sequences for measuring indicated gene expression: GAPDH (5'-GCGCCCAATACGACCAA-3', 5'-CTCTCTGCTCCTCCTGTTC-3'), RGS4 (5'-TGGTGCAAGAATCCAGGTTC-3', 5'-CCACAACAAGAAGGACAAAGTG-3') iNOS (5'-CACCATCCTCTTTGCGACA-3', 5'-CGAGCTCAGCCTGTACT-3'), SOD1 (5'-

CCTCGGAACCAGGACCT-3', 5'-TTAATGCTTCCCCACACCTT-3'), TGF-β (5'-CCGACTACTACGCCAAGGA-3', 5'-GTTCAGGTACCGCTTCTCG-3'), COX2 (5'-GCACTACATACTTACCCACTTCA -3', 5'-GCCATAGTCAGCATTGTAAGTTG-3').

Statistical analysis

For immunocytochemistry, data values shown represent the mean ± S.D. of at least three independent experiments. For each experiment, sample size (n) was determined as stated in the figure legends. For quantitative real time PCR analysis, each set of experiments was triplicated and performed three times. P-values were determined using ANOVA with Prism 6 software (GraphPad) or two-tailed student's t-test (degree of freedom = n-1). Statistical significance was determined as values of $p < 0.05$ (***$p < 0.001$; **$p < 0.01$; *$p < 0.05$).

Mass spectrometry analysis

Peptide sample preparation

$RGS4^{MYC}$ proteins are transiently expressed in HEK293T cells (4X 100mm dishes per sample) and treated with either MG132 (10 mM) or combination treatment of tBHP (250 mM) and BAF (20 nM) for 6hrs. Cells were harvested and lysed according to co-IP method and immunoprecipitated with MYC-agarose beads overnight (Invitrogen, 20169,100ul slurry per sample). Beads were washed with lysis buffer for 1hr at 4℃ and washes are repeated 5 times. Protein digestion of IP eluent was performed via the Filter-aided sample preparation (FASP) procedure as described with some modifications (103, 104). Briefly, 50ul of the elutes were mixed with 300ul of UA buffer (8 M Urea in 0.1 M Tris pH 8.5) and loaded onto a 30 K Amicon filter (Milipore). The buffer exchanges were performed with UA solution via centrifugation at 14,000xg for 15min. Following the exchange of buffer with 40 mM ammonium bicarbonate (ABC), protein digestion was

performed at 37°C overnight using a trypsin/LysC mixture (Promega) at a 100:1 protein-to-protease ratio. The digested peptides were collected by centrifugation. After the filter units were washed with 40 mM ABC, additional digestion was performed at 37°C for 2 hours using trypsin (enzyme-to-substrate ratio [w/w] of 1:1000). All resulting peptides were acidified with 10% TFA and desalted using homemade SDB-C18-StageTips as described (103, 104). Desalted samples were completely dried with a vacuum dryer and stored at -80°C.

LC-MS/MS analysis

LC-MS/MS analysis was performed using hybrid quadrupole Orbitrap mass spectrometers, Q-exactive plus (Thermo Fisher Scientific, Waltham, MA) coupled to an Ultimate 3000 RSLC systems (Dionex) via a nano electrospray source, as described with some modifications (103, 104). Peptide samples were separated on the 2-column setup with a trap column (300 mm I.D. x 5 mm, C18 3 mm, 100 Å) and an analytical column (50 mm I.D. x 50 cm, C18 1.9 mm, 100 Å). After the samples were loaded onto the nano LC, a 180-minute gradient from 8% to 26% solvent B (100% acetonitrile and 0.1% formic acid) was applied to all samples. The spray voltage was 2.0 kV in the positive ion mode, and the temperature of the heated capillary was set to 320°C. Mass spectra were acquired in data-dependent mode using a top 15 method. The Orbitrap analyzer scanned precursor ions with a mass range of 300–1800 m/z and a resolution of 70,000 at m/z 200. HCD scans were acquired at a resolution of 17,500 with the stepped normalized collision energy (NCE) of 27 ± 2%. The maximum ion injection time for the survey and MS/MS scans was 25 ms and 50 ms, respectively.

Data processing

MS raw files were processed by the Maxquant software version 1.6.1.0 (105). MS/MS

spectra were searched against the sequence of Human RGS4 protein with C-terminal Myc-tag using the Andromeda search engine (106). Primary searches were performed using a 6-ppm precursor ion tolerance. The MS/MS ion tolerance was set to 20 ppm. Digestion mode was set as “no digestion”. To identify modification sites of cysteine, carbamido-methylation, di-oxidation, and tri-oxidation on cysteine, N-terminal acetylation, and oxidation on methionine were set as variable modifications. The minimum score for the modified peptides was set to 40. To assign modification sites, localization probability of 0.75 was set as a threshold.

Wound healing assay

To analyze cell migration, proliferation and metastasis, HeLa cells were plated to a monolayer of 95% confluency. siRNA is transfected at the time of cell seeding using retro-transfection method. After cells are attached, cells were scratched with a sterile 200ul pipette tip and scratched cells were removed by changing media. Cells were treated with chemicals or purified exosomes diluted in medium and incubated for indicated time points. Photographs were obtained using a microscope.

Transmission electron microscopy (TEM)

For conventional transmission electron microscopy, A549 cells were transfected with negative control and ATE1 siRNA for 48h and treated with 250μM tBHP for 6 h. 1 x 10^8 cells were harvested by trypsinization and pelleted by centrifugation at 3000 rpm for 5 min. Pellets were washed with ice-cold PBS and re-pelleted by centrifugation. Pellets are incubated in 2.5% glutaraldeyhyde in 0.1M sodium cacodylate buffer (pH 7.4) (Electron Microscopy Sciences) for overnight at 4°C without resuspension. The fixative was replaced by cacodylate buffer for the last 6 hours, after which cells were embedded in Epon resin. Subsequently, 60-nm sections were cut and stained with uranyl acetate and

lead citrate using the Reichert Ultracut S Ultramicrotome (Leica Microsystems) and FEI Vitrobot Mark IV (Thermo Scientific), respectively. Cell sections were examined using the 120 kV transmission electron microscope JEM-1400Flash (JEOL) at the Seoul National University Hospital Biomedical Research Institute.

Exosome purification

Conditioned media of samples were harvested and centrifuged at 4°C, 2000 xg for 30 min to remove cell debris and floated cells. The supernatants of samples were transferred to new tubes, and an Exosome isolation kit (Thermo Fisher, 4478359) solution was added to and thoroughly mixed with samples. The volume of the solution should be half of the volume of samples. Then the mixtures were incubated at 4°C rotator overnight and centrifuged at 4°C 10000 xg for 1h. The isolated exosomes were resuspended in PBS with respect to volume of the cell lysates and lysed using 2× Laemmli sample buffer (Bio-Rad, 1610747) containing 10% β-mercaptoethanol. Samples were heated at 95°C for 10 min. followed by conventional western blotting process.

Discussion and Conclusion

Summary & follow-up

Here I report the sensing and responding mechanism of the cellular oxidative stress response through the Arg/N-degron pathway via proteolysis and protein secretion.

In the second part of the thesis, cysteine branch of the Arg/N-degron pathway is configured in the context of oxidative stress. Via characteristic modification of the oxidized Cys-secondary degron, two sets of N-recognin E3 ligases circuits are conditionally adopted for the repriming of the ubiquitin chain ligated on the substrate proteins. These series of proteolytic cascades reach the destination of the proteasome or autophagosome for substrate protein degradation. Specifically, the level of both O_2 and ROS are initially sensed by Nt-Cys residue, thereby resulted in production of $CysO_2$ and $CysO_3$, undergoing ATE1-mediated arginylation. Both arginylated-$CysO_2$ and -$CysO_3$ are recognized by either UBR1/UBR2 or KCMF1, respectively. Recognition of R-$CysO_3$ residue by KCMF1, forming a complex with UBR4, enables ligation of K63-linked poly-ubiquitin chain on the substrate in accordance with UBR4, which ligates K27-linked poly-ubiquitin chain on the identical substrate concurrently. These hetero ubiquitin chain ligated on the substrate recruits autophagic adaptor protein p62, which delivers ubiquitylated substrates to autophagosome as a destination. These multi-step process of Nt-Cys carrying substrate proteins are responsible for maintaining intracellular oxygen-homeostasis. These intricate protein regulatory mechanisms resemble that of the HIF1-α, one of the most well-studied proteins which also linked to oxygen homeostasis, yet better crafted to regulate multiple substrate proteins in a single signal, N-terminal oxidation of the cysteine residue. By regulating the stability of a protein and utilize the lagging phase for proper function, Nt-Cys modulating Arg/N-degron pathway becomes a part of the protein regulation methodology under hypoxia and oxidative stress throughout the whole kingdom.

The journey to the proteolysis of Nt-Cys substrates under the oxidative stress can also be re-routed to mitochondria where the unprocessable and undegradable proteins are headed to. Loss of ATE1 function underscores how important the Arg/N-degron pathway and proteolysis via the pathway are for maintain cellular homeostasis at the same time cellular integrity under oxidative stress. Obstruction of the Arg/N-degron pathway induces translocation of Nt-Cys substrate proteins to mitochondria precisely. Ironically referred as MAGIC (mitochondria as guardian of in cytosol), mitochondrial translocation of Nt-Cys substrate proteins under oxidative stress rather exhibits stronger cytotoxicity induced by enhanced fragmentation of the mitochondria. Moreover, acceleration of degradation flux of Nt-Cys substrate under oxidative stress drastically rescue cells from apoptosis and mitochondrial fragmentation as well. These series of findings support that the Arg/N-degron pathway is a guardian of cells from oxidative stress via mitochondrial integrity maintenance.

Several remained questions to be elucidated are the mechanism and conformation underlying the precise recognition of R-CysO_3 allowing the differential recognition of R-CysO_2 mediated by novel N-recognin E3 ligase KCMF1. Functionality and physiological characterization of KCMF1 E3 ligases are one of the major goals. Also, mechanism of which un-arginylated Nt-CysO_3 substrates are targeted to mitochondria needs further clarification.

Under the realm of intercellular communication, the Arg/N-degron pathway also exerts a significant effect on the exocytosis mechanism. The critical mechanistic part of the exocytosis, from initial biogenesis of the intraluminal vesicles inside MVB to targeting of ILV containing MVB, both processes are all linked to Nt-arginylation of the substrates. Nt-arginylation substrates partaking in exocytosis machinery change its functionality by differentiating its interactome upon arginylation. Specifically, RILP, a conditional arginylation substrate, is cleaved by Caspase-1 and exposes D75 residue for

subsequent arginylation. As oxidative stress induces activation of RILP cleaving Caspase-1, RILP is cleaved and arginylated under oxidative stress. Originally responsible for the interaction with Rab7 and lysosome, RILP interacts with ARL8 and VPS22 in its arginylated form for expected complex formation with motor protein kinesin for MVB transport. The RILP interactome shift under oxidative stress resulted in dissociation of RILP positive perinuclear aggregates and anterograde movement of RILP positive vesicles toward plasma membrane. RILP-mediated Arg/N-degron pathway linked exocytosis mechanism shone light to the mechanistic structure of the conditional release of exosomes yet to be elucidated.

Moreover, the mechanism of the signaling molecules assortment inside exosomes is also linked to arginylation. Formation of ILV, the process of preliminary exosomes formation with engulfing cytosolic contents, is critically inhibited by the abrogation of the Arg/N-degron pathway. Phenomenal observations showing the decreased number of ILV inside MVB along with enlargement of MVB are the main indication of the strong correlation in between exosome formation and the Arg/N-degron pathway. Identification of the ANXA1, the oxidative stress associated exosomal content protein, revealed that the arginylation functions as a bridge of cell-to-cell communication, expanding the range of effectors to distantly located cells for possible synchronization.

Taken together, these series of studies underscore the importance of the Arg/N-degron pathway as a sensor and responder as well as a global cell-to-cell communication pathway against oxidative stress. Given that those regulatory pathways have been validated in *in vitro*, I will additionally characterize these pathways in a broader context including tissue to organismal level. Also, further studies regarding the ubiquitin-recognition domains and specific conformations of ubiquitin chains are part of my scientific interests for postdoctoral fellowship.

REFERENCES

1. G. Manning, D. B. Whyte, R. Martinez, T. Hunter, S. Sudarsanam, The protein kinase complement of the human genome. *Science* **298**, 1912-1934 (2002).
2. C. Heride, S. Urbe, M. J. Clague, Ubiquitin code assembly and disassembly. *Curr Biol* **24**, R215-220 (2014).
3. R. M. Biondi, A. R. Nebreda, Signalling specificity of Ser/Thr protein kinases through docking-site-mediated interactions. *Biochem J* **372**, 1-13 (2003).
4. P. M. Holland, J. A. Cooper, Protein modification: docking sites for kinases. *Curr Biol* **9**, R329-331 (1999).
5. E. Mossessova, C. D. Lima, Ulp1-SUMO crystal structure and genetic analysis reveal conserved interactions and a regulatory element essential for cell growth in yeast. *Mol Cell* **5**, 865-876 (2000).
6. S. Muller, C. Hoege, G. Pyrowolakis, S. Jentsch, SUMO, ubiquitin's mysterious cousin. *Nat Rev Mol Cell Biol* **2**, 202-210 (2001).
7. A. Crow, R. K. Hughes, F. Taieb, E. Oswald, M. J. Banfield, The molecular basis of ubiquitin-like protein NEDD8 deamidation by the bacterial effector protein Cif. *Proc Natl Acad Sci U S A* **109**, E1830-1838 (2012).
8. R. Hjerpe *et al.*, Changes in the ratio of free NEDD8 to ubiquitin triggers NEDDylation by ubiquitin enzymes. *Biochem J* **441**, 927-936 (2012).
9. L. N. Shen *et al.*, Structural basis of NEDD8 ubiquitin discrimination by the deNEDDylating enzyme NEDP1. *EMBO J* **24**, 1341-1351 (2005).
10. A. L. Haas, P. Ahrens, P. M. Bright, H. Ankel, Interferon induces a 15-kilodalton protein exhibiting marked homology to ubiquitin. *J Biol Chem* **262**, 11315-11323 (1987).
11. K. R. Loeb, A. L. Haas, The interferon-inducible 15-kDa ubiquitin homolog conjugates to intracellular proteins. *J Biol Chem* **267**, 7806-7813 (1992).
12. W. Zou *et al.*, ISG15 modification of ubiquitin E2 Ubc13 disrupts its ability to form

thioester bond with ubiquitin. *Biochem Biophys Res Commun* **336**, 61-68 (2005).

13. A. Varshavsky, Naming a targeting signal. *Cell* **64**, 13-15 (1991).

14. A. Ciechanover, S. Elias, H. Heller, A. Hershko, "Covalent affinity" purification of ubiquitin-activating enzyme. *J Biol Chem* **257**, 2537-2542 (1982).

15. A. Hershko, Ubiquitin: roles in protein modification and breakdown. *Cell* **34**, 11-12 (1983).

16. A. Hershko, E. Leshinsky, D. Ganoth, H. Heller, ATP-dependent degradation of ubiquitin-protein conjugates. *Proc Natl Acad Sci U S A* **81**, 1619-1623 (1984).

17. A. Hershko, A. Ciechanover, A. Varshavsky, Basic Medical Research Award. The ubiquitin system. *Nat Med* **6**, 1073-1081 (2000).

18. C. Uchida, M. Kitagawa, RING-, HECT-, and RBR-type E3 Ubiquitin Ligases: Involvement in Human Cancer. *Curr Cancer Drug Targets* **16**, 157-174 (2016).

19. L. Hicke, Protein regulation by monoubiquitin. *Nat Rev Mol Cell Biol* **2**, 195-201 (2001).

20. A. Hershko, Lessons from the discovery of the ubiquitin system. *Trends Biochem Sci* **21**, 445-449 (1996).

21. A. Hershko, A. Ciechanover, The ubiquitin system. *Annu Rev Biochem* **67**, 425-479 (1998).

22. N. Zheng, N. Shabek, Ubiquitin Ligases: Structure, Function, and Regulation. *Annu Rev Biochem* **86**, 129-157 (2017).

23. C. H. Emmerich *et al.*, Activation of the canonical IKK complex by K63/M1-linked hybrid ubiquitin chains. *Proc Natl Acad Sci U S A* **110**, 15247-15252 (2013).

24. L. Jin, A. Williamson, S. Banerjee, I. Philipp, M. Rape, Mechanism of ubiquitin-chain formation by the human anaphase-promoting complex. *Cell* **133**, 653-665 (2008).

25. C. Liu, W. Liu, Y. Ye, W. Li, Ufd2p synthesizes branched ubiquitin chains to promote the degradation of substrates modified with atypical chains. *Nat Commun* **8**, 14274 (2017).

26. H. J. Meyer, M. Rape, Enhanced protein degradation by branched ubiquitin chains. *Cell* **157**, 910-921 (2014).

27. R. G. Yau *et al.*, Assembly and Function of Heterotypic Ubiquitin Chains in Cell-Cycle and Protein Quality Control. *Cell* **171**, 918-933 e920 (2017).

28. Y. T. Kwon, A. Ciechanover, The Ubiquitin Code in the Ubiquitin-Proteasome System and Autophagy. *Trends Biochem Sci* **42**, 873-886 (2017).

29. F. Ohtake, Y. Saeki, S. Ishido, J. Kanno, K. Tanaka, The K48-K63 Branched Ubiquitin Chain Regulates NF-kappaB Signaling. *Mol Cell* **64**, 251-266 (2016).

30. F. Ohtake, H. Tsuchiya, Y. Saeki, K. Tanaka, K63 ubiquitylation triggers proteasomal degradation by seeding branched ubiquitin chains. *Proc Natl Acad Sci U S A* **115**, E1401-E1408 (2018).

31. Y. Feng, D. He, Z. Yao, D. J. Klionsky, The machinery of macroautophagy. *Cell research* **24**, 24-41 (2014).

32. J. Kaur, J. Debnath, Autophagy at the crossroads of catabolism and anabolism. *Nature reviews. Molecular cell biology* **16**, 461-472 (2015).

33. G. Bjorkoy *et al.*, p62/SQSTM1 forms protein aggregates degraded by autophagy and has a protective effect on huntingtin-induced cell death. *J Cell Biol* **171**, 603-614 (2005).

34. V. Kirkin *et al.*, A role for NBR1 in autophagosomal degradation of ubiquitinated substrates. *Mol Cell* **33**, 505-516 (2009).

35. S. Pankiv *et al.*, p62/SQSTM1 binds directly to Atg8/LC3 to facilitate degradation of ubiquitinated protein aggregates by autophagy. *J Biol Chem* **282**, 24131-24145 (2007).

36. Z. Deng *et al.*, Autophagy Receptors and Neurodegenerative Diseases. *Trends in cell biology* **27**, 491-504 (2017).

37. C. H. Ji, Y. T. Kwon, Crosstalk and Interplay between the Ubiquitin-Proteasome System and Autophagy. *Mol Cells* **40**, 441-449 (2017).

38. A. E. Greijer, E. van der Wall, The role of hypoxia inducible factor 1 (HIF-1) in

hypoxia induced apoptosis. *J Clin Pathol* **57**, 1009-1014 (2004).

39. G. L. Wang, B. H. Jiang, E. A. Rue, G. L. Semenza, Hypoxia-inducible factor 1 is a basic-helix-loop-helix-PAS heterodimer regulated by cellular O2 tension. *Proc Natl Acad Sci U S A* **92**, 5510-5514 (1995).

40. R. K. Bruick, S. L. McKnight, A conserved family of prolyl-4-hydroxylases that modify HIF. *Science* **294**, 1337-1340 (2001).

41. A. C. Epstein *et al.*, C. elegans EGL-9 and mammalian homologs define a family of dioxygenases that regulate HIF by prolyl hydroxylation. *Cell* **107**, 43-54 (2001).

42. L. Holmquist-Mengelbier *et al.*, Recruitment of HIF-1alpha and HIF-2alpha to common target genes is differentially regulated in neuroblastoma: HIF-2alpha promotes an aggressive phenotype. *Cancer Cell* **10**, 413-423 (2006).

43. R. Chen *et al.*, Reactive Oxygen Species Formation in the Brain at Different Oxygen Levels: The Role of Hypoxia Inducible Factors. *Front Cell Dev Biol* **6**, 132 (2018).

44. J. L. Evans, I. D. Goldfine, B. A. Maddux, G. M. Grodsky, Oxidative stress and stress-activated signaling pathways: a unifying hypothesis of type 2 diabetes. *Endocr Rev* **23**, 599-622 (2002).

45. A. Bachmair, D. Finley, A. Varshavsky, In vivo half-life of a protein is a function of its amino-terminal residue. *Science* **234**, 179-186 (1986).

46. T. Tasaki, S. M. Sriram, K. S. Park, Y. T. Kwon, The N-end rule pathway. *Annu Rev Biochem* **81**, 261-289 (2012).

47. H. Cha-Molstad *et al.*, Amino-terminal arginylation targets endoplasmic reticulum chaperone BiP for autophagy through p62 binding. *Nat Cell Biol* **17**, 917-929 (2015).

48. H. Cha-Molstad *et al.*, p62/SQSTM1/Sequestosome-1 is an N-recognin of the N-end rule pathway which modulates autophagosome biogenesis. *Nat Commun* **8**, 102 (2017).

49. A. Varshavsky, N-degron and C-degron pathways of protein degradation. *Proc*

Natl Acad Sci U S A **116**, 358-366 (2019).

50. T. Tasaki *et al.*, A family of mammalian E3 ubiquitin ligases that contain the UBR box motif and recognize N-degrons. *Mol Cell Biol* **25**, 7120-7136 (2005).

51. R. G. Hu *et al.*, The N-end rule pathway as a nitric oxide sensor controlling the levels of multiple regulators. *Nature* **437**, 981-986 (2005).

52. M. J. Lee *et al.*, RGS4 and RGS5 are in vivo substrates of the N-end rule pathway. *Proc Natl Acad Sci U S A* **102**, 15030-15035 (2005).

53. M. D. White *et al.*, Plant cysteine oxidases are dioxygenases that directly enable arginyl transferase-catalysed arginylation of N-end rule targets. *Nat Commun* **8**, 14690 (2017).

54. N. Dissmeyer, Conditional Protein Function via N-Degron Pathway-Mediated Proteostasis in Stress Physiology. *Annu Rev Plant Biol* **70**, 83-117 (2019).

55. Y. T. Kwon *et al.*, An essential role of N-terminal arginylation in cardiovascular development. *Science* **297**, 96-99 (2002).

56. N. Masson *et al.*, Conserved N-terminal cysteine dioxygenases transduce responses to hypoxia in animals and plants. *Science* **365**, 65-69 (2019).

57. D. J. Gibbs *et al.*, Homeostatic response to hypoxia is regulated by the N-end rule pathway in plants. *Nature* **479**, 415-418 (2011).

58. D. A. Weits *et al.*, Plant cysteine oxidases control the oxygen-dependent branch of the N-end-rule pathway. *Nat Commun* **5**, 3425 (2014).

59. H. Cha-Molstad *et al.*, Modulation of SQSTM1/p62 activity by N-terminal arginylation of the endoplasmic reticulum chaperone HSPA5/GRP78/BiP. *Autophagy* **12**, 426-428 (2016).

60. J. Falck, J. Coates, S. P. Jackson, Conserved modes of recruitment of ATM, ATR and DNA-PKcs to sites of DNA damage. *Nature* **434**, 605-611 (2005).

61. A. N. Blackford, S. P. Jackson, ATM, ATR, and DNA-PK: The Trinity at the Heart of the DNA Damage Response. *Mol Cell* **66**, 801-817 (2017).

62. S. A. Wek, S. Zhu, R. C. Wek, The histidyl-tRNA synthetase-related sequence in

the eIF-2 alpha protein kinase GCN2 interacts with tRNA and is required for activation in response to starvation for different amino acids. *Mol Cell Biol* **15**, 4497-4506 (1995).

63. D. Garcia, R. J. Shaw, AMPK: Mechanisms of Cellular Energy Sensing and Restoration of Metabolic Balance. *Mol Cell* **66**, 789-800 (2017).

64. M. Wagegg *et al.*, Hypoxia promotes osteogenesis but suppresses adipogenesis of human mesenchymal stromal cells in a hypoxia-inducible factor-1 dependent manner. *PLoS One* **7**, e46483 (2012).

65. D. J. Gibbs *et al.*, Oxygen-dependent proteolysis regulates the stability of angiosperm polycomb repressive complex 2 subunit VERNALIZATION 2. *Nat Commun* **9**, 5438 (2018).

66. F. Licausi *et al.*, Oxygen sensing in plants is mediated by an N-end rule pathway for protein destabilization. *Nature* **479**, 419-422 (2011).

67. D. A. Weits *et al.*, An apical hypoxic niche sets the pace of shoot meristem activity. *Nature* **569**, 714-717 (2019).

68. J. Vicente *et al.*, The Cys-Arg/N-End Rule Pathway Is a General Sensor of Abiotic Stress in Flowering Plants. *Curr Biol* **27**, 3183-3190 e3184 (2017).

69. J. W. Tobias, T. E. Shrader, G. Rocap, A. Varshavsky, The N-end rule in bacteria. *Science* **254**, 1374-1377 (1991).

70. R. I. Astuti, R. Nasuno, H. Takagi, Nitric oxide signaling in yeast. *Appl Microbiol Biotechnol* **100**, 9483-9497 (2016).

71. T. H. Rushmore, M. R. Morton, C. B. Pickett, The antioxidant responsive element. Activation by oxidative stress and identification of the DNA consensus sequence required for functional activity. *J Biol Chem* **266**, 11632-11639 (1991).

72. J. D. Hayes, D. J. Pulford, The glutathione S-transferase supergene family: regulation of GST and the contribution of the isoenzymes to cancer chemoprotection and drug resistance. *Crit Rev Biochem Mol Biol* **30**, 445-600 (1995).

73. J. D. Hayes, R. C. Strange, Potential contribution of the glutathione S-transferase supergene family to resistance to oxidative stress. *Free Radic Res* **22**, 193-207 (1995).

74. C. Richter *et al.*, Oxidants in mitochondria: from physiology to diseases. *Biochim Biophys Acta* **1271**, 67-74 (1995).

75. J. D. Hayes, E. M. Ellis, G. E. Neal, D. J. Harrison, M. M. Manson, Cellular response to cancer chemopreventive agents: contribution of the antioxidant responsive element to the adaptive response to oxidative and chemical stress. *Biochem Soc Symp* **64**, 141-168 (1999).

76. P. C. Lee, M. E. Sowa, S. P. Gygi, J. W. Harper, Alternative ubiquitin activation/conjugation cascades interact with N-end rule ubiquitin ligases to control degradation of RGS proteins. *Mol Cell* **43**, 392-405 (2011).

77. Y. D. Yoo *et al.*, N-terminal arginylation generates a bimodal degron that modulates autophagic proteolysis. *Proc Natl Acad Sci U S A* **115**, E2716-E2724 (2018).

78. D. Blum *et al.*, Molecular pathways involved in the neurotoxicity of 6-OHDA, dopamine and MPTP: contribution to the apoptotic theory in Parkinson's disease. *Prog Neurobiol* **65**, 135-172 (2001).

79. C. I. Sze *et al.*, A cascade of protein aggregation bombards mitochondria for neurodegeneration and apoptosis under WWOX deficiency. *Cell Death Dis* **6**, e1881 (2015).

80. L. Ruan *et al.*, Cytosolic proteostasis through importing of misfolded proteins into mitochondria. *Nature* **543**, 443-446 (2017).

81. J. W. Heck, S. K. Cheung, R. Y. Hampton, Cytoplasmic protein quality control degradation mediated by parallel actions of the E3 ubiquitin ligases Ubr1 and San1. *Proc Natl Acad Sci U S A* **107**, 1106-1111 (2010).

82. J. S. Bhatti, G. K. Bhatti, P. H. Reddy, Mitochondrial dysfunction and oxidative stress in metabolic disorders - A step towards mitochondria based therapeutic

strategies. *Biochim Biophys Acta Mol Basis Dis* **1863**, 1066-1077 (2017).

83. S. Sifuentes-Franco, F. P. Pacheco-Moises, A. D. Rodriguez-Carrizalez, A. G. Miranda-Diaz, The Role of Oxidative Stress, Mitochondrial Function, and Autophagy in Diabetic Polyneuropathy. *J Diabetes Res* **2017**, 1673081 (2017).

84. S. Sifuentes-Franco, D. E. Padilla-Tejeda, S. Carrillo-Ibarra, A. G. Miranda-Diaz, Oxidative Stress, Apoptosis, and Mitochondrial Function in Diabetic Nephropathy. *Int J Endocrinol* **2018**, 1875870 (2018).

85. N. Suematsu *et al.*, Oxidative stress mediates tumor necrosis factor-alpha-induced mitochondrial DNA damage and dysfunction in cardiac myocytes. *Circulation* **107**, 1418-1423 (2003).

86. H. Nojiri *et al.*, Oxidative stress causes heart failure with impaired mitochondrial respiration. *J Biol Chem* **281**, 33789-33801 (2006).

87. J. R. Mayers *et al.*, ESCRT-0 assembles as a heterotetrameric complex on membranes and binds multiple ubiquitinylated cargoes simultaneously. *J Biol Chem* **286**, 9636-9645 (2011).

88. X. Ren *et al.*, Hybrid structural model of the complete human ESCRT-0 complex. *Structure* **17**, 406-416 (2009).

89. D. J. Gill *et al.*, Structural insight into the ESCRT-I/-II link and its role in MVB trafficking. *EMBO J* **26**, 600-612 (2007).

90. H. Teo *et al.*, ESCRT-I core and ESCRT-II GLUE domain structures reveal role for GLUE in linking to ESCRT-I and membranes. *Cell* **125**, 99-111 (2006).

91. M. Babst, B. Wendland, E. J. Estepa, S. D. Emr, The Vps4p AAA ATPase regulates membrane association of a Vps protein complex required for normal endosome function. *EMBO J* **17**, 2982-2993 (1998).

92. C. Kieffer *et al.*, Two distinct modes of ESCRT-III recognition are required for VPS4 functions in lysosomal protein targeting and HIV-1 budding. *Dev Cell* **15**, 62-73 (2008).

93. S. Lata *et al.*, Helical structures of ESCRT-III are disassembled by VPS4. *Science*

321, 1354-1357 (2008).

94. S. Shim, S. A. Merrill, P. I. Hanson, Novel interactions of ESCRT-III with LIP5 and VPS4 and their implications for ESCRT-III disassembly. *Mol Biol Cell* **19**, 2661-2672 (2008).

95. G. Palade, Intracellular aspects of the process of protein synthesis. *Science* **189**, 867 (1975).

96. T. L. Burgess, R. B. Kelly, Constitutive and regulated secretion of proteins. *Annu Rev Cell Biol* **3**, 243-293 (1987).

97. N. V. Khobrekar, S. Quintremil, T. J. Dantas, R. B. Vallee, The Dynein Adaptor RILP Controls Neuronal Autophagosome Biogenesis, Transport, and Clearance. *Dev Cell* **53**, 141-153 e144 (2020).

98. C. Rosa-Ferreira, S. T. Sweeney, S. Munro, The small G protein Arl8 contributes to lysosomal function and long-range axonal transport in Drosophila. *Biol Open* **7** (2018).

99. L. Parente, E. Solito, Annexin 1: more than an anti-phospholipase protein. *Inflamm Res* **53**, 125-132 (2004).

100. D. Kim *et al.*, Identification of disulfide cross-linked tau dimer responsible for tau propagation. *Sci Rep* **5**, 15231 (2015).

101. S. T. Kim *et al.*, The N-recognin UBR4 of the N-end rule pathway is targeted to and required for the biogenesis of the early endosome. *J Cell Sci* **131** (2018).

102. Y. T. Kwon, Z. Xia, I. V. Davydov, S. H. Lecker, A. Varshavsky, Construction and analysis of mouse strains lacking the ubiquitin ligase UBR1 (E3alpha) of the N-end rule pathway. *Mol Cell Biol* **21**, 8007-8021 (2001).

103. D. Han, J. Jin, J. Woo, H. Min, Y. Kim, Proteomic analysis of mouse astrocytes and their secretome by a combination of FASP and StageTip-based, high pH, reversed-phase fractionation. *Proteomics* **14**, 1604-1609 (2014).

104. J. Woo, D. Han, J. Park, S. J. Kim, Y. Kim, In-depth characterization of the secretome of mouse CNS cell lines by LC-MS/MS without prefractionation.

Proteomics **15**, 3617-3622 (2015).

105. S. Tyanova, T. Temu, J. Cox, The MaxQuant computational platform for mass spectrometry-based shotgun proteomics. *Nat Protoc* **11**, 2301-2319 (2016).

106. J. Cox *et al.*, Andromeda: a peptide search engine integrated into the MaxQuant environment. *J Proteome Res* **10**, 1794-1805 (2011).

초록

허아정
의과학과, 의과학전공
서울대학교 대학원

가변적인 환경 변화에 대한 적응은 세포 내 항상성 조절에 필수적이다. 적응을 위해서는 환경변화에 대한 “인지” 와 “반응” 두 가지 측면이 동등하게 필수적으로 작용하는데, 이 때, 단백질은 그 자신이 변화의 주체로서, 이러한 인지와 반응 매커니즘을 매개한다. 특히나 단백질은 스트레스 상황을 포함한 특정 컨디션에서 그 자신의 형태적 변경을 통해, 기본적으로 자신이 실행하던 기능에서 벗어난 새로운 기능을 수행하게 되며, 이는 단백질 자체의 안정성 조절과 전사 유도 (transcriptional induction)를 통한 양적 기능변화, 그리고 번역 후 수정 (post-translational modification) 과 같은 여러 조절기전들을 통해 일어나게 된다.

이 논문에서, 필자는 세포 내 산화적 스트레스 하에서 시스테인/N-말단 경로의 역할을 단백질의 안정성 조절과 번역 후 수정의 관점에서 다룰 것이다. N-말단 법칙은 진화적 관점에서 고도로 보존된 단백질의 조절기전으로, 모든 계(界, kingdom)를 통틀어 적용되어왔다. N-말단 법칙은 단백질이 잘려지거나 혹은 처리되며 노출되는 N-말단부의 아미노산이 단백질의 안정성을 조절한다는 단백질 분해 기전의 한 줄기로, 말단부에 노출된 아미노산의 종류에 따라 다양한 가지로 나뉘어 연구되고 있다. 그 중에서도 아르기닌 N-말단 법칙의 일부인 N-말단 시스테인의 경우, 황화수소 잔기(sulfhydryl side chain)를 가지는 유일한 아미노산으로 산소 원자와 결합, 변형이 가능하다는 특이점을 가진다. 이러한 시스테인 잔기의 특이성은 자동적으로 시스테인/N-말단 법칙이 세포 내 산화 스트레스에 의한 변화의 주체로서 산화 스트레스 인지와 반응의 매개체일 것이라는 확신을 부여한다.

이 논문의 첫 부분은 세포 내에서 일어나는 산화와 환원력 사이의 섬세한 밸런스를 단백질 분해의 관점에서 풀어나갈 것이다. 세포 내 급성 저산소증과 만성적 저산소증, 그리고 만성적 저산소 상태로 인해 초래된 산화스트레스로 일어나는 단백질 변화에 대한 기전연구에 대해 논할 것이다. 특히나, N-말단에 노출된 시스테인이 이러한 상황에서 어떻게 단백질의 구조, 기능적 변화를 유도하고 그에 따른

단백질의 분해 과정까지 영향을 미치는지에 대하여 자세하게 다룰 것이다. N-말단 아르기닌화가 가능한 두가지 종류의 산화 시스테인인 시스테인 설핀산(cysteine sulfinic acid; $CysO_2H$) 과 시스테인 설폰산 (cysteine sulfonic acid; $CysO_3H$)은 각각 동일한 N-말단 경로 기질의 분해 방법을 유비퀴틴-프로테아좀 시스템 (Ubiquitin-proteasome system) 과 오토파지-리소좀 경로 (autophagy) 로 이원화하며, 이러한 분해경로의 이원화는 N-레코그닌 E3 리가제인 UBR1/UBR2를 이용한 노선과 새로운 N-레코그닌인 KCMF1-UBR4 리가제 노선으로 분리됨에 따라 유비퀴틴 코드가 전위되며 일어나게 된다. 이러한 일련의 발견들은 아르기닌/N-말단 경로에 있어 최말단부 뒤에 위치하는 두번째 잔기의 역할이 단순히 최말단부의 데그론을 유치하는데 필요한 단순 중개자가 아닌, 결정자로서 작용하여 단백질의 분해에 있어 그 특징과 변화가 중요하다는 것을 밝혀냄으로서 두번째 위치의 N-데그론(secondary N-degron)에 대한 개념을 확장할 것이다. 또한, 이러한 시스테인 N-말단 경로를 통한 산화스트레스의 인지와 반응을 생체적 관점에서 미토콘드리아 항상성과 엮어 풀어낼 것이다.

논문의 다음 파트는 이전 파트들에서 다뤄왔던 세포 내부의 산화 스트레스를 인지 및 반응을 세포간 통신을 통한 외부 세포-세포 간 반응의 영역으로 확장한다. 필자는 이러한 산화스트레스에 대한 세포간 신호전달에 있어 아르기닌/N-말단 경로가 작용하는 기전에 대해 중점적으로 다룰 것이다. 구체적으로는 산화스트레스에 의해 잘려지고 아르기닌화 되는 Arg/N-말단 경로의 기질인 RILP 단백질을 동정하였으며, 이러한 RILP 단백질로 인해 매개된 다낭체 (MVB)-ARL8b-키네신 (kinesin) 단백질 복합체 형성과 이를 통한 MVB의 원형질막(plasma membrane) 타겟팅 기전에 대해 논할 것이다. 뿐만 아니라, ATE1에 의존적으로 일어나는 MVB의 내강소포(intraluminal vesicle)형성 또한 아르기닌/N-말단 경로가 이중 기전을 통해 엑소좀 형성과 수송에 관여하며 궁극적으로 산화 스트레스에 대항한 항상성 조절에 중요하다는 것을 시사한다.

마지막으로, 필자는 본 논문에 대한 요약과 추후 논의를 통해 논문을 마무리하려고 한다. 이 논문에서 다루어진 발견들은 진화적으로 보존된 Arg/N-말단 경로가 포유류 세포에서 산화스트레스에 대항하여 두 가지 모드의 단백질 분해와 엑소좀의 분비를 통해 세포 내 외적 항상성을 조절할 수 있음을 의미한다.

Keywords : 아르기닌/N-말단 법칙, 시스테인/N-말단 법칙, 산화스트레스 센서, 저산소 센서, KCMF1, 엑소사이토시스
Student Number : 2014-25077

Acknowledgements
감사의 글

7 년 반의 대학원 생활이 끝나고 드디어 제가 학위논문을 제출하게 되었습니다.
학위논문을 작성하고 졸업 심사를 거치며 그 동안의 생활을 돌아보게 되었습니다.
현재까지의 인생을 통틀어 절대 짧지 않은 기간 이였고 그 동안 많은 경험과
사람들을 만나 지금의 제가 되었습니다

자기 주장 강하고 지도하기 쉽지 않던 저를 긴 시간동안 이끌어 주시고 기다려 주시며 과학자로서 거듭날 수 있도록 기본기와 소양을 키워 주신 권용태 교수님께 큰 감사의 인사를 올립니다.

졸업 심사에서 마지막까지 학업적으로도 개인적으로도 좋은 연구자가 될 수 있도록 많은 가르침을 주신 이민재 교수님, 전양숙 교수님, 한도현 교수님, 독일학회부터 개인적 조언까지 물심양면으로 많은 도움을 주신 송현규 교수님, 모두 정말 감사드립니다.

같이 밤새워 실험실에서 함께 디스커션하고, 논문을 작성했고, 데이터 하나에 같이 울고 웃으며 긴 시간 질곡과 애환의 모든 순간을 함께한 서포터이자 코워커가 되어 준 내 친구 지창훈 박사. 나란히 손잡고 졸업하는 동기 이수현 언니, 잘 따라와 주고 의지와 손발이 되어 준 부사수 김수빈, 이수진, 권순철 학생과, 실험실 생활을 함께해온 이민주 학생, 김호선 선생님께 감사의 인사를 드립니다. 또한 미처 다 언급하지 못하였으나 쉽지 않고 다사다난하던 연구에 도움을 주신 많은 분들께 깊이 감사드립니다.

늦은 나이까지 공부한다고 맏이 노릇 제대로 못하는 큰 딸 옆에서 지켜봐 주시고 믿어 주시고 아낌없는 응원과 함께 기다려 주신 부모님, 여느 언니들처럼 잘 해주지 못해 항상 마음에 걸리고 미안한 유정이, 이러한 가족들의 사랑과 전폭적인 지지가 버팀목이 되어 힘든 시간들을 견디어 낼 수 있었던 것 같습니다.
감사하고 사랑합니다.

그 모든 분들의 도움으로 제가 성장해서 박사 졸업을 앞두게 되었습니다.

감사하다는 말 한마디로는 전부 표현할 수는 없지만,

모든 분들께 오롯이 제 마음을 담아 진심 어린 감사의 인사를 올립니다.